Sequential Position And Covariance Estimation

(SPACE)

Trajectory Program

ANALYTICAL MANUAL

April 1965

Contract No.: NAS-5-3509

Prepared by

Sperry Rand Systems Group
Sperry Gyroscope Company
Division of Sperry Rand Corporation
Great Neck, New York

(Sperry Report No. AB-21-0001)

for

Goddard Space Flight Center
Greenbelt, Maryland

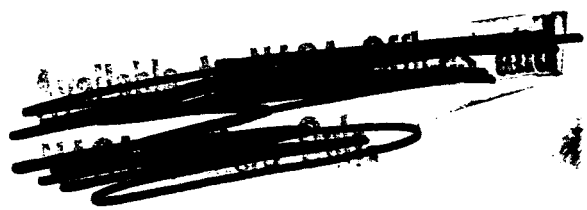

Sequential Position And Covariance Estimation

(SPACE)

Trajectory Program

ANALYTICAL MANUAL

April 1965

Contract No.: NAS-5-3509

Prepared by

Sperry Rand Systems Group
Sperry Gyroscope Company
Division of Sperry Rand Corporation
Great Neck, New York

(Sperry Report No. AB-21-0001)

for

Goddard Space Flight Center
Greenbelt, Maryland

ERRATA

PAGE	CORRECTION
5-21/5-22	In Table 5-1, the division lines apply only to the partial derivatives. The 1,1 element, for example, should appear as $$1 + \sum_{m=0}^{\infty} \frac{\partial a_{m+2}}{\partial x_o} \quad t^{(m+2)}$$ Similarly, the 4,1 element should be $$\sum_{m=0}^{\infty} (m+2) \frac{\partial a_{m+2}}{\partial x_o} \quad t^{(m+1)}$$
6-7	$A = \mathrm{Tan}^{-1} \frac{\rho_B \cdot \bar{e}_B}{\rho_B \cdot \bar{n}_B}, \quad 0 \le A \le 2\pi$ (8)
6-8	$(RA) = \mathrm{Tan}^{-1} \frac{\rho_B \cdot \bar{y}}{\rho_B \cdot \bar{x}}, \quad 0 \le (RA) < 2\pi$ (13)
6-11	$f_3 = 930.150 \times 10^{-6} - 30\left(\frac{96}{89}\right)\left(\frac{31}{32}\right)(FRQ)\left\{1 - \frac{(\dot{\rho}_i - \dot{\rho}_2)}{c}\right\}$ (28)
6-15	$\frac{\partial A}{\partial \ell} = \frac{\mathrm{Cos}\ A}{\mathrm{Cos}\ E}; \quad \frac{\partial E}{\partial m} = \frac{-\mathrm{Sin}\ A}{\mathrm{Cos}\ E}$ (43c)
	$M_{EV} = \left[-(\bar{e}_B \mathrm{SinA}\ \mathrm{SinE} + \bar{n}_B \mathrm{CosA}\ \mathrm{SinE} - \bar{h}_B \mathrm{CosE}) \quad 0 \quad 0 \quad 0\right]$ (44a)
	$\frac{\partial E}{\partial \ell} = \frac{-\mathrm{Sin}\ A}{\mathrm{Sin}\ E}; \quad \frac{\partial E}{\partial m} = \frac{-\mathrm{Cos}\ A}{\mathrm{Sin}\ E}$ (44c)
6-16	$M_{\rho V} = 2\left[\frac{\rho_B}{\rho_B} \quad 0 \quad 0 \quad 0\right]$ (45a)
6-17	$M_{\dot{\rho} V} = \frac{1}{\rho_B}\left[\left(\dot{R}_c - \dot{R}_{SB} - \dot{\rho}\frac{\rho_B}{\rho_c}\right) \quad \rho_B\right]$ (46a)

PAGE

CORRECTIONS

6-18

$$\frac{\partial h}{\partial E} = \frac{\text{Sin}^2 h \ \text{Sec}^2 E \ \text{Cos} \ \phi_G}{\text{Sin A}} \qquad (47b)$$

$$\frac{\partial h}{\partial A} = \frac{\text{Cos}^2 h \ (\text{Sin} \ \phi_G - \text{Tan E Cos A Cos} \ \phi_G)}{(\text{Cos A Sin} \ \phi_G - \text{Tan E Cos} \ \phi_G)^2}$$

$$\frac{\partial \zeta}{\partial A} = - \frac{\text{Cos E Sin A Cos} \ \phi_G}{\text{Cos} \delta} \qquad (48b)$$

TABLE OF CONTENTS

TABLE OF CONTENTS (CONT)

TABLE OF CONTENTS (CONT)

TABLE OF CONTENTS (CONT)

TABLE OF CONTENTS (CONT)

LIST OF ILLUSTRATIONS

LIST OF ILLUSTRATIONS (CONT)

LIST OF TABLES

SECTION 1

INTRODUCTION

The Goddard Orbit Determination Program (GODP) described in this manual was developed for the Special Projects Branch, Theoretical Division, Goddard Space Flight Center by the Sperry Rand Systems Group.

The historical background to the present Program began with the development of a prototype routine by Analytical Mechanics Associates to demonstrate the feasibility of a minimum variance estimator (Kalman filter) applied to the updating of satellite orbits. Subsequently, the prototype program was modified and extended by the Systems Group, under contract to the Special Projects Branch, to accommodate the processing of real data. As a consequence of these efforts, a single-precision orbit determination program was designed using FORTRAN II and FAP. Identified as the Phase I Program, it has been employed to compute orbits for the IMP, RELAY and TIROS satellites.

Using the same design features which characterize the Phase I Program, a double-precision orbit determination program was developed by the Systems Group. This Phase II Program is the one described in this manual. It is written entirely in FORTRAN IV and offers many options both in its trajectory computation and statistical estimation modes. One essential advance of the present Program over the Phase I version is the ability of the former to obtain estimates of biases in the dynamical and observational models. It is capable, therefore, of updating geodetic and astrophysical parameters as well as of correcting tracking station survey errors and instrument biases. The double-precision program is also able to update trajectories during periods of thrust and to use measurements made on board a satellite.

Data editing routines have been developed for rejecting data with unacceptable formats, time-ordering data from various tracking systems, merging the data in proper time sequence, inserting time corrections, and converting the data formats to a standard format suitable to both Phase I and Phase II Programs. These data editing routines are subsidiary to and separate from the orbit determination Programs.

The Goddard Orbit Determination Program was developed under Contract NAS5-35-9. This Contract was monitored for the Theoretical Division by Mr. R.K. Squires and Mr. D.S. Woolston, Special Projects Branch.

SECTION 2
PROGRAM DESCRIPTION

2.1 INTRODUCTION

Orbit determination entails the statistical estimation of orbital elements, or equivalently, satellite position and velocity, from tracking data. In the usual situation, these data consist of measurements of range, range-rate, and angles from ground-based stations. The data are processed by an orbit determination program in which full use is made of a priori information in the estimation process.

To carry out its functions, an orbit determination program requires two major components; (1) a routine for orbit prediction or trajectory computation; (2) a routine for statistical estimation. This section introduces these two components in terms of the contents of the Program, thereby providing an over-all view of the material to be described in succeeding sections. Specifically, detailed discussions of trajectory computation are given in Sections 3 and 4; the elements of statistical estimation are covered in Section 5.

2.2 TRAJECTORY COMPUTATION

Orbit prediction, or trajectory computation, is the process of calculating the position and velocity of a spacecraft at any time later than some initial time, given the vehicle's position and velocity at the initial time. To accomplish this prediction, one makes use of the laws of celestial mechanics as embodied in the differential equations of motion. Forcing functions for these equations are obtained from a dynamic model which accounts for the accelerations acting on the spacecraft. A reference frame is erected to express the components of the various vector quantities, and the equations of motion are numerically integrated, subject to the given initial conditions.

The coordinate system used in this Program is based upon the mean Earth's equator and equinox obtaining at 0^h January 1 of the year subsequent to the initial time. Coordinate directions of this frame are inertial with respect to the fixed stars; the center of origin of the system, however, may be transferred from one central body to another, so that the spacecraft motion is specified relative to a point mass which itself has a proper motion. This reference frame is called the Base Date System.

Observations made from the Earth are necessarily in a system different from the Base Date System; the actual coordinate frame is called the true system of date. The true

system differs from the Base Date System because of the Earth's nutation and the precession of the equinox. In going from one frame to the other, the true system of date is reduced to the mean system of date by a nutation transformation. A vector expressed in the resulting mean system is then transformed to the Base Date System by a precession matrix.

For observations made on the Moon, account must be taken of lunar libration. In this instance, a transformation is made from a coordinate frame rigidly attached to the Moon to the true system of date. Nutation and precession transformations then rotate the observation into the Base Date System.

All accelerations acting on the vehicle are specified in the Base Date System. The gravitational attractions of bodies in the solar system are functions only of position with respect to the vehicle; consequently, the Program employs an ephemeris giving planetary coordinates relative to the Sun and lunar coordinates relative to the Earth, all in a Base Date System. A Base Date System is specified for overlapping two-year blocks of data, the Date corresponding to the middle of the two-year file. Specifying an initial time causes the Program to choose an ephemeris file having as its Base Date the beginning of the year following the initial time. In this way, at least one full year of ephemeris information is available before a change of reference system is necessary.

Another acceleration specified in the Base Date System without transformation is that arising from solar radiation pressure. Since this acceleration is a function of relative position between the Sun and the vehicle, its direction is given in the proper frame by manipulating information from the ephemeris.

Other accelerations, such as Earth oblateness effects and atmospheric drag must be transformed through nutation and precession to the proper frame. Higher gravitational terms arising from the Moon's field are subject to the additional transformation of libration. Thrust accelerations, on the other hand, may be specified in an arbitrary coordinate frame. If they are given in the Base Date System, no transformations are necessary, whereas if they are described in any other frame, rotation matrices appropriate to the situation must be used.

Spacecraft motion is always computed relative to some reference body: a planet; the Moon; the Sun. Consequently, the equations of motion contain a term which accounts for the acceleration of the reference body on the spacecraft. The remaining accelerations are usually, but not always, much smaller than this primary acceleration and are therefore called perturbations. In most cases, they can be regarded as giving rise to small disturbances in the orbit determined by the reference body and the initial conditions. Two exceptions arise in the cases of motion through a dense atmosphere, and the application of high thrust to the vehicle. In both these instances, the perturbation acceleration may equal or exceed the primary acceleration.

Reference bodies are changed during a trajectory calculation when the spacecraft leaves the "region of influence" associated with a particular body. Regions of influence are computed for a body with respect to the object of which it is a satellite. Hence, each planet has a region of influence defined relative to the Sun, and the Moon has a similar region defined relative to the Earth. In transferring into or out of such a region, velocity as well as position with respect to the new reference body must be calculated.

Since no analytic solution exists for the equations of motion, numerical methods are employed to compute the components of position and velocity. In the Program, a choice may be made between using straightforward integration and using Encke's method. The former technique, called Cowell's method, is conceptually simple, but suffers from precision and machine running time problems. Encke's method, although somewhat more complicated, gives dividends in both precision and machine efficiency. In this procedure, the Keplerian orbit arising from the reference body central force field is taken as a nominal trajectory. The perturbation accelerations are integrated and the resulting position and velocity increments are added to the Keplerian solutions. Naturally, Encke's method is most effective when the perturbations are small. This Program employs an extension of the Encke procedure for powered flight in which the central gravitational force and the thrust accelerations define the nominal trajectory. Perturbations to this more comprehensive reference orbit are then integrated to obtain the total trajectory.

Both ground-based and on-board observations can be computed in the Program. Such observations may be corrupted with random noise of specified variance to give fictitious data. These "data" find application in various types of systems studies. The Program also generates acquisition information for tracking stations.

Corrections are provided in the Program for the refraction of an electromagnetic signal by the troposphere or by the ionosphere. Adjustments are computed for errors in elevation angle, range, and radial velocity; other angular corrections are calculated from the adjustment in elevation angle.

2.3 STATISTICAL COMPUTATIONS

Orbit determination has come to mean, in modern usage, the aggregate of those methods whereby initial estimates of a spacecraft's position and velocity are statistically updated from observations. Updating need not be restricted to position and velocity, but may also be applied to uncertainties in the dynamical and observational models. Uncertainties in both models give rise to inaccuracies in the prediction of spacecraft motion, and affect, as well, the confidence to be placed in the prediction.

To implement the estimation of the vehicle state, and to correct the constants of the dynamical and observational models, the available data must be processed by some statistical technique within the Program. Before reaching this point, however, the information from the tracking stations is first subjected to a data editing routine external to the Program. In this routine, the data are time-ordered, time-corrected, and data points which have been labelled as bad at the tracking station are removed from the resulting data tape. The Program can then process this tape and edit out any data point which falls outside a designated statistical limit. A final tape is thereby produced which is loaded into the Program as the raw material of orbit determination.

The estimation procedure may be recursive or non-recursive, and may use various criteria to define a "best estimate" of the quantities to be updated. Recursive estimation is typified by minimum variance, or Kalman, filtering in which data points are processed successively in their natural time order. Non-recursive estimation, like least-squares, processes "batches" of data taken over relatively long time arcs. The Program provides a

choice between Baye's estimation (which includes least-squares) and minimum variance. Baye's estimate may be made either recursively or non-recursively.

All of the estimation procedures make use of a linearized state vector, the components of which are the position and velocity deviations from a nominal trajectory, and the uncertainties in the constants of the dynamical and observational models. The employment of a linearized vector necessitates the calculation of three matrices: the state transition matrix; the covariance matrix; the matrix of observation partial derivatives.

A state transition matrix relates the linearized state vector at one time to the state vector at some other time. A covariance matrix contains as diagonal elements the variances of the state vector components, whereas the off-diagonal elements are the covariances among these same components. The matrix of observation partials establishes the deterministic relationship between the linearized observation residuals and the state vector. Each of these matrices is used in computing an optimal estimate of the state.

Recursive procedures give the optimal estimate at each data time. Non-recursive estimation, on the other hand, updates the vehicle state at one point in the "batch" of data; an optimal estimate at any other point is obtained by integrating the trajectory from the updated state.

The Program does not use the conventional linearized position and velocity components in the state vector. Rather, it uses a set of differential parameters for which the statistical correction matrix can be computed over a longer time span than can the corresponding matrix for the conventional vector. A closed-form point transformation has been developed relating the conventional state vector and the parameter vector. The parameter transition matrix is also available in closed form when computed for a Keplerian orbit. Throughout this Program, it is assumed that the Keplerian transition matrix is a good approximation to the true transition matrix.

2.4 SCOPE OF THE MANUAL

The Analytical Manual is one of three manuals which have been written to describe the Orbit Determination Program. The other two volumes are concerned with programming aspects and user's information.

This volume gives the mathematical derivations behind important routines and indicates features which are unique in the Program. Section 3 covers the equations of motion, integration techniques, the special treatment of powered flight trajectories, and the procedure for reference body transfer. Section 4 deals with all the perturbations considered in trajectory computation, including planetary attractions, planetary oblateness, atmospheric drag, and radiation pressure. Statistical calculations are treated in Section 5, and Section 6 develops the computation of observables, the matrices of observation partial derivatives, and certain corrections employed with the observations. Three appendices describe: the coordinate systems used in the Program together with the complement of transformations employed; a special transformation used in powered flight computations; propagation corrections made to raw data provided to the Program by tracking stations.

SECTION 3

TRAJECTORY DETERMINATION

3.1 GENERAL

The equations of motion for a space vehicle are second-order differential equations which describe the accelerations arising from the forces acting on the vehicle. These forces are generally classified as follows:

a. Gravitational, primary

b. Gravitational, harmonic

c. Thrust

d. Drag

e. Radiation pressure.

The simplest gravitational force field is that due to a single point mass. In this case, the equations of motion are

$$\ddot{\mathbf{R}} = -\frac{\mu \mathbf{R}}{R^3} \tag{1}$$

where

$\mu = GM$

G = the universal gravitational constant

M = mass of the vehicle

$\mathbf{R}$ = position of the vehicle with respect to the point mass

With initial conditions $\mathbf{R}_0$ and $\dot{\mathbf{R}}_0$, equation (1) defines a "two-body" or Keplerian orbit which may be described in closed form in terms of its true anomaly or eccentric anomaly.

A more complicated gravitational field may be constructed by considering the forces contributed by additional point masses. In this instance, the equations of motion become

$$\ddot{\mathbf{R}} = -\frac{\mu \mathbf{R}}{R^3} + \mathbf{P}_1 \tag{2}$$

where the sum of the accelerations, P_1, caused by the other point masses is small compared to the acceleration of the original mass. The P_1 acceleration is given by

$$P_1 = \sum_j \mu_j \left[\frac{R_{vj}}{R^3_{vj}} - \frac{R_j}{R_j{}^3} \right] \qquad (3)$$

where

$\mu_j = GM_j$, where M_j is the mass of the jth body

R_{vj} = vector from the vehicle to the jth body

R_j = vector from original mass to the jth body.

The form of equation (2) implies that the original point mass provides the major portion of the vehicle's acceleration and that the remaining accelerations are perturbations. It is customary to erect a reference frame, for the equations of motion, having the predominant contributor to the force field at the origin. Consequently, the original mass is frequently called the reference body.

For a realistic model, the reference body cannot be considered as a point mass; for trajectories close to this body, it will be necessary to compute accelerations arising from harmonics in the body's gravitational potential. The Earth's potential, for example, is usually expressed in terms of associated spherical harmonics, whereas the Moon's potential is given by the moments of inertia about its three major axes.

A homogeneous ponderable body, i.e., a homogeneous body having appreciable weight, which is perfectly spherical in shape may be considered as a point mass for potential calculations. Therefore, accelerations due to gravitational harmonics result from the oblateness, i.e., deviation from purely spherical shape, of the associated body. Designating these oblateness perturbations as P_2, the equations of motion become

$$\ddot{R} = -\frac{\mu R}{R^3} + P_1 + P_2 \qquad (4)$$

Thrust accelerations, designated by P_3, may in fact be larger than the primary gravitational acceleration of the reference body. In such cases, the thrust acceleration is not considered a perturbation. A similar situation may exist for drag acceleration, P_4.

The final perturbation considered here is the effect of radiation pressure on space vehicles having a high ratio of surface area to mass. Radiation pressure may arise from three sources:

a. Direct sunlight

b. Reflected sunlight

c. Planetary radiation

In the Program, only the first source is considered; the vehicle acceleration from sunlight is designated P_5. Since the vehicle is not always in full sunlight, but may be in the umbra or penumbra of a planet, (figure 3.1-1), it is necessary to compute the vehicle's position relative to the cones of shadowing. If the vehicle is in a penumbra, an illumination factor is computed which indicates the percentage of total sunlight available for illuminating the vehicle.

Accounting for the primary gravitational field of the reference body and the five types of perturbative accelerations, the equations of motion become

$$\ddot{R} = -\frac{\mu R}{R^3} + \sum_{i=1}^{5} P_i \qquad (5)$$

There are two basic methods by which the solution to equation (5) may be obtained, Encke's method and Cowell's method. If equation (5) were to be numerically integrated in a straight-forward manner, the integration would be known as Cowell's method. The simplicity of this method is offset by the large accelerations which must be integrated. As a consequence of the acceleration magnitudes, small time increments have to be used in the integration, and machine roundoff error accumulates rapidly. Independent evaluations at many companies and universities have shown that Cowell's method requires more machine time (by a factor of ten) than other perturbational schemes. Despite these drawbacks, Cowell's integration is still widely used and is included in the Program to permit a direct comparison of results with facilities employing this technique.

Historically, Encke's method is older than Cowell's, although the former is more sophisticated. Cowell's method requires a modern high-speed computer to be practical, whereas Encke's was developed for hand computation. In Encke's method, it is assumed that the perturbative accelerations, P_i, are small compared to the reference body acceleration. Consequently, when neither the drag nor the thrust accelerations are very large, the solution of equation (1) is a good approximation to the true orbit. Under these conditions, it is only necessary to integrate the difference between the accelerations on the two-body orbit and the total accelerations acting on the vehicle. The equations of motion then become second-order differential equations describing the acceleration differences. Let

$$\xi = R - R_{TB} \qquad (6)$$

where R_{TB} is the position of the vehicle in terms of the two-body orbit. Then,

$$\ddot{\xi} = -\mu\left[\frac{R}{R^3} - \frac{R_{TB}}{R_{TB}^3}\right] + \sum_{i=1}^{5} P_i \qquad (7)$$

Equation (7) is integrated to obtain $\dot{\xi}$ and ξ. These quantities are then added to $\dot{R}_{TB}$ and R_{TB}, respectively, to obtain the instantaneous position (R) and velocity ($\dot{R}$) of the vehicle. The quantity ξ is commonly referred to as the "Encke" term.

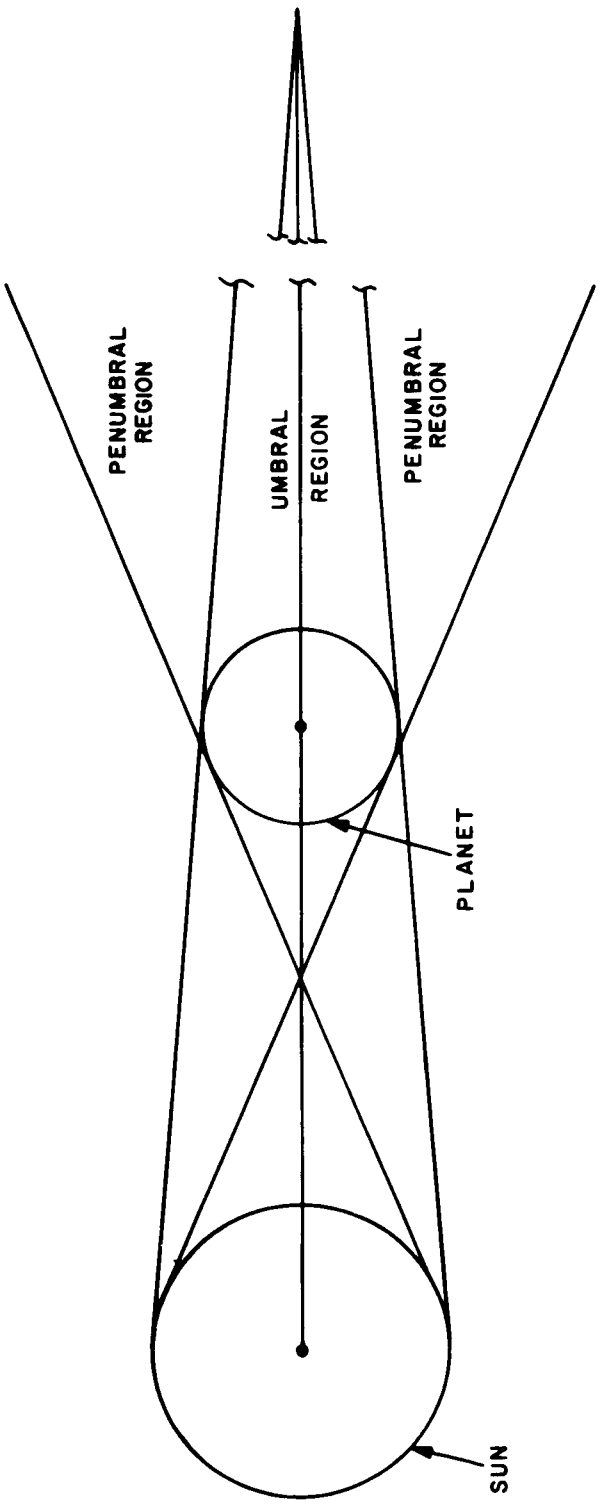

Figure 3.1-1. Vehicle Shadowing

If the thrust or drag accelerations approach the reference body acceleration in magnitude, a new reference trajectory must somehow be obtained if Encke's method is to be used. In this program, vehicle altitudes are limited to those at which atmospheric drag can safely be treated as a perturbation. For thrust, however, a subroutine has been designed which computes the trajectory arising from the reference body gravitational field and a specified thrust schedule. Using this solution as the nominal trajectory, the equations of motion now describe the acceleration difference between positions on this orbit and the actual instantaneous vehicle positions. Let

$$\xi' = R - R_N \tag{8}$$

where R_N is the position of the vehicle in terms of the nominal trajectory. Then,

$$\ddot{\xi}' = -\mu\left[\frac{R}{R^3} - \frac{R_N}{R_N^3}\right] + \sum_{\substack{i=1 \\ i\neq 3}}^{5} P_i \tag{9}$$

Detailed descriptions of the Program's implementation of Encke's and Cowell's methods are provided in paragraphs 3.2 and 3.3, respectively. The special case where the thrust acceleration is too large to be treated as a perturbation is described in paragraph 3.4. The method and criteria for selecting the reference body and transfering from one reference body to another is discussed in paragraph 3.5.

3.2 ENCKE'S METHOD

3.2.1 EQUATIONS OF MOTION. As described in paragraph 3.1, the basic equations for Encke's method are as follows:
When P_3 can be considered as a perturbation,

$$R = R_{TB} + \xi \tag{1}$$

and

$$\ddot{\xi} = -\mu\left[\frac{R}{R^3} - \frac{R_{TB}}{R_{TB}^3}\right] + \sum_{i=1}^{5} P_i \tag{2}$$

When P_3 is too large to be treated as a perturbation,

$$R = R_N + \xi' \tag{3}$$

and

$$\ddot{\xi}' = -\mu\left[\frac{R}{R^3} - \frac{R_N}{R_N^3}\right] + \sum_{\substack{i=1 \\ i\neq 3}}^{5} P_i \tag{4}$$

The determination of position and velocity of the vehicle, R_{TB} and $\dot{R}_{TB}$, in a two-body orbit, is described in paragraph 3.2.2. The determination of the powered flight nominal trajectory vectors, R_N and $\dot{R}_N$, is discussed in paragraph 3.4.

Paragraph 3.2.3 discusses the integration scheme used by the Program to implement equations (1) and (2) or (3) and (4).

The use of a reference orbit in Encke's method assumes that the perturbations are kept small. Therefore, the size of the Encke term ξ (or ξ') must be monitored. When the magnitude of this term becomes too large, a new reference orbit is computed. The process of computing the new reference orbit is commonly referred to as "rectification". In the Program, the following rectification criteria are employed:

$$\frac{\xi}{R_{TB}} \leq \epsilon_1 \tag{5}$$

and

$$\frac{\dot{\xi}}{R_{TB}} \leq \epsilon_2 \tag{6}$$

NOTE: Equations (5) and (6) apply when P_3 is small. When P_3 is large, substitute ξ' for ξ and R_N for R_{TB} in the equations.

3.2.2 DETERMINATION OF TWO-BODY ORBIT VECTORS. The position and velocity, R_{TB} and $\dot{R}_{TB}$, respectively, of the vehicle in a Kepler orbit can be written in terms of the initial position and velocity, R_{TB_o} and $\dot{R}_{TB_o}$, respectively, as follows:

$$R_{TB} = f\, R_{TB_o} + g\, \dot{R}_{TB_o} \tag{1}$$

and

$$\dot{R}_{TB} = \dot{f}\, R_{TB_o} + \dot{g}\, \dot{R}_{TB_o} \tag{2}$$

where f and g are explicit functions of the differential eccentric anomaly of the Kepler orbit. Equations (1) and (2) are solved, using Herrick's method as summarized in the following analysis, to yield the R_{TB} and $\dot{R}_{TB}$ at any instant on the same two-body orbit as R_{TB_o} and $\dot{R}_{TB_o}$. Herrick's method first determines f, $\dot{f}$, g, and $\dot{g}$, and then computes R_{TB} and $\dot{R}_{TB}$ from equations (1) and (2). According to Herrick,

$$f = 1 - \frac{C}{R_{TB_o}} \tag{3}$$

$$f = \frac{M - U}{\sqrt{\mu}} \tag{4}$$

$$\dot{f} = \frac{-\sqrt{\mu} S}{A R_{TB_o}} \tag{5}$$

$$\dot{g} = 1 - \frac{C}{A} \tag{6}$$

where

$$M = \sqrt{\mu}\,(t - t_o) = R_{TB_o} X + d_o C + c_o U \tag{7}$$

$$C = X^2 \left[\frac{1}{2!} - \frac{X^2}{4!a} + \frac{X^4}{6!a^2} - \frac{X^6}{8!a^3} + \ldots \right] \tag{8}$$

$$U = X^3 \left[\frac{1}{3!} - \frac{X^2}{5!a} + \frac{X^4}{7!a^2} - \frac{X^6}{9!a^3} + \ldots \right] \tag{9}$$

$$S = X - \frac{U}{a} \tag{10}$$

$$A = R_{TB_o} + d_o S + c_o C \tag{11}$$

$$d_o = \frac{R_{TB_o} \cdot \dot{R}_{TB_o}}{\sqrt{\mu}} \tag{12}$$

$$c_o = \frac{R_{TB_o} \dot{S}_o^2}{\mu} - 1 \tag{13}$$

$$\frac{1}{a} = \frac{2}{R_{TB_o}} - \frac{\dot{S}_o^2}{\mu} = \text{reciprocal of semi major axis of Kepler orbit} \tag{14}$$

$$\dot{S}_o^2 = \dot{R}_{TB_o} \cdot \dot{R}_{TB_o} \tag{15}$$

X = Herrick's variable, a linear function of differential eccentric anomaly

t = time corresponding to R_{TB} and $\dot{R}_{TB}$

t_o = time corresponding to R_{TB_o} and $\dot{R}_{TB_o}$

μ = universal gravitation constant

Solution of equations (3) through (6) requires the determination of X. Initially, a first approximation of X is made. Then a Newton-Raphson iterative process is used on equations (7), (8), and (9) to yield a more accurate estimate of X.

Having obtained a satisfactory estimate of X, equations (3) through (6) are solved using equations (7) through (15). The computed values of f, $\dot{f}$, g, and $\dot{g}$ are then substituted into equations (1) and (2) to determine R_{TB} and $\dot{R}_{TB}$. The functions U and C (equations (8) and (9)) are infinite series expansions. Since the argument X^2/a could under given conditions become very large, a great many terms would have to be employed to limit the truncation error. However, the use of many terms results in an increased accumulation of machine roundoff error. A shifting epoch concept is used to cope with this problem. To calculate R_{TB} and $\dot{R}_{TB}$ at time t_j where $t_j - t_o$ is large, select an intermediate time t_i such that $t_j > t_i > t_o$. The epoch is shifted by employing

$$\left.\begin{aligned} R_{TB_i} &= f_i\, R_{TB_o} + g_i\, \dot{R}_{TB_o} \\ \dot{R}_{TB_i} &= \dot{f}_i\, R_{TB_o} + \dot{g}_i\, \dot{R}_{TB_o} \end{aligned}\right\} \qquad (16)$$

Then,

$$\left.\begin{aligned} R_{TB_j} &= f_{ij}\, R_{TB_i} + g_{ij}\, \dot{R}_{TB_i} \\ \dot{R}_{TB_j} &= \dot{f}_{ij}\, R_{TB_i} + \dot{g}_{ij}\, \dot{R}_{TB_i} \end{aligned}\right\} \qquad (17)$$

By careful selection of $t_j - t_i$, the argument X^2_{ij}/a may be kept small.

3.2.3 INTEGRATION TECHNIQUE

3.2.3.1 Introduction. Equation (4) of paragraph 3.2.1 is integrated numerically by the Program. The numerical integration process is divided into two stages: a starting procedure and a long-term procedure. (Most long-term numerical integration procedures require knowledge of previous data points. Thus, the starting procedure is needed to provide the initial data points for the long-term numerical procedure.)

The long-term numerical integration procedure presently in use in the ITEM and MINIVAR programs is an Adams sixth-order predictor method (without corrector) for second-order differential equations. It was desired, however, to test a broader class of procedures before deciding on one for use as the long-term numerical integration procedure to be used

in the Program. Accordingly, a program was written to test predictor, predictor-corrector, and iterated predictor-corrector, i.e., repeated application of correctors, techniques of various orders of approximation and with or without modifiers.

The following results were obtained:

a. Modifiers were found to leave the error unchanged. There is therefore no reason to use them.

b. As time interval increases, there is more tendency for the solution to become unstable. Error increases with a large power of the time interval.

c. As the degree of the approximating polynomial increases, a decrease in stability is noted. Error decreases about 3:1 for unit increase in degree of the approximating polynomial.

d. Predictor-only methods (degree and time interval held fixed) are about 30:1 less accurate than predictor-corrector methods, i.e., one application of the corrector removes 97% of the error in the predictor. A second iteration of the corrector does not reduce the error, but does improve stability at the expense of a 2:1 increase in running time. The increase in running time is intolerable; therefore, a predictor-corrector method will be used with no iteration of the corrector.

e. Either a fifth or sixth degree approximating polynomial yields a good compromise between accuracy and stability.

The final choice of a long-term integrating procedure involves considerations other than only accuracy and stability:

a. The ease of transforming the output of the starting procedure to the form of input starting data needed by the long-term procedure.

b. Whether the long-term procedure can easily accommodate a change in the time interval.

c. Whether the long term procedure can easily interpolate to find conditions at an intermediate time at which data are desired.

There are at least three forms in which the Adams long-term predictor-corrector formulas can be written. The only difference is in mathematical form; therefore, the accuracy and stability are the same for all three.

The first form is the conventional one in terms of the successive backward differences; this is the form in which the ITEM program was originally written. The second is in terms of the successive values of the function, as in the present ITEM program. The third is due to Nordsieck and uses the successive higher derivatives of the approximating polynomial. Each of the three forms has certain advantages and certain disadvantages which will be discussed now.

The backward difference form is fairly easy to start but interpolation is somewhat difficult, and it is virtually impossible to change intervals except by use of the

starting procedure. The successive value form of the method is trivial to start up, but interpolation involves the Lagrangian interpolation formulas, and changing intervals is, again, almost impossible. The inability to change intervals immediately after starting causes, as in the present ITEM program, a situation where the starting solution is called 28 times, but used only 7 times.

The Nordsieck method is fairly difficult to start, but very amenable to arbitrary changes of time intervals and to interpolation to intermediate points. Five points are all that are needed to start after a change in time interval (of about 4:1).

Due to its versatility, the Nordsieck method of degree 5 (called m = 6 by Nordseick) without iteration and without choice of interval is used in the Program. Paragraph 3.2.3.2 summarizes the Nordsieck method as applied in the Program. Paragraph 3.2.3.3 describes the starting procedure selected for the Program. Paragraph 3.2.3.4 describes the transformation of the starting values to the form required by the Nordsieck method.

3.2.3.2 **Nordsieck Method.** The Nordsieck method of long-term numerical integration (reference 1) is used to solve a system of equations of the form

$$\frac{dy_i}{dx} = f\ (x, y_1, y_2, \ldots) \qquad (1)$$

where

$$i = 1, 2, 3 \ldots$$

Equations (1) are often shortened to

$$\frac{dy}{dx} = f\ (x,\ y) \qquad (2)$$

When the solution to equation (2) is approximated by a polynomial of degree five, the predictor is given by

$$y(x_o + h) = y(x_o) + h\left[y'(x_o) + \frac{h}{2!}\, y''\ (x_o) + \frac{h^2}{3!}\, y'''\ (x_o)\right.$$

$$\left. + \frac{h^3}{4!}\, y''''\ (x_o) + \frac{h^4}{5!}\, y'''''(x_o) + \frac{h^5}{6!}\, y''''''\ (x_o)\right] \qquad (3)$$

where

h is the integration step size (interval)

x_o is the value of x at last integration

y( ) is the value of y at ( ) value of x

primes denote derivatives with respect to x

Let

$$f(x_o) = y'(x_o) \tag{4}$$

$$a(x_o) = \frac{h}{2!} y''(x_o) \tag{5}$$

$$b(x_o) = \frac{h^2}{3!} y'''(x_o) \tag{6}$$

$$c(x_o) = \frac{h^3}{4!} y''''(x_o) \tag{7}$$

$$d(x_o) = \frac{h^4}{5!} y'''''(x_o) \tag{8}$$

$$e(x_o) = \frac{h^5}{6!} y''''''(x_o) \tag{9}$$

Nordsieck's corrector is given by equation (10):

$$\text{Corrector} = K_1 h \left[f(x_o + h) - f^P \right] \tag{10}$$

where

K_1 is a constant (0.315591931)

$f(x_o + h)$ is the value of $f(x,y)$ computed at $x = x_o + h$, $y(x_o + h)$

f^P is a predicted value for $f(x,y)$ at $x = x_o + h$, and is given by

$$f^P = f(x_o) + 2a(x_o) + 3b(x_o) + 4c(x_o) + 5d(x_o) + 6e(x_o) \tag{11}$$

Hence, from equations (3) through (11), the value of y at $x = x_o + h$ is given by

$$y(x_o + h) = y(x_o) + h \left[f(x_o) + a(x_o) + b(x_o) + c(x_o) + d(x_o) + e(x_o) + K_1 \{ f(x_o + h) - f^P \} \right] \tag{12}$$

The values of the successive higher derivatives (a (x), b (x), c (x), d (x), e (x)) at $x = x_o + h$ are given in terms of their values at $x = x_o$ by

$$a(x_o + h) = a(x_o) + 3b(x_o) + 6c(x_o) + 10d(x_o) + 15e(x_o) + K_2\left[f(x_o + h) - f^P\right] \quad (13)$$

$$b(x_o + h) = b(x_o) + 4c(x_o) + 10d(x_o) + 20e(x_o) + K_3\left[f(x_o + h) - f^P\right] \quad (14)$$

$$c(x_o + h) = c(x_o) + 5d(x_o) + 15e(x_o) + K_4\left[f(x_o + h) - f^P\right] \quad (15)$$

$$d(x_o + h) = d(x_o) + 6e(x_o) + K_5\left[f(x_o + h) - f^P\right] \quad (16)$$

$$e(x_o + h) = e(x_o) + K_6\left[f(x_o + h) - f^P\right] \quad (17)$$

where

$$K_2 = 1.141666667$$

$$K_3 = 0.6250$$

$$K_4 = 0.177083333$$

$$K_5 = 0.0250$$

$$K_6 = 0.0013888889$$

Successive applications of equations (12) through (17) are used to provide a solution to equations (1).

The integration interval, h, is readily changed, the change being accomplished by using new values of a(x), b(x), c(x), d(x), and e(x). These new values are obtained from the following equations:

$$B = \frac{h_n}{h_o} \quad (18)$$

$$a_n(x) = Ba_o(x) \quad (19)$$

$$b_n(x) = B^2b_o(x) \quad (20)$$

$$c_n(x) = B^3c_o(x) \quad (21)$$

$$d_n(x) = B^4d_o(x) \quad (22)$$

$$e_n(x) = B^5c_o(x) \quad (23)$$

where the subscripts n and o stand for new and old, respectively.

Interpolation between computed solutions for y is also easily accomplished. Let

$$\alpha = (x_2 - x_1)h \tag{24}$$

where

x_2 = value of x at which the value of y is desired

x_1 = value of x at which y was computed

Then,

$$y(x_2) = y(x_1) + h\left[f(x_1) + \alpha a(x_1) + \alpha^2 b(x_1) + \alpha^3 c(x_1) + \alpha^4 d(x_1) + \alpha^5 e(x_1)\right] \tag{25}$$

In the Encke method, the Nordsieck method is used to integrate the differential equations of the Encke term. For this integration, y of equation (3) represents $\dot{\xi}$, $\dot{y}$ represents $\ddot{\xi}$, and x represents time, t.

3.2.3.3 Starting Method. The Nordsieck method (paragraph 3.2.3.2) is used to continue the solution of the Encke differential equations, once a starting procedure generates the numerical solution at enough points to evaluate the successive higher derivatives of the approximating polynomial at the start of the Nordsieck method.

Nordsieck's method may be used in a self-starting mode. When it is used that way, it assumes that there is no discontinuity in the solution for five time steps. Since the minimum variance technique introduces a rectification (discontinuity) at each data point, and many data points may occur in five time steps, the condition for continuity will not in general be satisfied.

Most of the starting procedures involve analytic differentiation of the Encke terms. This is not feasible.

There remains the Runge-Kutta procedure which is self-starting and has been used successfully previously. The Program uses the Gill modification of Runge-Kutta (reference 2), for the starting procedure, because it introduces some simplicity and error reduction. The differences between Gill and Runge-Kutta are minor, and do not require a new substantiation of its use as a starting procedure.

Each entry into the Runge-Kutta-Gill (RKG) method yields a pair of values for $y(t)$ and $\dot{y}(t)$. The RKG method develops the values of $y(t)$ and $\dot{y}(t)$ in a 4-step process by dividing the integration interval, h, by four. The following equations summarize the development of $y(t)$ for a given entry into the RKG method:

$$y(t)_j = y(t)_{j-1} + ha_j\ (\dot{y}(t)_{j-1} - b_j\ q_{j-1}) \tag{1}$$

and

$$q_j = q_{j-1} + 3\ \{a_j\ [\dot{y}(t)_{j-1} - b_j\ q_{j-1}]\} - c_j\ \dot{y}(t)_{j-1} \tag{2}$$

where

j = the RKG step number (varies from 1 through 4)

a_j, b_j, and c_j are constants

The values of $\dot{y}(t)_{j-1}$ are determined external to the RKG method; they are computed by summing the perturbation accelerations at the corresponding time.

The Runge-Kutta-Gill (RKG) procedure is entered five times. The values of a(t), b(t), c(t), d(t), and e(t) are computed by fitting a polynomial to the six sequential points corresponding to the RKG data plus the initial estimate used in the RKG method. The equations for this fitting are given in paragraph 3.2.3.4.

3.2.3.4 Transformation of RKG Data Into Form Suitable for Nordsieck Method. The starting procedure yields the solutions of the differential equations and their rates of change at six successive times. It is necessary to transform these data into the form required by the Nordsieck long-term numerical integration procedure.

For each first-order differential equation, the Nordsieck method requires the following five higher derivatives evaluated at $t = t_o$:

$$\left.\begin{aligned} a(t_o) &= \frac{h\,\ddot{y}(t_o)}{2!} \\ b(t_o) &= \frac{h^2\,\dddot{y}(t_o)}{3!} \\ c(t_o) &= \frac{h^3\,\ddddot{y}(t_o)}{4!} \\ d(t_o) &= \frac{h^4\,\dddddot{y}(t_o)}{5!} \\ e(t_o) &= \frac{h^5\,\ddddddot{y}(t_o)}{6!} \end{aligned}\right\} \qquad (1)$$

The RKG starting method provides data for $y(t)$ and $\dot{y}(t)$ at the six time intervals up to and including t_o, i.e., RKG provides:

$y(t_o)$	$\dot{y}(t_o)$
$y(t_o - h)$	$\dot{y}(t_o - h)$
$y(t_o - 2h)$	$\dot{y}(t_o - 2h)$
$y(t_o - 3h)$	$\dot{y}(t_o - 3h)$

$$y(t_o - 4h) \qquad \dot{y}(t_o - 4h)$$

$$y(t_o - 5h) \qquad \dot{y}(t_o - 5h)$$

The required values for $a(t_o)$, $b(t_o)$, $c(t_o)$, $d(t_o)$, and $e(t_o)$ will be found by using Lagrange's Interpolation Formula to fit a power series of degree five to the $\dot{y}(t)$ data provided by the RKG method. The power series will then be successively differentiated to obtain the required data. Let

$$x = \frac{t - t_o}{h} \tag{2}$$

and let primes denote derivatives with respect to x. Therefore,

$$\left.\begin{aligned} y'(t) &= h\,\dot{y}\,(t) \\ y''(t) &= h^2\,\ddot{y}\,(t) \\ y'''(t) &= h^3\,\dddot{y}\,(t) \\ y''''(t) &= h^4\,\ddddot{y}\,(t) \\ y'''''(t) &= h^5\,\dddddot{y}\,(t) \\ y''''''(t) &= h^6\,\ddddddot{y}\,(t) \end{aligned}\right\} \tag{3}$$

From Lagrange's Interpolation Formula,

$$y(x) = \sum_{i=0}^{5} F_i(x) y_i \tag{4}$$

where $y(x)$ is the desired power series

$$F_o(x) = \frac{(x+1)(x+2)(x+3)(x+4)(x+5)}{120} \tag{5}$$

$$F_1(x) = \frac{-x(x+2)(x+3)(x+4)(x+5)}{24} \tag{6}$$

$$F_2(x) = \frac{x(x+1)(x+3)(x+4)(x+5)}{12} \tag{7}$$

$$F_3(x) = \frac{-x(x+1)(x+2)(x+4)(x+5)}{12} \tag{8}$$

$$F_4(x) = \frac{x(x+1)(x+2)(x+3)(x+5)}{24} \tag{9}$$

$$F_5(x) = \frac{-x(x+1)(x+2)(x+3)(x+4)}{120} \tag{10}$$

y_i are the values determined by the RKG method. Multiplying out the factors in equations (5) through (10) yields

$$F_0(x) = \frac{x^5 + 15\,x^4 + 85\,x^3 + 225\,x^2 + 274\,x + 120}{120} \tag{11}$$

$$F_1(x) = \frac{-(x^5 + 14\,x^4 + 71\,x^3 + 154\,x^2 + 120x)}{24} \tag{12}$$

$$F_2(x) = \frac{x^5 + 13\,x^4 + 59\,x^3 + 107\,x^2 + 60x}{12} \tag{13}$$

$$F_3(x) = \frac{-(x^5 + 12\,x^4 + 49\,x^3 + 78\,x^2 + 40x)}{12} \tag{14}$$

$$F_4(x) = \frac{x^5 + 11\,x^4 + 41\,x^3 + 6\,x^2 + 30x}{24} \tag{15}$$

$$F_5(x) = \frac{-(x^5 + 10\,x^4 + 35\,x^3 + 50\,x^2 + 24x)}{120} \tag{16}$$

From equations (1) and (3),

$$\left.\begin{aligned} a(t_o) &= \frac{y'(0)}{2!} \\ b(t_o) &= \frac{y''(0)}{3!} \\ c(t_o) &= \frac{y'''(0)}{4!} \\ d(t_o) &= \frac{y''''(0)}{5!} \\ e(t_o) &= \frac{y'''''(0)}{6!} \end{aligned}\right\} \tag{17}$$

Successively differentiating equation (4) with respect to x, (using equations (12) through (16)), setting $x = 0$, and substituting into equations (17) yields the following in matrix notation;

$$\begin{bmatrix} 2a(t_o) \\ 3b(t_o) \\ 4c(t_o) \\ 5d(t_o) \\ 6e(t_o) \\ \end{bmatrix} = \frac{1}{120} \cdot \begin{bmatrix} -24 & 150 & -400 & 600 & -600 & 274 \\ -50 & 305 & -780 & 1070 & -770 & 225 \\ -35 & 205 & -490 & 590 & -355 & 85 \\ -10 & 55 & -120 & 130 & -70 & 15 \\ -1 & 5 & -10 & 10 & -5 & 1 \\ \end{bmatrix} \cdot \begin{bmatrix} \dot{y}(t_o - 5h) \\ \dot{y}(t_o - 4h) \\ \dot{y}(t_o - 3h) \\ \dot{y}(t_o - 2h) \\ \dot{y}(t_o - h) \\ \dot{y}(t_o) \end{bmatrix} \tag{18}$$

or

$$\begin{bmatrix} a(t_o) \\ b(t_o) \\ c(t_o) \\ d(t_o) \\ e(t_o) \\ \end{bmatrix} = \frac{1}{1440} \cdot \begin{bmatrix} -144 & 900 & -2400 & 3600 & -3600 & 1644 \\ -200 & 1220 & -3120 & 4280 & -3080 & 900 \\ -105 & 615 & -1470 & 1770 & -1065 & 255 \\ -24 & 132 & -288 & 312 & -168 & 36 \\ -2 & 10 & -20 & 20 & -10 & 2 \\ \end{bmatrix} \cdot \begin{bmatrix} \dot{y}(t_o - 5h) \\ \dot{y}(t_o - 4h) \\ \dot{y}(t_o - 3h) \\ \dot{y}(t_o - 2h) \\ \dot{y}(t_o - h) \\ \dot{y}(t_o) \end{bmatrix} \tag{19}$$

3.3 COWELL'S METHOD

As described in paragraph 3.1, the general equations of motion of a space vehicle are

$$\ddot{\mathbf{R}} = -\frac{\mu \mathbf{R}}{R^3} + \sum_{i=1}^{5} \mathbf{P}_i .$$

In Cowell's method, these equations are integrated, using numerical techniques, to obtain the instantaneous position and velocity of the vehicle. The Program performs the integration using the same techniques as it does for the Encke method. The RKG starting procedure (paragraph 3.2.3.3) provides the initial data, and the Nordseick method (paragraph 3.2.3.2) is used as the long-term integration procedure. To make the accuracy of the results of the two methods compatible, the Cowell's method of integration is performed completely in double precision.

3.4 POWERED FLIGHT

3.4.1 INTRODUCTION. For powered flight, the dynamic model of the vehicle's trajectory includes the thrust acceleration components as well as the accelerations arising from gravitation, drag, and radiation pressure. In the following development, the thrust acceleration components are assumed available in the form of a polynomial expansion with time as the variable. It is further assumed that: (a) no guidance loop is included in the analysis, so that thrust is independent of the vehicle state; (b) the vehicle has sufficient altitude so that drag forces may be treated as small perturbations.

During powered flight, the equations of motion are

$$\ddot{\mathbf{R}} = \frac{-\mu \mathbf{R}}{R^3} + \mathbf{P}_1 + \mathbf{P}_2 + \mathbf{P}_3 + \mathbf{P}_4 + \mathbf{P}_5 \tag{1}$$

in which

$\mathbf{R}$ = position of vehicle with respect to the central body

$\mathbf{P}_1$ = planetary perturbation accelerations

$\mathbf{P}_2$ = oblateness accelerations

$\mathbf{P}_3$ = thrust acceleration

$\mathbf{P}_4$ = atmospheric drag acceleration

$\mathbf{P}_5$ = radiation pressure acceleration.

In most computations involving powered flight, $\mathbf{P}_1$ and $\mathbf{P}_5$ may be neglected. The equations then become

$$\ddot{\mathbf{R}} = \frac{-\mu \mathbf{R}}{R^3} + \mathbf{P}_3 + (\mathbf{P}_2 + \mathbf{P}_4) \tag{2}$$

The computational advantages of Encke's method (paragraph 3.2) may be extended to trajectories involving large thrust forces if a suitable nominal trajectory can be found. For the problem analyzed here, the nominal orbit is computed from

$$\ddot{\mathbf{R}} = \frac{-\mu \mathbf{R}}{R^3} + \mathbf{P}_3 \tag{3}$$

where $\mathbf{P}_3$ is expressed as a polynomial expansion in time, i.e.,

$$\mathbf{P}_3 = \sum_{i=0}^{k} \sigma_i \tau^i \tag{4}$$

where

$$\sigma_i = \alpha_i \bar{x} + \beta_i \bar{y} + \gamma_i \bar{z} \qquad (5)$$

and $\bar{x}$, $\bar{y}$, $\bar{z}$ are the unit vectors of the coordinate system in which the thrust acceleration is computed.

Paragraph 3.4.2 develops a power series for the nominal trajectory described by equation (3). The nominal trajectory is computed in double precision whereas the integrations of the Encke accelerations, $\ddot{\xi}'$, are carried out in single precision. The summation of the nominal trajectory components and the Encke components are performed in double precision. To obtain double-precision expansions of R_N and $\dot{R}_N$ which hold over the same time interval for which the thrust acceleration polynomial is valid would, in general, require a large number of terms in the R_N and $\dot{R}_N$ power series. In order to overcome this difficulty and to maintain high precision in the computations, the power series for R_N and $\dot{R}_N$ are transformed to shifted Chebyshev polynomial expansions. The latter expansions are more accurate for a given number of terms. (Refer to Appendix B of this manual.) Paragraph 3.4.3 develops this transformation.

Paragraph 3.4.4 develops a power series formulation for the thrust acceleration (equation (4)).

The analysis of paragraph 3.4.2 applies to the "forward integration," i.e., forward in time, of the equations of motion of a vehicle in powered flight. It may be necessary for the Program to integrate backwards in time, over an interval during which the vehicle was in powered flight. Paragraph 3.4.5 describes the computations for the case of backwards integration.

3.4.2 TRAJECTORY DETERMINATION. Solutions to equation (3) of paragraph 3.4.1 may be given in terms of a power series; thus, the state vector of the nominal trajectory may be written as

$$R_N = \sum_i S_i \tau^i \qquad (1)$$

and

$$\dot{R}_N = \sum_i i S_i \tau^{(i-1)} \qquad (2)$$

Recursion relations will be developed giving S_i in terms of σ_i (equations (4) and (5) of paragraph 3.4.1) and the vehicle's initial conditions, R_o and $\dot{R}_o$. Having the nominal trajectory given by equations (1) and (2), the Encke equations of motion are obtained by subtracting equation (3) of paragraph 3.4.1 from equation (2) of paragraph 3.4.1:

$$\ddot{\xi}' = \ddot{R} - \ddot{R}_N = -\mu \left[\frac{R}{R^3} - \frac{R_N}{R_N^3} \right] + (P_2 + P_4). \qquad (3)$$

Solution of equation (3) with the initial conditions $\xi' = 0$, $\dot{\xi}' = 0$ leads to the calculation of vehicle position and velocity:

$$\left.\begin{aligned} \mathbf{R} &= \mathbf{R}_N + \xi' \\ \dot{\mathbf{R}} &= \dot{\mathbf{R}}_N + \dot{\xi}' \end{aligned}\right\} \tag{4}$$

Simple recursion formulas may be developed for the S_i coefficients by considering the expansion of equation (1):

$$\left.\begin{aligned} x_N &= \sum_{i=0}^{\infty} a_i \tau^i \\ y_N &= \sum_{i=0}^{\infty} b_i \tau^i \\ z_N &= \sum_{i=0}^{\infty} c_i \tau^i \end{aligned}\right\} \tag{5}$$

where x_N, y_N, and z_N are the magnitudes of the $\bar{x}$, $\bar{y}$, $\bar{z}$ components of $\mathbf{R}_N$ and

$$S_i = a_i \bar{x} + b_i \bar{y} + c_i \bar{z} \tag{6}$$

Let

$$\sum_{i=0}^{\infty} D_i \tau^i = R_N^2 = x_N^2 + y_N^2 + z_N^2, \tag{7}$$

and

$$\sum_{i=0}^{\infty} d_i \tau^i = R_N^{-3} = (x_N^2 + y_N^2 + z_N^2)^{-3/2} \tag{8}$$

The coefficients of equation (7) are obtained by definition from equation (5):

$$D_i = \sum_{j=0}^{i} (a_j a_{i-j} + b_j b_{i-j} + c_j c_{i-j}) \tag{9}$$

To evaluate the coefficients of equation (8), let

$$z = (R_N^2)^p. \tag{10}$$

Taking the natural logarithm of both sides,

$$p\ln(R_N^2) = \ln(z) \tag{11}$$

Differentiating with respect to τ,

$$p\frac{(\dot{R_N^2})}{R_N^2} = \frac{\dot{z}}{z}$$

$$p(\dot{R_N^2})z = \dot{z}\,R_N^2 \tag{12}$$

Setting $p = -3/2$, performing the indicated differentiation, and equating coefficients in equation (12) yields

$$d_i = \frac{-1}{iD_o}\sum_{j=1}^{i} D_j d_{i-j}\left[\frac{j}{2} + i\right] \tag{13}$$

$$d_o = (D_o)^{-3/2} \tag{14}$$

Differentiating equations (5) twice:

$$\left.\begin{aligned}
\ddot{x}_N &= \sum_{i=0}^{\infty} i(i-1)\,a_i\,\tau^{(i-2)} \\
\ddot{y}_N &= \sum_{i=0}^{\infty} i(i-1)\,b_i\,\tau^{(i-2)} \\
\ddot{z}_N &= \sum_{i=0}^{\infty} i(i-1)\,c_i\,\tau^{(i-2)}
\end{aligned}\right\} \tag{15}$$

Let the thrust acceleration polynomial of equation (4) of paragraph 3.4.1 be developed in components so that

$$\left.\begin{aligned}(P_3)_x &= \sum_{i=0}^{k} \alpha_i \tau^i \\ (P_3)_y &= \sum_{i=0}^{k} \beta_i \tau^i \\ (P_3)_z &= \sum_{i=0}^{k} \gamma_i \tau^i\end{aligned}\right\} \qquad (16)$$

where α_i, β_i, γ_i are the coefficients defined in equation (5) of paragraph 3.4.1.

Substituting equations (5), (8), (15), and (16) into equation (3) of paragraph 3.4.1, and equating coefficients of like powers, the recursion formulae for the S_i coefficients are obtained:

$$\left.\begin{aligned}a_0 &= x_o \qquad b_0 = y_o \qquad c_0 = z_o \\ a_1 &= \dot{x}_o \qquad b_1 = \dot{y}_o \qquad c_1 = \dot{z}_o\end{aligned}\right\} \qquad (17)$$

$$\left.\begin{aligned}a_{i+2} &= \frac{1}{(i+1)(i+2)}\left[\alpha_i - \mu \sum_{j=0}^{i} a_j d_{i-j}\right] \\ b_{i+2} &= \frac{1}{(i+1)(i+2)}\left[\beta_i - \mu \sum_{j=0}^{i} b_j d_{i-j}\right] \\ c_{i+2} &= \frac{1}{(i+1)(i+2)}\left[\gamma_i - \mu \sum_{j=0}^{i} c_j d_{i-j}\right]\end{aligned}\right\} \qquad (18)$$

$$i = 0, 1, 2, \ldots$$

NOTE: In equations (17) the subscript "0" indicates initial conditions.

With these coefficients, positions on the reference orbit are obtained from equations (5); velocity components on the orbit are given by the first derivatives of x_N, y_N, and z_N:

$$\left.\begin{aligned} \dot{x}_N &= \sum_{i=0}^{\infty} i a_i \tau^{(i-1)} \\ \dot{y}_N &= \sum_{i=0}^{\infty} i b_i \tau^{(i-1)} \\ \dot{z}_N &= \sum_{i=0}^{\infty} i c_i \tau^{(i-1)} \end{aligned}\right\} \qquad (19)$$

3.4.3 EXPANSION OF R_N AND $\dot{R}_N$ IN SHIFTED CHEBYSHEV POLYNOMIALS. Let the thrust acceleration polynomials of equation (4) of paragraph 3.4.1 be valid in the range $0 \leq \tau \leq \tau_{MAX}$. Over this span, the normalized time variable is

$$t = \frac{\tau}{\tau_{MAX}}. \qquad (1)$$

For shifted Chebyshev polynomials, the normalized time variable is

$$t' = \frac{1 + t}{2} \qquad (2)$$

and the thrust acceleration as a function of t' is given by

$$f(t') = \frac{K_o}{2} + K_1 T_1^*(t') + K_2 T_2^*(t') + \ldots + K_r T_r^*(t') + \ldots. \qquad (3)$$

Calculation of the K_r given the power series coefficients of $f(t')$ has been described in Appendix B. The pertinent equations, however, are summarized here in a consistent notation. Rearranging equations (5) of paragraph 3.4.2 in terms of the normalized variable t:

$$\left.\begin{aligned} x_N &= \sum_{i=0}^{\infty} a_i (\tau_{MAX})^i \left[\frac{\tau}{\tau_{MAX}}\right]^i = \sum_{i=0}^{\infty} a'_i (t)^i \\ y_N &= \sum_{i=0}^{\infty} b'_i (t)^i \\ z_N &= \sum_{i=0}^{\infty} c'_i (t)^i \end{aligned}\right\} \qquad (4)$$

so that

$$\left.\begin{aligned} a_i' &= a_i(\tau_{MAX})^i \\ b_i' &= b_i(\tau_{MAX})^i \\ c_i' &= c_i(\tau_{MAX})^i \end{aligned}\right\} \tag{5}$$

Similarly for the velocity component expansions of equations (19) of paragraph 3.4.2:

$$\left.\begin{aligned} \dot{x}_N &= \sum_{i=0}^{\infty} i a_i'(t)^{(i-1)} \\ \dot{y}_N &= \sum_{i=0}^{\infty} i b_i'(t)^{(i-1)} \\ \dot{z}_N &= \sum_{i=0}^{\infty} i c_i'(t)^{(i-1)} \end{aligned}\right\} \tag{6}$$

Let P_i stand for any of the coefficients a_i', b_i', c_i'; then,

$$K_o = 2P_o + 2 \sum_{q=1}^{\infty} C_o(2q) P_{2q} \tag{7}$$

$$C_o(2q) = \frac{(2q-1)(2q-3)(2q-5)\ldots 3 \cdot 1}{(2q)(2q-2)(2q-4)\ldots 4 \cdot 2} \tag{8}$$

The remaining coefficients are obtained from

$$K_r = 2 \sum_{q=1}^{\infty} C_r C_o(2q) P_{2q}, \text{ if } r \text{ is even} \tag{9}$$

$$K_r = 2 \sum_{q=1}^{\infty} C_r' C_o(2q) P_{2q-1}, \text{ if } r \text{ is odd} \tag{10}$$

where

$$C_r = \frac{(2q)(2q-2)(2q-4)\ldots(2q-r+2)}{(2q+2)(2q+4)(2q+6)\ldots(2q+r)}, \quad r \text{ even} \tag{11}$$

$$C_r' = \frac{(2q-2)(2q-4)(2q-6)\ldots(2q-r+1)}{(2q+2)(2q+4)(2q+6)\ldots(2q+r-1)}, \quad r \text{ odd.} \tag{12}$$

3.4.4 THRUST ACCELERATION POWER SERIES FORMULATION. At altitudes well above the dense portion of the atmosphere, rocket thrust may be expressed in terms of parameters which are independent of altitude. In general, the thrust force is some function of time:

$$F_3 = G(t) \tag{1}$$

Mass rate is generally constant, so that the instantaneous mass may be described by

$$m = m_o + \dot{m}_o t. \tag{2}$$

With these assumptions, the thrust acceleration is given by

$$P_3 = \frac{G(t)}{m_o\left[1 + \frac{\dot{m}_o}{m_o} t\right]} \tag{3}$$

In the development presented in paragraph 3.4.2, it was assumed that P_3 was representable as a polynomial expansion in time. Let $(P_3)_\xi$ and $G_\xi(t)$ be the magnitudes of the ξ-components of acceleration and force, respectively. If $(P_3)_\xi$ can be given as a power series in time, then

$$(P_3)_\xi = \frac{G_\xi'(t)}{(1+kt)} = \delta_0 + \delta_1 t + \delta_2 t^2 + \ldots + \delta_n t^n + \ldots, \tag{4}$$

where

$$G_\xi'(t) = \frac{G_\xi(t)}{m_o} \tag{5}$$

$$k = \frac{\dot{m}_o}{m_o} \tag{6}$$

and

$$\delta_p = \frac{1}{P!} \frac{d^{(P)}(P_3)_\xi}{dt^{(P)}}\Bigg]_{t=0} \tag{7}$$

To obtain the general formulation of equation (7), write the ratio of equation (4):

$$(P_3)_\xi = \frac{G'_\xi(t)}{D(t)} \tag{8}$$

Taking natural logarithms

$$\ln (P_3)_\xi = \ln G_\xi'(t) - \ln D(t) \tag{9}$$

Differentiating equation (9)

$$\frac{\dot{(P_3)}_\xi}{(P_3)_\xi} = \frac{\dot{G}_\xi'}{G_\xi'} - \frac{\dot{D}}{D} \tag{10}$$

Multiplying through by G_ξ',

$$D\dot{(P_3)}_\xi = \dot{G}_\xi' - \dot{D}(P_3)_\xi \tag{11}$$

Since $D(t) = 1 + kt$, $\dot{D} = k$ and all higher derivatives of $D(t)$ are zero. Consequently, equation (11) becomes

$$D\dot{(P_3)}_\xi = \dot{G}_\xi' - k(P_3)_\xi \tag{12}$$

The P^{th} derivative of equation (12) is readily seen to be

$$D(P_3)_\xi^{(P)} = G_\xi'^{(P)} - pk(P_3)_\xi^{(P-1)} \tag{13}$$

Evaluating equation (13) at $t = 0$,

$$(P_3)_\xi^{(P)} = [G_\xi'^{(P)}]_o - Pk[(P_3)_\xi^{(P-1)}]_o \tag{14}$$

Hence, the P^{th} coefficient as given by equation (7) is

$$\delta_P = \frac{[G_\xi'^{(P)}]_o - Pk[(P_3)_\xi^{(P-1)}]_o}{P!} \tag{15}$$

3.4.5 BACKWARD INTEGRATION DURING POWERED FLIGHT. To compute powered flight nominal trajectory in the forward direction, the following quantities are required:

a. R_o - initial position vector

b. $\dot{R}_o$ - initial velocity vector

c. σ_i - coefficients of thrust acceleration polynomial

d. t_b - start of burn

e. t_f - end of burn

In the backward integration mode, the following quantities are available:

a. R_T - terminal position vector

b. $\dot{R}_T$ - terminal velocity vector

c. $\tilde{\sigma}_i$ - best estimate of thrust acceleration coefficients

d. $\tilde{t}_b$ - best estimate of start of burn

e. $\tilde{t}_f$ - best estimate of end of burn

The equations of motion to be solved are the same in either mode:

$$\ddot{R} = -\mu \frac{R}{R^3} + T \tag{1}$$

In the backward mode, however, the series solutions to equations (1) become

$$R_N = \sum_{i=o}^{\infty} S_i' \, (\tau - \tau_{MAX})^i \tag{2}$$

$$\dot{R}_N = \sum_{i=o}^{\infty} i \, S_i' \, (\tau - \tau_{MAX})^i . \tag{3}$$

Thrust acceleration is given by

$$T = \sum_{i=o}^{N} \tilde{\sigma}_i \, \tau^i \tag{4}$$

Expanding the function about τ_{MAX}.

$$T = \sum_{i=o}^{N} \sigma_i' \, (\tau - \tau_{MAX})^i \tag{5}$$

The σ_i' may be derived from the $\tilde{\sigma}_i$ by means of the relation

$$\sigma_k' = \sum_{i=o}^{N} {}_iC_k \, \tilde{\sigma}_i \, \tau_{MAX}^{(i-k)} \tag{6}$$

where

$${}_iC_k = \frac{i!}{k!\,(i-k)!} \tag{7}$$

The coefficients S_i' may be computed from the coefficients of equation (6) and the terminal conditions, R_T and $\dot{R}_T$. These S_i' are then converted to Chebyshev polynomial coefficients. To make this conversion, the time parameters must be defined.

$$\begin{aligned} 0 &\leq \tau \leq \tau_{MAX} \\ \tau_{MAX} &= \tilde{t}_f - \tilde{t}_b \\ t &= \tau - \tau_{MAX} \\ -\tau_{MAX} &\leq t \leq 0 \end{aligned} \tag{8}$$

In terms of the variable t, equations (2) and (3) become

$$R_N = \sum_{i=o}^{\infty} S_i' \, (t)^i \tag{9}$$

$$\dot{R}_N = \sum_{i=o}^{\infty} i \, S_i' \, (t)^{(i-1)} \tag{10}$$

For conversion to Chebyshev coefficients, the S_i' are normalized by

$$S_i'' = S_i' \, (\tau_{MAX})^i \tag{11}$$

The time variable corresponding to this nomalization lies in the range

$$-1 \leq t' \leq 0 \tag{12}$$

whereas the Chebyshev time variable has the range

$$0 \leq t'' \leq \frac{1}{2} \tag{13}$$

3.5 REFERENCE BODY TRANSFER

3.5.1 INTRODUCTION. When several central bodies are to be used in trajectory computation, criteria are necessary for determining when one central body is to be taken as the coordinate origin in preference to another. The most common criteria are based on "regions of influence" surrounding the planets in a heliocentric system, or surrounding a satellite in a planetocentric system. The following paragraphs derive a general expression for computing regions of influence, and evaluate the expression for both the solar system and the earth-moon system.

The only transformation involved in changing reference bodies is a translation of the reference frame from one origin to another. The directions of the coordinate axes are defined by the base date system: the x- and y-axes lie in the mean equator of base date, with the positive x-direction specified by the equinox of base date.

To refer velocities from one reference system to another, the relative velocities between the new and the old reference bodies must be known. Components of this velocity are obtained by the evaluation of polynomials which have been fitted to ephemeris data.

3.5.2 THE REGION OF INFLUENCE. Reference 3 defines an "activity sphere" as follows:

> "Activity sphere: the region within which the planet (or moon) rather than the sun (or planet) should be regarded as the center body for the orbit of a body moving at hyperbolic speed[1] in the planet's gravitational field. Within the limits of this sphere,...the ratio of center force to perturbative force is greater in the planetocentric coordinate system than in the heliocentric coordinate system."

The region of influence based on this definition is not truly spherical; however, in most cases it is unnecessary to compensate for the small flattening and bulging of the actual region. Therefore, a spherical shape may be assumed, except in earth-moon space. A general expression is now derived for the earth-moon system following the development of reference 4. Simplifying approximations are then applied to make this expression suitable for heliocentric space.

From the geometry shown in figure 3.5-1, the gravitational acceleration, per unit mass, of the vehicle is seen to be

$$a_E = -\frac{\mu_E R_E}{R_E^3} \qquad (1)$$

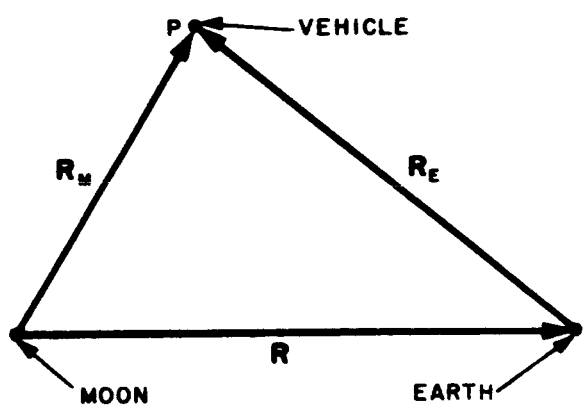

Figure 3.5-1. Vehicle In Earth-Moon Space

[1] At a speed equal to or greater than the escape velocity.

from the Earth, and

$$a_M = -\frac{\mu_M R_M}{R_M^3} \tag{2}$$

from the moon. The gravitational acceleration of the moon because of the Earth is

$$a_{ME} = -\frac{\mu_E R}{R^3}, \tag{3}$$

whereas the acceleration of the earth because of the moon is

$$a_{EM} = -\frac{\mu_M R}{R^3}. \tag{4}$$

Only the magnitudes of the above accelerations are employed in computing the sphere of influence. The use of magnitudes rather than total vectors essentially restricts the vehicle position to the earth-moon line. This restriction is not serious since the angle subtended at the Earth by the sphere of influence is in the order of 10 degrees. Using the aforementioned definition for the activity sphere, the defining equation for this region becomes

$$\frac{a_E - a_{ME}}{a_M} = \frac{a_M - a_{EM}}{a_E} \tag{5}$$

$$\frac{\mu_E^2}{R_E^2}\left(\frac{1}{R_E^2} - \frac{1}{R^2}\right) = \frac{\mu_M^2}{R_M^2}\left(\frac{1}{R_M^2} - \frac{1}{R^2}\right). \tag{6}$$

Rearranging equation (6)

$$R_M^4 = \left[\frac{\mu_M}{\mu_E}\right]^2 \left[R_E^4 \frac{(R + R_M)(R - R_M)}{(R + R_E)(R - R_E)}\right]. \tag{7}$$

Along the earth-moon line,

$$R_M = R - R_E \tag{8}$$

so that R_M is positive when the vehicle is in front of the moon and negative when it is behind. Substituting equation (8) into equation (7):

$$R_M^5 = \left[\frac{\mu_M}{\mu_E}\right]^2 \left[(R - R_M)^5\right] \left[\frac{R + R_M}{2R - R_M}\right] \tag{9}$$

Let

$$r = R_M/R \tag{10}$$

$$K = \mu_M/\mu_E \tag{11}$$

Then

$$r = K^{2/5} (1 - r) \left[\frac{1 + r}{2 - r}\right]^{1/5} \tag{12}$$

Equation (12) is also applicable to a heliocentric system; in that instance,

$$r = \frac{R_P}{R_{SP}} << 1$$

where

R_P = distance from the vehicle to the planet

R_{SP} = distance from the planet to the Sun

and

$$R_{ACT} \approx R_{SP} \left(\frac{K^2}{2}\right)^{1/5} \tag{13}$$

where

R_{ACT} is radius of activity sphere

K is in this case μ_P/μ_S

Mean values for R_{SP} may be used for all the planets of the solar system.

For the earth-moon system, equation (12) may be solved for the radius of the activity sphere. In this case, however, consideration must be given to the fact that, because of the proximity of the Earth, the lunar region of influence is not quite spherical. On the side of the moon closest to the Earth, the radius of the region of influence is

$$r_m = K^{2/5} (1 - r_m) \left[\frac{(1 + r_m)}{(2 - r_m)} \right]^{1/5} \tag{14}$$

where

r_m = minimum value of r, i.e., when $R_M = R - R_E$ is positive

The maximum radius is obtained when

$$R_M = R_E - R \tag{15}$$

is positive. Under this condition, equation (12) becomes

$$r_M = K^{2/5} (1 + r_M) \left[\frac{(1 - r_M)}{(2 + r_M)} \right]^{1/5} \tag{16}$$

Expanding the fifth roots by the binomial theorem, and retaining terms up to second order:

$$\left[\frac{1 + r_m}{2 - r_m} \right]^{1/5} = \frac{1}{2^{1/5}} (0.1 r_m^2 + 0.3 r_m + 1) \tag{17}$$

$$\left[\frac{1 - r_M}{2 + r_M} \right]^{1/5} = \frac{1}{2^{1/5}} (0.1 r_M^2 - 0.3 r_M + 1) \tag{18}$$

Substituting equations (17) and (18) into equations (14) and (16), respectively, and retaining terms up to the second order:

$$0.2\theta r_m^2 + (1 + 0.7\theta) r_m - \theta = 0 \tag{19}$$

$$0.2\theta r_M^2 + (1 - 0.7\theta) r_M - \theta = 0 \tag{20}$$

where

$$\theta = \left(\frac{K^2}{2} \right)^{1/5} \tag{21}$$

Then

$$r_m = \frac{\sqrt{1.29\theta^2 + 1.4\theta + 1} - (1 + 0.7\theta)}{0.4\theta} \tag{22}$$

$$r_M = \frac{\sqrt{1.29\theta^2 - 1.4\theta + 1} - (1 - 0.7\theta)}{0.4\theta} \tag{23}$$

The moon's region of influence may conveniently be described by an ellipsoid having one focus at the moon. Computing the ellipsoid's major axis:

$$2a = (r_m + r_M)R \tag{24}$$

The ellipsoid's eccentricity is obtained from

$$Rr_m = a(1 - e)$$

or

$$e = \frac{r_M - r_m}{r_M + r_m} \tag{25}$$

The ellipsoid's minor axis is given by

$$2b = 2a\sqrt{1 - e^2} \tag{26}$$

For the $\bar{x}$, $\bar{y}$, $\bar{z}$ coordinate system of figure 3.5-2, the center of the ellipsoid is (x_o, 0, 0), where

$$x_o = a - r_m R$$

$$x_o = \frac{1}{2}(r_M - r_m)R \tag{27}$$

The quantity R, the earth-moon distance, is actually a function of time, so that the figure of the ellipsoid changes with time. It is customary to assign this quantity a value corresponding to the mean lunar orbital radius.

Reference body transfer criteria in earth-moon space is determined by vehicle position with respect to the activity ellipsoid, the equation for which is

$$\frac{(x_e - x_o)^2}{a^2} + \frac{y_e^2}{b^2} + \frac{z_e^2}{b^2} = 1 \tag{28}$$

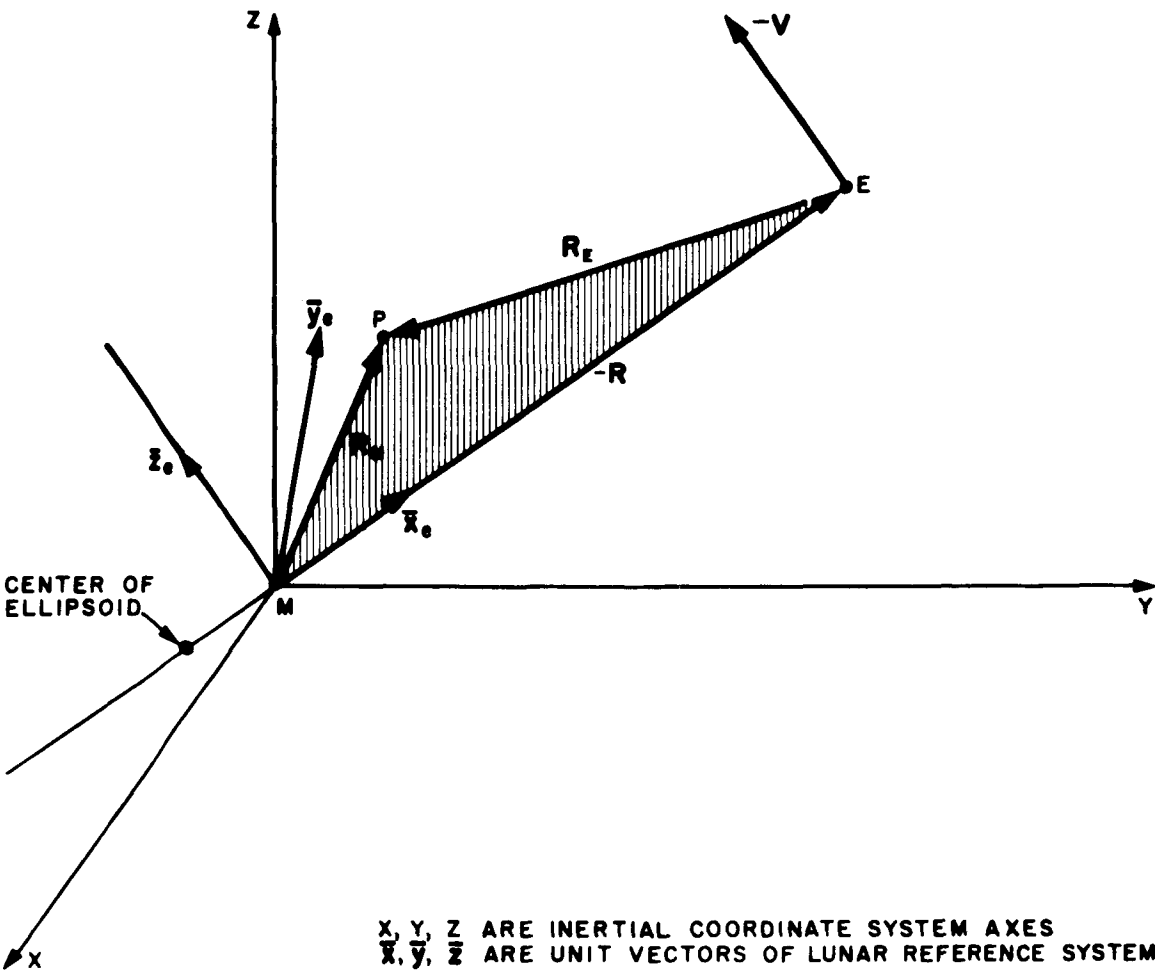

Figure 3.5-2. Inertial and Lunar Reference Frames

The vector $\mathbf{R}_e$ is the vehicle position with respect to the moon specified in a coordinate system in which the x-axis is directed along the earth-moon line from the moon to the Earth, and in which the z-axis is determined by the angular momentum vector of the earth-moon system. If $\mathbf{R}$ is lunar position with respect to the Earth and $\mathbf{V}$ is lunar orbital velocity, both as obtained from the ephemeris, then the unit vectors of the lunar coordinate system (figure 3.5-2) are:

$$\bar{x}_e = -\frac{\mathbf{R}}{R} \tag{29}$$

$$\bar{z}_e = \frac{\mathbf{R} \times \mathbf{V}}{|\mathbf{R} \times \mathbf{V}|} \tag{30}$$

$$\bar{y}_e = \bar{z}_e \times \bar{x}_e \tag{31}$$

Let R_M be vehicle position with respect to the moon in base date inertial coordinates. Then,

$$\left.\begin{aligned} x_e &= R_M \cdot \bar{x}_e \\ y_e &= R_M \cdot \bar{y}_e \\ z_e &= R_M \cdot \bar{z}_e \end{aligned}\right\} \tag{32}$$

The substitution of these values into equation (28) permits the development of the following criteria:

$$\Xi = \frac{(x_e - x_o)^2}{a^2} + \frac{y_e^2}{b^2} + \frac{z_e^2}{b^2} \tag{33}$$

If $\Xi > 1$, vehicle is outside ellipsoid of influence.
If $\Xi = 1$, vehicle is on ellipsoid of influence.
If $\Xi < 1$, vehicle is inside ellipsoid of influence.

Methods for employing these criteria are discussed in paragraph 3.5.4.

3.5.3 EQUATIONS OF TRANSFER. The transfer equations are simple transformations. For position transfer from body 1 to body 2:

$$R_2 = R_1 - R \tag{34}$$

where

R = position of second body with respect to the first

R_1 = vehicle position with respect to first body

R_2 = vehicle position with respect to second body

R, R_1, and R_2 are specified in the base date inertial coordinate system.

For velocity transfer from body 1 to body 2:

$$\dot{R}_2 = \dot{R}_1 - \dot{R} \tag{35}$$

where

$\dot{R}$ = velocity of second body with respect to the first

$\dot{R}_1$ = vehicle velocity with respect to first body

$\dot{R}_2$ = vehicle velocity with respect to second body

3.5.4 APPLICATION OF TRANSFER CRITERIA

3.5.4.1 Heliocentric System. The activity radii, R_{ACT}, for the solar system planets considered in this program are listed in table 3.5-1. The values were computed using equation (13) of paragraph 3.5.2. The vehicle's distance from each of these planets is computed, and the distances compared with the associated activity radii. If the vehicle is outside of the spheres of influence of all of the planets, the Sun is used as the reference body.

Table 3.5-1. Activity Radii for Planets of the Solar System

Planet	R_{ACT} (In Astronomical Units)
Venus	0.003586
Earth	0.005384
Mars	0.003364
Jupiter	0.176967
Saturn	0.317538

3.5.4.2 Earth-Moon Space. In considering lunar transfer, the Earth's proximity must be considered in designating the region of influence. If the region were spherical, i.e., if equation (13) of paragraph 3.5.2 were applicable, its radius would change by about ±2000 miles from perigee to apogee of the moon's orbit about the Earth. The radius of the sphere is about 36,000 miles; therefore, this change will be considered negligible and the mean earth-moon distance will be used in computing the region of influence.

Calculating the elements of the ellipsoid gives rise to the list in table 3.5-2.

Since a and b are nearly equal, the moon's region of influence may also be taken as spherical with

$$a = b = 9.12 \text{ E.R.} = R_{ACT}.$$

The displacement of the center of the region of influence from the moon's center, x_o, is nearly 4000 miles, sufficiently significant to be retained in positioning the sphere. Equation (33) of paragraph 3.5.2 therefore can be rewritten as

$$\Xi = \frac{(x_e - x_o)^2 + y_e^2 + z_e^2}{a^2}$$

Table 3.5-2. Lunar Region of Influence Ellipsoid Parameters

θ	= 0.150	
r_m	= 0.135	Normalized Distances
r_M	= 0.167	Normalized Distances
a	= 0.151	Normalized Distances
b	= 0.150	Normalized Distances
e	= 0.106	
R	= 60.39 E.R.	
x_o	= 0.966 E.R.	

SECTION 4

PERTURBATIONS

4.1 INTRODUCTION

This section develops expressions for the components of vehicle acceleration due to the following perturbing influences: planetary attractions; oblateness of the Earth and Moon; atmospheric drag; solar radiation pressure. Where necessary, descriptions are provided of the general methods used by the Program to implement these expressions.

4.2 PLANETARY ATTRACTIONS

The general expression for the perturbation acceleration, P_1, of a space vehicle due to the gravitational influence of the Sun, Moon, and planets (excluding the reference body) is given by (refer to Section 3)

$$P_1 = \sum_j \mu_j \left[\frac{R_{vj}}{R_{vj}^3} - \frac{R_{rj}}{R_{rj}^3} \right] \qquad (1)$$

where

$\mu_j = GM_j$

G = gravitational constant

M_j = mass of j^{th} body

R_{vj} = position of vehicle with respect to the j^{th} body (figure 4.2-1)

R_{rj} = position of reference body with respect to the j^{th} body

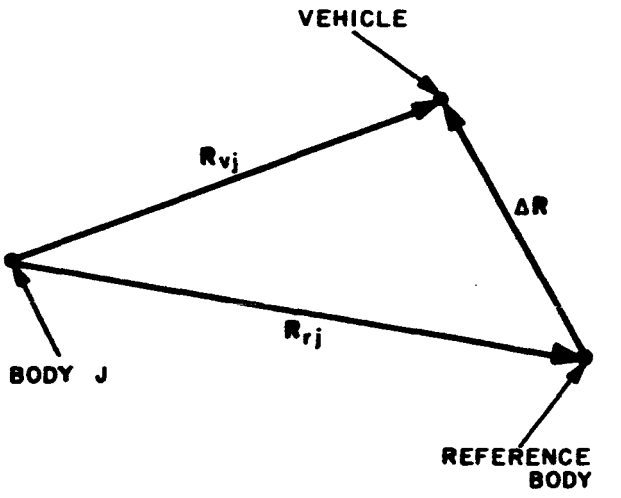

Figure 4.2-1. Planetary Attraction

If the two terms of the bracketed expression in equation (1) are nearly equal, the

indicated subtraction will result in a loss of accuracy due to round-off errors introduced by machine computations. Battin (reference 5) has rewritten equation (1) in a form which eliminates the problem:

$$P_1 = \sum_j \frac{\mu_j}{R_{vj}^3} \left[R_{rj} \{f(U)\} - \Delta R \right] \tag{2}$$

where

$$U = \frac{2}{R_{rj}^2} \left[R_{rj} + \frac{\Delta R}{2} \right] \cdot \Delta R \tag{3}$$

$$f(U) = \frac{U[3 + U(3 + U)]}{1 + (1 + U)^{3/2}} \tag{4}$$

$$\Delta R = R_{vj} - R_{rj} \tag{5}$$

4.3 OBLATENESS

4.3.1 GENERAL. The Program takes into consideration perturbations due to the oblateness of the Earth and the Moon. Paragraph 4.3.2 provides a derivation of a space vehicle's perturbation acceleration due to the Earth's oblateness. Paragraph 4.3.3 provides a similar discussion for the Moon.

> NOTE: The notation used throughout the discussion in paragraph 4.3.2 is consistent with that used by Kaula and Kozai with the exception of the sign of the potential.

4.3.2 EARTH'S OBLATENESS. Consider a ponderable body having an arbitrary figure and an arbitrary mass distribution as shown in figure 4.3-1. The contribution of the mass element dm to the potential at point P is given by

$$dU = - \frac{Gdm}{\Delta r} \tag{1}$$

$$dU = -Gdm[r^2 - 2Rr \cos \gamma + R^2]^{-1/2} \tag{2}$$

where

dU = differential potential

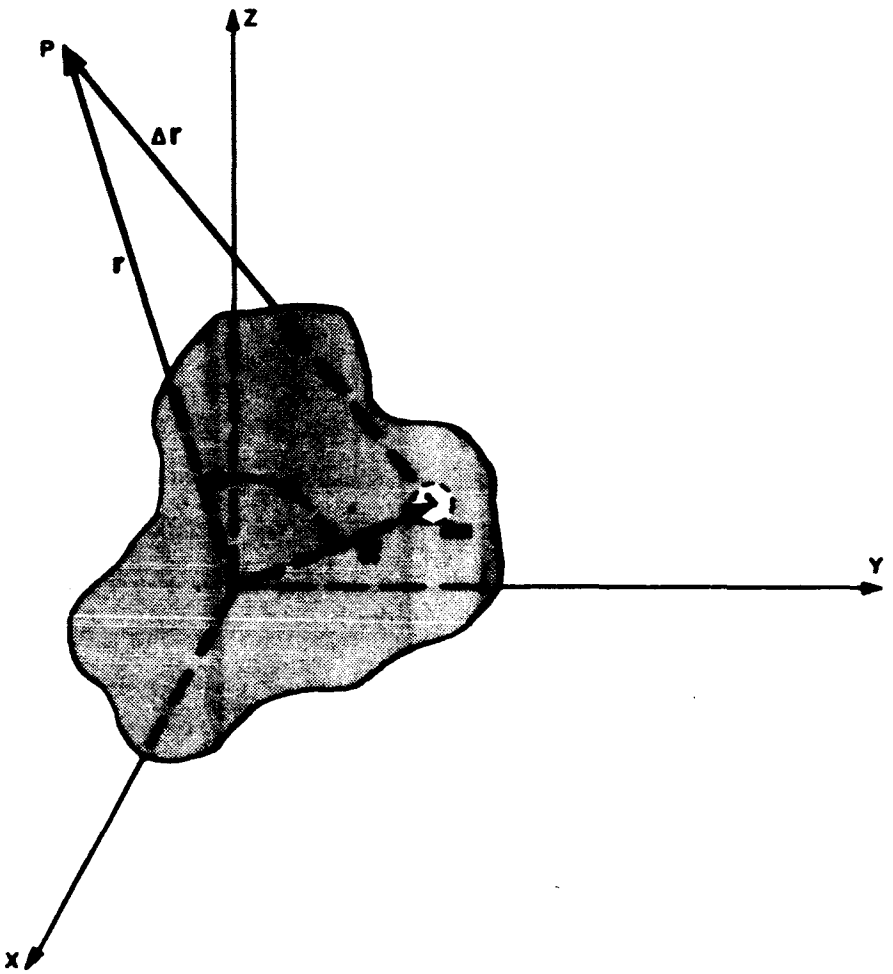

Figure 4.3-1. Calculation of Potential

dm = differential mass element

r = distance from center of coordinates to point at which dU is computed

R = distance from center of coordinates to mass element dm

γ = angle between the vectors r and R

Δ r = magnitude of the vector difference of r - R

Equation (2) may be reformulated by expanding the bracketed terms in a Legendre series in (R/r):

$$dU = -\frac{Gdm}{r} \sum_{n=0}^{\infty} \left[P_n(\cos \gamma) \left[\frac{R}{r} \right]^n \right] \tag{3}$$

in which $P_n(\cos \gamma)$ is the n^{th} order Legendre polynomial. In spherical coordinates, let (R, θ_M, λ_M) and (r, θ, λ) represent the positions of the mass element and the point of interest, respectively. The angles θ_M and θ are co-latitudes of the two points, whereas the angles λ_M and λ are their longitudes. It can be shown that

$$\cos \gamma = \cos \theta_M \cos \theta + \sin \theta_M \sin \theta(\cos \lambda_M \cos \lambda + \sin \lambda_M \sin \lambda) \tag{4}$$

The Legendre polynomials can now be expressed in terms of the associated spherical harmonics $P_n^m(\tau)$:

$$P_n(\cos \gamma) = \sum_{m=0}^{n} \left[\frac{(n - m)!}{(n + m)!} \frac{2}{a_m} P_n^m(\cos \theta_M) P_n^m(\cos \theta) \cos m(\lambda_M - \lambda) \right] \tag{5}$$

where

$$\begin{aligned} a_m &= 2 \text{ when } m = 0 \\ a_m &= 1 \text{ when } m \neq 0 \end{aligned} \tag{6}$$

Substitution of equations (5) and (6) into equation (3) yields an expression for dU in terms of tesseral harmonics. Integrating this expression over all mass elements in the ponderable body gives the potential at point P (figure 4.3-1):

$$U = -\frac{G}{r} \sum_{n=0}^{\infty} \left[\frac{R_o}{r} \right]^n \sum_{m=0}^{n} [P_n^m(\sin \beta)(C_{n,m} \cos m\lambda + S_{n,m} \sin m\lambda)] \tag{7}$$

where

R_o is the mean equatorial radius of the ponderable body

R_o^n, $C_{n,m}$ and $S_{n,m}$ incorporate the results of the integration

β is the latitude of P above the equatorial plane.

In the preceding general formulation, the range of the indices (m, n) is unrestricted. For practical computational purposes, however, the following limits on the range are employed:

Range of Indices (m,n)	
m	n
0,1,2	2
0,1,2,3	3
0,1,2,3,4	4
0,1,2,3	5
0,1,2	6
0,1	7
0	8
0	9
0	10

The fundamental term is given by the 0,0 combination. Zonal harmonics (which indicate the variation of the expression with latitude) are obtained from combinations in which $m = 0$, while sectorial harmonics (which indicate the variation of the expression with longitude) arise when $m = n$; the remaining combinations are truly "tesseral" or "square" in that the function

$$P_n^m(\sin \beta) \begin{cases} \sin m\lambda \\ \cos m\lambda \end{cases}$$

vanishes both along a number (n-m) of parallels of latitude and a number (2m) of meridians of longitude. Figure 4.3-2 provides an illustration of zonal, sectorial, and tesseral harmonic variations for a sample set.

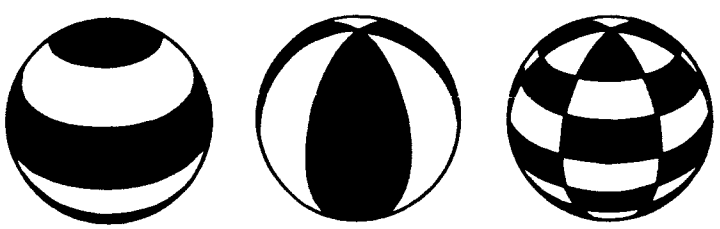

ZONAL HARMONIC FOR n = 4 m = 0

SECTORIAL HARMONIC FOR n = 3 m = 3

TESSERAL HARMONIC FOR n = 8 m = 3

Figure 4.3-2. Sample Spherical Harmonics

With the coordinate system defined as follows, equation (7) describes the Earth's gravitational potential at any point in space:

(a) The center of coordinates is the Earth's center of mass.

(b) The $\bar{x}$-$\bar{y}$ plane is the true equatorial plane of date. The $\bar{x}$-axis passes through the Greenwich meridian.

(c) The $\bar{z}$-axis is the Earth's spin axis.

With these definitions, equation (7) describes the Earth's gravitational potential at any point in space; the gradient of this potential gives the corresponding force field. The force field, however, is described with respect to a moving coordinate system; if the field is to be employed in trajectory computation, it must be transformed to an inertial base date coordinate frame.

The components of gravitational acceleration will now be expressed by a general recursive formulation valid for any n, m combination. First, it is necessary to develop expansions for cos $m\lambda$ and sin $m\lambda$ in terms of cos λ and sin λ. Let

$$z = (\alpha + j\beta) = e^{j\lambda} \tag{8}$$

Then,

$$z^m = (\alpha + j\beta)^m = e^{jm\lambda} = \cos m\lambda + j \sin m\lambda \tag{9}$$

Expanding $(\alpha + j\beta)^m = (\cos \lambda + j \sin \lambda)^m$ by the binomial theorem, and equating real and imaginary parts in equation (9):

$$\cos m\lambda = \sum_{k=0}^{P(m)} \left[(-1)^{(k+2)} {}_mC_{2k} (\cos \lambda)^{(m-2k)} (\sin \lambda)^{(2k)}\right] \tag{10}$$

$$\sin m\lambda = \sum_{k=0}^{P'(m)} \left[(-1)^{(k)} {}_mC_{2k+1} (\cos \lambda)^{(m-2k-1)} (\sin \lambda)^{(2k+1)}\right] \tag{11}$$

where

$${}_mC_r = \frac{m!}{r!(m-r)!} \tag{12}$$

$$P(m) = \begin{cases} \dfrac{m}{2} & \text{if m is even} \\ \dfrac{m-1}{2} & \text{if m is odd} \end{cases} \tag{13}$$

$$P'(m) = \begin{cases} \dfrac{m}{2} - 1 & \text{if } m \text{ is even} \\ \dfrac{m-1}{2} & \text{if } m \text{ is odd} \end{cases} \qquad (14)$$

The definition of equations (13) and (14) maintain positive exponents for equations (10) and (11).

From the definition of spherical coordinates:

$$\left.\begin{aligned} \sin\beta &= \frac{z}{r} \\ \cos\beta\cos\lambda &= \frac{x}{r} \\ \cos\beta\sin\lambda &= \frac{y}{r} \end{aligned}\right\} \qquad (15)$$

Multiplying and dividing equations (10) and (11) by $\cos^m\beta$, and using equations (15),

$$\cos m\lambda = \frac{1}{r^m \cos^m\beta} \sum_{k=0}^{P(m)} \left[(-1)^{(k+2)}\, {}_mC_{2k}\, (x)^{(m-2k)}\, (y)^{(2k)}\right] \qquad (16)$$

$$\sin m\lambda = \frac{1}{r^m \cos^m\beta} \sum_{k=0}^{P'(m)} \left[(-1)^{(k)}\, {}_mC_{2k+1}\, (x)^{(m-2k-1)}\, (y)^{(2k+1)}\right] \qquad (17)$$

Substituting equations (16) and (17) into equation (7),

$$U = -\mu \sum_{n=0}^{\infty} \frac{R_o^n}{r^{n+1}} \sum_{m=0}^{n} \frac{P_n^m(\sin\beta)}{r^m \cos^m\beta} \cdot G(x,y) \qquad (18)$$

$$G(x,y) = C_{n,m} \sum_{k=0}^{P(m)} \left[(-1)^{(k+2)}\, {}_mC_{2k}\, (x)^{(m-2k)}\, (y)^{(2k)}\right]$$

$$+ S_{n,m} \sum_{k=0}^{P'(m)} \left[(-1)^{(k)}\, {}_mC_{2k+1}\, (x)^{(m-2k-1)}\, (y)^{(2k+1)}\right] \qquad (19)$$

For given values of m and n,

$$U_{n,m} = \frac{-\mu R_o^{\,n}}{r^{n+m+1}} \cdot \frac{P_n^{\,m}(\sin\beta)}{\cos^m\beta} \cdot G(x,y) \tag{20}$$

From the definition of Legendre coefficients,

$$\left.\begin{aligned} \frac{P_n^{\,m}(\sin\beta)}{\cos^m\beta} &= \frac{1}{2^n n!}\,\frac{d^{m+n}}{d\tau^{m+n}}\,(\tau^2-1)^n \\ \tau &= \sin\beta \end{aligned}\right\} \tag{21}$$

Upon substitution of equation (21) into equation (20),

$$U_{n,m} = \frac{-\mu R_o^{\,n}}{2^n n!\, r^{n+m+1}}\,\frac{d^{m+n}}{d\tau^{m+n}}\,(\tau^2-1)^n \cdot G(x,y) \tag{22}$$

Gravitational acceleration is computed by taking the gradient of the potential function of equation (22). The general derivative in the gradient will be taken with respect to ξ, where ξ takes on the values of x, y, and z. Consequently, the magnitude of the ξ-component of acceleration will be designated by $A^{\xi}_{n,m}$ and

$$\begin{aligned} A^{x}_{n,m} &= \ddot{X}_{n,m} \\ A^{y}_{n,m} &= \ddot{Y}_{n,m} \\ A^{z}_{n,m} &= \ddot{Z}_{n,m} \end{aligned} \tag{23}$$

With these definitions,

$$A^{\xi}_{n,m} = \frac{\partial U_{n,m}}{\partial \xi} \tag{24}$$

Carrying out the indicated operations,

$$A^{\xi}_{n,m} = \frac{GR_o^{\,n}}{2^n n!\, r^{m+n+1}} \left[\frac{(m+n+1)\xi}{r^2} \cdot G(x,y) \frac{d^{m+n}}{d\tau^{m+n}} (\tau^2 - 1)^n \right.$$

$$- \frac{G(x,y)}{r} \left[\frac{\partial z}{\partial \xi} - \frac{z\xi}{r^2} \right] \frac{d^{m+n+1}}{d\tau^{m+n+1}} (\tau^2 - 1)^n$$

$$\left. - \frac{d^{m+n}}{d\tau^{m+n}} (\tau^2 - 1)^n \cdot \frac{\partial G(x,y)}{\partial \xi} \right] \tag{25}$$

in which

$$\frac{1}{r} \left[\frac{\partial z}{\partial \xi} - \frac{z\xi}{r^2} \right] = \frac{\partial \tau}{\partial \xi} \tag{26}$$

and

$$\frac{\partial G(x,y)}{\partial \xi} = C_{n,m} \sum_{k=0}^{P(m)} \left[(-1)^{(k+2)} {}_mC_{2k} \left[(m-2k)(x)^{(m-2k-1)}(y)^{(2k)} \frac{\partial x}{\partial \xi} \right. \right.$$

$$\left. + 2k(x)^{(m-2k)}(y)^{(2k-1)} \frac{\partial y}{\partial \xi} \right] \Bigg]$$

$$+ S_{n,m} \sum_{k=0}^{P'(m)} \left[(-1)^{(k)} {}_mC_{2k+1} \left[(m-2k-1)(x)^{(m-2k-2)}(y)^{(2k+1)} \frac{\partial x}{\partial \xi} \right. \right.$$

$$\left. \left. + (2k+1)(x)^{(m-2k-1)}(y)^{(2k)} \frac{\partial y}{\partial \xi} \right] \right] \tag{27}$$

From Rodrigues' formula

$$\frac{d^{m+n}}{d\tau^{m+n}} (\tau^2 - 1)^n = \sum_{g=0}^{P(n)} \frac{(-1)^g n!(2n-2g)!}{g!(n-g)!(n-2g-m)!} \tau^{(n-2g-m)} \tag{28}$$

$$\frac{d^{m+n+1}}{d\tau^{m+n+1}} (\tau^2 - 1)^n = \sum_{g=0}^{P(n)} \frac{(-1)^g n!(2n-2g)!}{g!(n-g)!(n-2g-m-1)!} \tau^{(n-2g-m-1)} \tag{29}$$

where P(n) is the integral part of (n-m)/2.

In addition,

$$\frac{\partial x}{\partial \xi} = \begin{cases} 1 \text{ if } x = \xi \\ 0 \text{ if } x \neq \xi \end{cases} \quad \frac{\partial y}{\partial \xi} = \begin{cases} 1 \text{ if } y = \xi \\ 0 \text{ if } y \neq \xi \end{cases} \quad \frac{\partial z}{\partial \xi} = \begin{cases} 1 \text{ if } z = \xi \\ 0 \text{ if } z \neq \xi \end{cases} \tag{30}$$

Substituting equations (28) and (29) into equation (25), combining terms, and changing the sign in accordance with the usual convention:

$$A^{\xi}_{n,m} = \frac{-\mu R_o^{\,n}}{2^n n! r^{m+n+1}} \sum_{g=0}^{P(n)} \left\{ \left[\frac{(-1)^g n! (2n-2g)!}{g!(n-g)!(n-2g-m)!} \left[\frac{z}{r}\right]^{(n-2g-m-1)} \right] \right.$$
$$\left. \times \left[\left[(2n-2g+1) \frac{\xi z}{r^3} - \frac{(n-2g-m)}{r} \frac{\partial z}{\partial \xi} \right] G(x,y) - \left[\frac{z}{r}\right] \frac{\partial G(x,y)}{\partial \xi} \right] \right\} \tag{31}$$

since

$$\tau = \sin \beta = \frac{z}{r} \tag{32}$$

Tables 4.3-1 and 4.3-2 list the appropriate values of coefficients $C_{n,m}$ and $S_{n,m}$, respectively, to relate equation (31) to the Earth's gravitational field. The values listed are for the range of n and m suggested earlier. Note that values are not supplied in tables 4.3-1 and 4.3-2 for the fundamental ($n = m = 0$) term of the $A_{n,m}$ expansion. The fundamental term represents the vehicle's acceleration due to a spherical Earth, while the other terms account for the Earth's oblateness. Thus,

$$(P_2)_E = \sum_{n=1}^{\infty} \sum_{m=0}^{n} A_{n,m} \tag{33}$$

where $(P_2)_E$ is the vehicle's perturbation acceleration due to the Earth's oblateness.

4.3.3 MOON'S OBLATENESS. The potential, U_M, at a point P (figure 4.3-3) due to the Moon's gravitational field is given by

$$U_M = -\int_M G dm \frac{1}{|R_M - r|} \tag{1}$$

where

dm is a differential element of lunar mass

G is the gravitational constant

Table 4.3-1. Earth Values of $C_{n,m}$

m \ n	1	2	3	4	5	6	7	8	9	10
0	0	-1082.30×10^{-6}	$+2.3 \times 10^{-6}$	$+1.8 \times 10^{-6}$	$+0.064 \times 10^{-6}$	-0.39×10^{-6}	$+0.470 \times 10^{-6}$	$+0.02 \times 10^{-6}$	-0.117×10^{-6}	
1	0	4×10^{-8}	-170×10^{-8}	-43×10^{-8}						
2		31×10^{-8}								
3										
4										

Table 4.3-2. Earth Values of $S_{n,m}$

m \ n	1	2	3	4	5	6	7	8	9	10
0	0	0	0	0	0	0	0	0	0	0
1	0	110×10^{-8}	582×10^{-8}	27×10^{-8}						
2		-150×10^{-8}								
3										
4										

R_M is the selenocentric position of the vehicle

r is the selenocentric position of dm

M is the mass of the Moon

Rewriting equation (1),

$$U_M = -\mu \int_M \frac{dm}{R_M} \left[1 - \frac{2r \cdot R_M}{R_M^2} + \frac{r^2}{R_M^2} \right]^{-1/2} \tag{2}$$

Considering the bracketed expression of equation (2) to be of the form $(1 + a)^{-1/2}$, where

$$a = \frac{r^2}{R_M^2} - \frac{2r \cdot R_M}{R_M^2}, \tag{3}$$

equation (2) is rewritten, using a binomial expansion, as

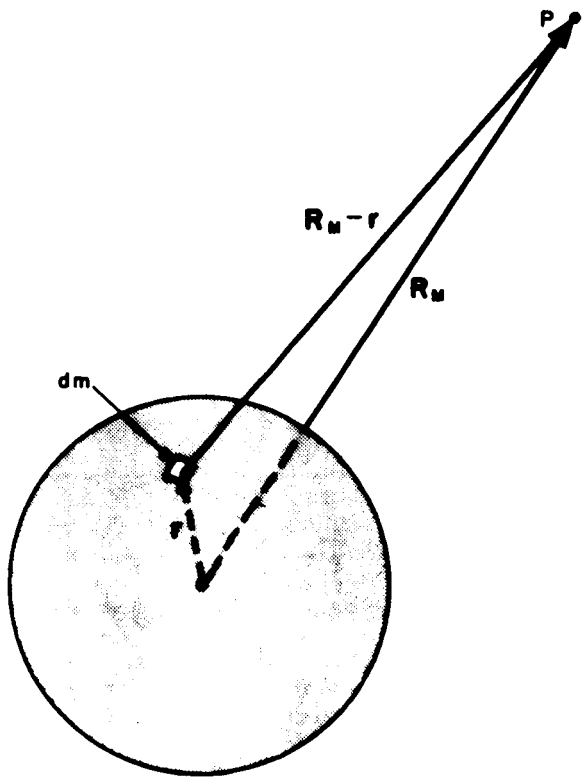

Figure 4.3-3. Lunar Potential

$$U_M = -\mu \int_M \frac{dm}{R_M} \left[1 + \frac{r \cdot R_M}{R_M^2} - \frac{1}{2} \frac{r^2}{R_M^2} + \frac{3}{8} \left[\frac{2r \cdot R_M}{R_M^2} \right]^2 + \ldots \right] \tag{4}$$

The quantity

$$\frac{3}{8} \left[\frac{2r \cdot R_M}{R_M^2} \right]^2$$

can be rewritten as

$$\frac{3}{2} \frac{\bar{R}_M \cdot [rr] \cdot \bar{R}_M}{R_M^2}$$

where $[rr]$ is a dyadic of order 1. Therefore, neglecting all terms in equation (4) of an order higher than that shown in the equation,

$$U_M \approx -\frac{\mu}{R_M}\left[M + \int_M \frac{r\cdot R_M}{R_M^2}\,dm - \frac{1}{2}\int_M \frac{r^2 dm}{R_M^2} - 3\bar{R}_M\cdot\int_M \frac{[rr]}{R_M^2}\,dm\cdot\bar{R}_M\right] \tag{5}$$

Over the entire mass of the Moon,

$$\int_M \frac{r\cdot R_M}{R_M^2}\,dm = 0. \tag{6}$$

Therefore,

$$U_M \approx -\frac{\mu}{R_M}\left[M - \frac{1}{2}\int_M \frac{r^2 dm}{R_M^2} - 3\bar{R}_M\cdot\int_M \frac{[rr]}{R_M^2}\,dm\cdot\bar{R}_M\right] \tag{7}$$

Equation (7) can be rewritten as

$$U_M \approx -\frac{\mu M}{R_M} + \frac{\mu}{2R_M^3}\,\bar{R}_M\cdot\left[\int_M (r^2[I] - 3[rr])\,dm\right]\cdot\bar{R}_M \tag{8}$$

where $[I]$ is a unit dyadic.

Let

$$[V_M] = \int_M (r^2[I] - 3[rr])\,dm \tag{9}$$

Therefore,

$$U_M \approx -\frac{\mu M}{R_M} + \frac{\mu}{2R_M^5}\,R_M\cdot[V_M]\cdot R_M \tag{10}$$

The quantity $[V_M]$ represents the lunar oblateness dyadic. This dyadic, which is independent of vehicle position, may be written as follows in terms of lunar constants in the lunar principal axis coordinate system ($\bar{x}_M$, $\bar{y}_M$, $\bar{z}_M$) defined in Appendix A to this manual:

$$[V_M]_M = \begin{bmatrix} 2A-B-C & 0 & 0 \\ 0 & 2B-A-C & 0 \\ 0 & 0 & 2C-A-B \end{bmatrix} \tag{11}$$

where

A = principal moment of inertia on $\bar{x}_M = \int_M (Y^2 + Z^2)dm$

B = principal moment of inertia on $\bar{y}_M = \int_M (X^2 + Z^2)dm$

C = principal moment of inertia on $\bar{z}_M = \int_M (X^2 + Y^2)dm$

Reference 6 gives the following values for A, B, and C:

$$A = 0.88746 \times 10^{29} \text{ kg - km}^2$$

$$B = 0.88764 \times 10^{29} \text{ kg - km}^2$$

$$C = 0.88801 \times 10^{29} \text{ kg - km}^2$$

In these units,

$$[V_M]_M = \begin{bmatrix} 7.3 & 0 & 0 \\ 0 & 1.9 & 0 \\ 0 & 0 & -9.2 \end{bmatrix} \text{kg-km}^2 \tag{12}$$

The vehicle's acceleration due to the Moon's oblateness is given by the gradient of the oblateness term of equation (10):

$$(P_2)_M = \nabla \left[\frac{G}{2R_M^5} R_M \cdot [V_M] \cdot R_M \right] \tag{13}$$

$$(P_2)_M = \frac{G}{2} \left[\nabla(R_M^{-5}) R_M \cdot [V_M] \cdot R_M + R_M^{-5} \nabla(R_M \cdot [V_M] \cdot R_M) \right] \tag{14}$$

Now,

$$\nabla(R_M^{-5}) = -5R_M^{-6} \nabla R_M \tag{15}$$

Since

$$\nabla R_M = \frac{R_M}{R_M}, \tag{16}$$

$$\nabla(R_M^{-5}) = \frac{-5R_M}{R_M^7} \tag{17}$$

$$\nabla(R_M \cdot [V_M] \cdot R_M) = \nabla R_M \cdot \begin{bmatrix} V_{11} & 0 & 0 \\ 0 & V_{22} & 0 \\ 0 & 0 & V_{33} \end{bmatrix} \cdot R_M$$

$$= \nabla(V_{11} X_M^2 + V_{22} Y_M^2 + V_{33} Z_M^2)$$

$$= 2V_{11} \bar{X}_M + 2V_{22} \bar{Y}_M + 2V_{33} \bar{Z}_M$$

$$= 2[V_M] \cdot R_M \tag{18}$$

where R_M is written in the coordinate system for which $[V_M]$ is a diagonal dyadic.

Therefore,

$$(P_2)_M = -\frac{5}{2} \frac{\mu}{R_M^7} R_M [R_M \cdot [V_M] \cdot R_M] + \frac{\mu}{R_M^5} ([V_M] \cdot R_M) \tag{19}$$

In the trajectory calculations of the Program, R_M is given in the base date $(\bar{X}_B, \bar{Y}_B, \bar{Z}_B)$ system. It is therefore necessary to transform $[\bar{V}_M]_M$ into that system. This may be done by a composite transformation composed of precession, nutation, and libration. Thus ,

$$[V_M]_B = [A][N][L][V_M]_M [L]^{-1}[N]^{-1}[A]^{-1} \tag{20}$$

where [A], [N], and [L] are given in Appendix A.

It should be noted that the lunar oblateness perturbation acceleration, $(P_2)_M$, is appreciable only if R_M is less than 40,000 km. For values of R_M greater than this value, the lunar oblateness perturbation acceleration may be assumed to be zero.

4.4 ATMOSPHERIC DRAG

4.4.1 INTRODUCTION. Accurate simulation of the trajectory of an artificial satellite or space probe requires consideration of vehicle deceleration resulting from atmospheric drag. At the present time, there is evidence that Mars, Venus, Jupiter, as well as the Earth have sufficiently dense atmospheres to retard the motion of a space vehicle.

The following paragraphs describe the general equations used for drag computations, some of the problems involved in simulating planetary atmospheres, and the effects, on the simulation, of making certain simplifying assumptions. The concluding paragraphs describe a method of simulating atmospheric drag representing a complexity commensurate with the state-of-the-art.

An analysis of the effects of atmospheric drag must take into account the mission of the vehicle. There are three missions in which atmospheric drag could play an important part. The first mission is a low-eccentricity orbit about the Earth or another planet. The second mission is planetary re-entry, and the third is a fly-by orbit (pass around a planet or moon) of the space vehicle. In the following discussion, the three cases will be referred to as the "orbiting", "reentry" and "fly-by" cases.

4.4.2 DRAG EQUATIONS

4.4.2.1 General. The form of the equation used to compute the magnitude of the vehicle deceleration, P_4, resulting from atmospheric drag depends on the diffuseness of the atmosphere. For relatively dense atmospheres where the assumption of continuum flow is valid, the following equation is commonly used:

$$P_4 = \frac{1}{2m} \{\rho V_a{}^2 C_D S\} \tag{1}$$

where

ρ is the density of the atmosphere at the vehicle

V_a is the magnitude of the velocity of the vehicle with respect to the atmosphere

C_D is the drag coefficient of the vehicle

S is the effective surface area presented by the vehicle

m is the mass of the vehicle

As the atmosphere becomes more and more diffuse, the mean free path (average distance between impacts of air molecules) increases. Figure 4.4-1, obtained from reference 7, shows mean free path plotted as a function of altitude. When the mean free path becomes greater than the diameter of the vehicle, the collisions become two-body collisions and the assumption of continuity of the air mass (continuum flow) is no longer applicable. The assumption of a diffuse atmosphere, where all collisions are two-body and the mean-free-path exceeds the dimension of the vehicle passing through, is called free molecular flow.

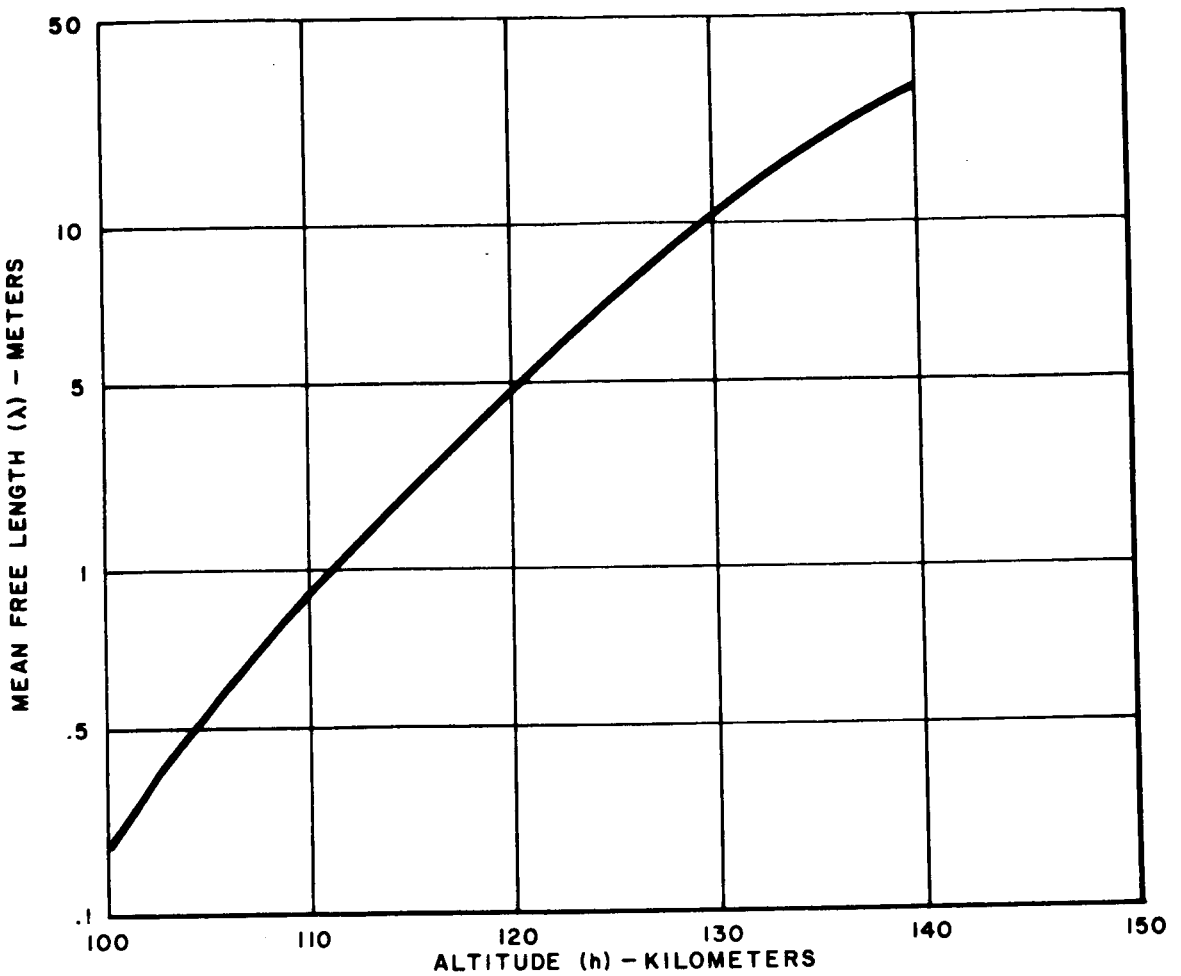

Figure 4.4-1. Variation of Mean Free Length With Geocentric Altitude

Ketchum (reference 8) has derived, using the Maxwell-Boltzman Distribution Law, the following formula for the magnitude of the drag deceleration in free molecular flow:

$$P_4 = \frac{\pi}{8m} \left[(1+2R/\lambda)\ \rho V_a C_{av} S\right] \qquad (2)$$

where

R is the radius of the vehicle

λ is the mean free path

C_{av} is the average velocity of particles in the medium

Ketchum is uncertain as to the validity of the $(1 + 2R/\lambda)$ term in equation (2). A more correct equation may be

$$P_4 = \frac{\pi}{8m} [\rho V_a \, C_{av} \, S]$$

This program uses the latter equation. From figure 4.4-1, it is seen that λ varies very rapidly with altitude so that the change from $2R = \lambda$ (where the transition from continuum flow occurs) to $2R = 0.1 \lambda$ (where the correction becomes negligible) takes a short time.

4.4.2.2 Direction of Drag Force. By definition, the drag force acts in a direction opposite to that of the vehicle's velocity with respect to the air mass, V_a. Paragraph 4.4.2.5 describes the computation of V_a. The direction of the drag force is obtained by normalizing this vector.

4.4.2.3 Vehicle Mass. In the most general case, the vehicle mass terms in the drag equations must be considered as variable with time. In the orbiting case or the fly-by case, a step change in mass representing the separation of a landing craft is conceivable. A long-term steady-state mass flow rate, however, would probably be small.

For the reentry case, if the reentry vehicle is of the heat-sink type, the mass would be constant. For an ablative nose cone (i.e., one which loses, due to friction, mass when moving at high speeds), the mass flow rate is a function of the drag. For ballistic missile applications, this mass change is usually ignored. In any event, such changes in mass represent a small error in the location of the impact point.

4.4.2.4 Surface Area. The effective surface area term S, in the drag equation is not simply the cross-sectional area of the vehicle. The vehicle, in passing through the air, produces a shock wave which skirts the missile thereby placing the effective cross-sectional area at a point somewhat close to the nose. Since the shock wave changes with air speed, so does the effective cross-sectional area. In practice, S is made constant and any variation with speed is included in the coefficient of drag.

> NOTE: The preceding discussion assumes that the angle of attack of the vehicle is zero, i.e., that the vehicle velocity relative to the air mass is in line with the vehicle longitudinal axis.

4.4.2.5 Air Speed. The velocity of the vehicle is computationally available in an inertial coordinate system. The vehicle velocity with respect to the moving air mass, V_a, in the same coordinate system, is obtained by subtracting the velocity of the air mass from the vehicle velocity. The air speed is the magnitude of V_a. A good first approximation to the velocity of the air mass is obtained by assuming the air mass to be rigidly attached to the rotating planet.

A better approximation could be obtained by including the effects of wind velocity. The purely local effects have to be neglected, but the long-term horizontal effects are known as a function both of position on the Earth's surface and of altitude. The effects of the wind velocity's direction (independent of altitude but dependent on latitude and longitude) and magnitude (strongly dependent on altitude, less strongly on latitude, and least on

longitude) would have to be included. The error made by neglecting Earth winds is about 1500 feet at impact for a typical ICBM mission. It should be noted that winds are of importance only in the Earth's lower atmosphere, mainly for the reentry case.

4.4.2.6 **Drag Coefficient.** The drag coefficient, C_D, is sometimes considered to be constant, but a much more accurate representation is obtained by considering it to be a function of Mach number, where the Mach number is defined as air speed (paragraph 4.4.2.5) divided by the speed of sound.

The speed of sound is a function of altitude but is easily computed, from a stored table, using a table look-up procedure. Linear interpolation is used between tabulated values. A different table is required for each planet.

It should be noted that as altitude increases, the atmosphere becomes rarified to the point that the speed of sound loses its physical significance.

In practice, C_D is tabulated for about 25 different Mach numbers. These numbers are denser for speeds below Mach 2 than those above, and very dense in the region around Mach 1. For intermediate values of Mach number, linear interpolation is used.

Inadequate knowledge of the drag coefficient is one of the major sources of inaccuracy in the simulation of drag. Since drag coefficient is a function of Mach number, drag coefficient data are obtained by wind tunnel measurements made at a range of Mach numbers. These data are tabulated to a precision of 1 part in 30. At best then, the tolerance is half of 1 part in 30, or ±1.7%. It is believed, however, that the total error is more in the order of ±3%, even at the tabulated points.

4.4.2.7 **Discontinuity Between Continuum and Free Molecular Flow.** It is readily seen that the formula for drag (paragraph 4.4.2.1) in the region of free molecular flow is different from that in the region of continuum flow. Even if the two formulas were to agree at one altitude for a given V_a and C_{av}, permitting a continuous transition from one formula to the other, there would be no continuity at the junction of the regions for a different V_a or C_{av}.

A possible solution is to introduce a transition region in which a weighted average is taken between the drag values computed by the two methods and gradually slide the weight from unity for free molecular flow and zero for continuum flow to unity for continuum flow and zero for free molecular flow.

4.4.3 ATMOSPHERIC MODELS

4.4.3.1 **Introduction.** The following paragraphs provide a summary of current knowledge of the composition of the atmospheres of Jupiter, Mars, Venus, and the Earth. A discussion is provided of the models currently being used (or developed) to simulate these atmospheres.

4.4.3.2 **Jupiter.** Current studies are concentrated on determining the composition of Jupiter's atmosphere. At the present time, it is considered premature to even begin to consider the relationship of density to altitude.

4.4.3.3 **Mars.** Density versus altitude data for Mars are fairly well agreed upon for altitudes up to about 30 km. For altitudes up to 80 km, Schilling (reference 9) gives

values for density with a maximum uncertainty of about 8:1, and a standard deviation of about 3:1. Schilling's model is easily approximated by an exponential interpolation: tabular listings of logarithm of density versus altitude are made; linear interpolation is used between tabulated values; and the antilog is obtained. With a 7-value table of density and altitude, a maximum error of 1.4% can be obtained for the Schilling Model II Mars atmosphere.

4.4.3.4 Venus. Because the surface of Venus is always obscured from view, there is little agreement about its atmospheric model, or composition within the cloud level (at about 30 km in altitude). However, in 1959, the star Regulus was occulted at 100 km in altitude, thereby providing fairly definite data.

There are the three theories of the model of Venus' atmosphere: greenhouse; aeolosphere; and ionosphere. However, no one theory explains all of the available information about Venus. At the present time, there is no generally acceptable density versus altitude curve for Venus.

4.4.3.5 Earth

4.4.3.5.1 General. Although knowledge of the Earth's atmosphere is not complete, the known effects are far more complete than for any of the other planets and represent an adequate model of the Earth's atmosphere even at altitudes of 2000 km (about 6.6 million feet). It is convenient to separate the atmosphere into two parts, the lower atmosphere and upper atmosphere, with the separation occurring at about 120 km (400,000 ft.). Drag in the lower atmosphere is large and a vehicle entering it will usually be slowed down sufficiently to be captured by the Earth. Thus, the lower atmosphere is primarily of concern in the reentry case. The upper atmosphere is characterized by smaller drag effects which are of significance mainly over long time arcs (orbiting mission). In the cases of reentry and fly-by, the upper atmosphere can probably be neglected.

4.4.3.5.2 Lower Atmosphere. Data for an average model have been well established for the lower atmosphere. There are five sources for these data: U.S. Standard Atmosphere, 1962; COSPAR International Reference Atmosphere (CIRA), 1961; COESA Table for Tropical Latitudes, 1962; ARDC Model Atmosphere 1956, 1959. Table 4.4-1 shows the density deviation (in percent), as a function of altitude, of each of the others from the U.S. Standard Atmosphere values. From the table, it is evident that, except for the COESA tables, there is good agreement between the various tables at low altitudes. Note that the U.S. Standard Atmosphere and CIRA tables are in excellent agreement all the way to 120 km (400,000 feet).

The lower atmosphere is characterized by seasonal, diurnal, and latitude variations; however, none of these are sufficiently well documented. The only effect of omitting them is that the impact point of a re-entering body would be slightly different. It was estimated in 1958 that the standard deviation for a heat-sink type nose cone used in the ICBM application is only about 0.5 nm.

The speed of sound in the lower atmosphere can also be obtained from the five sources given earlier, but only in the range 0 to 90 km. However, for the U.S. Standard Atmosphere and CIRA sources, values up to 120 km can be computed from absolute temperature and mean molecular weight data tabulated in these tables.

Table 4.4-1. Comparison of Sources of Density Data

Altitude		U.S. Standard Atmosphere Density Values (Reference)	Percent Deviation From Reference			
km	ft	slugs/ft^3	ARDC 1956	ARDC 1959	CIRA 1961	COESA 1962
0	0	2.38^{-3}	0	0	0.55	- 4.77
3.0	10,000	1.76^{-3}	0	0	-0.91	- 5.32
5.5	18,000	1.36^{-3}	0.04	0	1.85	- 1.67
10.1	33,000	7.97^{-4}	0.05	0	1.68	1.92
14.6	48,000	4.00^{-4}	0.09	0	2.36	15.5
20.4	67,000	1.61^{-4}	3.28	0.16	0.48	6.80
29.0	95,000	4.20^{-5}	0.59	- 2.36	0.10	0.46
33.5	110,000	2.07^{-5}	- 3.13	- 3.13	0.68	2.53
48.8	160,000	2.32^{-6}	4.77	4.77	0.77	8.93
67.1	220,000	2.50^{-7}	15.0	15.5	1.30	8.10
91.4	300,000	4.62^{-9}	31.2	-10.8	0.11	--
121.9	400,000	3.62^{-11}	81.5	-35.0	1.17	--

4.4.3.5.3 Upper Atmosphere. Models of the Earth's upper atmosphere must take into account solar activity. There is evidence that solar activity occurs cyclically at periods of 27 days, 6 months, 1 year, and 11 years.

Theoretical models do not exist for the 27-day, 6-month, and 1-year cycles. Diurnal variations, if any, of the models for these cycles are not known. Completion of synthesis of the 27-day model is not anticipated until mid-1964; completion of the synthesis of the other two models will be later than that. Investigation of the 11-year cycle (corresponding to the sunspot period) in solar flux has lead to the Harris-Priester model of the upper atmosphere. This model (references 10 and 11) has diurnal and solar flux variations. R. Bryant of the Goddard Space Flight Center (GSFC) has had excellent results using density data from this model to predict the orbit of the Echo Satellite over an extensive period of time.

Roemer (reference 12), assuming the exosphere to start at 600 km, performed a Fourier analysis on the temperature variations of solar flux below that altitude and assumed

isothermal conditions above. The resulting numerical approximation was accurate to ±2%. A program (written by R. Devaney of GSFC) based on these results occupies 1530 words of storage on the IBM 7094 computer. Approximately 1710 words of storage are needed for constants. Harris indicated that the start of the exosphere could be reduced to 400 km which would reduce the constants storage to 1450 words, but leave the program size unchanged (at 1530), for a total of 2980 words.

In an attempt to shorten computation and reduce storage without causing a significant deterioration in accuracy, the use of a simple table-lookup procedure for density was investigated. The result is a table comprising 1074 words of storage. Density data are stored at each combination of 16 values of altitude, 13 values of local solar time (difference between the right ascensions, on the celestial sphere, of the vehicle and the Sun), and 5 values of solar flux. The values of altitude, time, and solar flux are also stored, adding 34 values. For a maximum error of 2.7%, linear exponential interpolation (in 3 dimensions) is satisfactory. This maximum error would only be obtained if, simultaneously, solar flux is high, local time is at 14 hours, and altitude is half-way between two tabulated values. The average error would probably be below 1%. The program size was estimated from the equations as 645 for a total of 1900, after adding 10% of the total for contingency.

There is an intuitive difficulty in using local solar time as one of the parameters: At the North or South pole, there is no midnight and noon, local solar time being undefined. Since there is no evidence of direct variation of the Harris-Priester model with vehicle latitude, it has been suggested that the use of zenith angle in place of local solar time might give more intuitively satisfying results. (Zenith angle is the angle subtended on the celestial sphere between the vehicle position and the Sun's position.) Unfortunately, the use of zenith angle introduces an unacceptable discontinuity. The zenith angle for a vehicle α degrees above the ecliptic decreases to α degrees at noon (minimum) and then increases again; it can never decrease below α degrees. This is evident from figure 4.4-2. To yield a cyclic time function, zenith angle would have to be arbitrarily made negative before noon, going to $-\alpha$ degrees at noon, and $+\alpha$ degrees instantaneously after noon. This discontinuity is unsatisfactory. Therefore, the use of local solar time is recommended despite the inherent difficulty at noon and midnight.

The upper atmosphere has a delaying effect on solar radiation. It takes several hours for the Sun's heat to pass through the atmosphere and reach the Earth's surface. The Harris-Priester model is based on densities computed at the Earth's equator. Intuitively, it is expected that it will take longer for the solar flux to reach the poles as opposed to the equator. Therefore, it is considered that there is an effective variation of solar flux with latitude. This variation is implemented in the Program by applying the Harris-Priester model at the equator and a stored table of "twilight" densities at the poles. The cosine of the latitude of the vehicle is used as a weighting factor to interpolate between the two sets of data.

4.4.3.5.4 Density Discontinuity Between Lower and Upper Atmospheres. In the Harris-Priester model, the density at 120 km is fixed independently of solar flux and time of day, and is 34% higher than the U.S. Standard Atmosphere value. No other model for the lower atmosphere gives a value close to it so that there is a discontinuity in density between the Harris-Priester model and all of the models of the lower atmosphere.

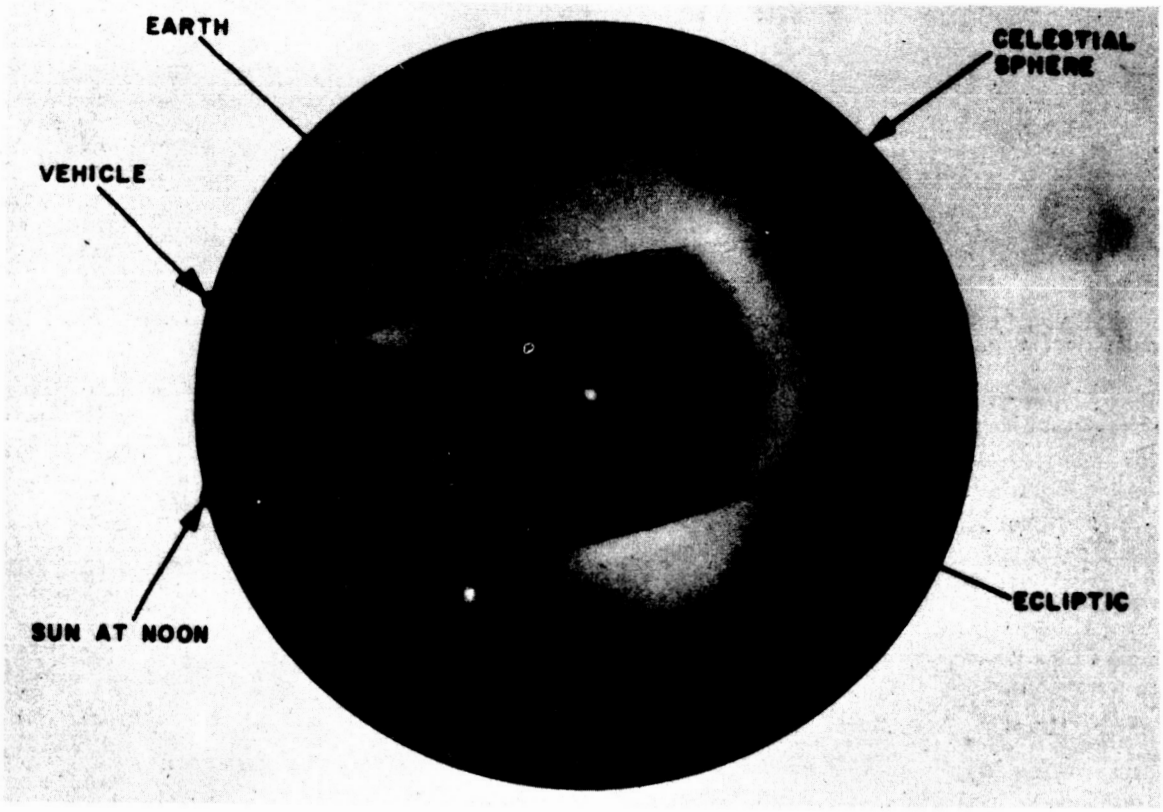

Figure 4.4-2. Zenith Angle Variation

4.4.3.6 General Considerations for Atmospheric Simulation

4.4.3.6.1 Definition of Altitude. Harris has suggested that the geocentric altitude above the oblate earth should be used for the Harris-Priester model of the upper atmosphere. For the lower atmosphere, the same definition of altitude should be used.

For all other planets, geocentric altitude above an ellipsoidal or spherical planet could be used.

4.4.3.6.2 Medium Velocity. The average velocity of particles in the medium (C_{av}) is of importance only when the altitude is high enough so that free molecular flow is valid. Free molecular flow is of concern only for the Earth since, for other planets, the atmospheres are not known to a high enough altitude. For the Earth, from figure 4.4-1, it is seen that for the usual space vehicle dimensions, free molecular flow occurs in the upper atmosphere. From equations I. 3.4-(1) and I. 2.6-(1) of reference 7, C_{av} is found to be proportional to $\sqrt{T/M}$:

$$C_{av} \propto \sqrt{\frac{T}{M}}$$

where

T is absolute temperature

M is mean molecular weight

The medium velocity can be computed using values of T and M from the Harris-Priester model. The variation in C_{av} with local time and solar flux was ±22% for altitudes below 500 km and ±14% for altitudes above 500 km. Therefore, were C_{av} to be approximated by a function of altitude only, an error in drag of ±22% would be introduced. An error of this order of magnitude is intolerable.

Thus, drag is linearly proportional to both density and medium velocity, both of which are functions of the same three parameters (altitude, local time, and solar flux). It is natural then, for altitudes where free molecular flow pertains, to store the product of density and medium velocity (as a function of the three parameters) instead of both density and medium velocity separately.

4.4.3.6.3 Accuracy. From the foregoing analyses, it is concluded that the computation of drag is probably accurate to ±5% in the Earth's lower atmosphere, and is less accurate in the upper atmosphere. For Mars, the knowledge of drag is probably not as accurate as ±10%, and for Venus considerably worse. Therefore, calculation of drag and its constituent parameters can always be computed in single precision without degrading the over-all precision of computation.

4.4.4 DRAG COMPUTATION METHODS USED BY PROGRAM

4.4.4.1 General. The following methods for drag computations represent, in most cases, a compromise between state-of-the-art and ease of computation.

Programs and tables are included for computing drag over any combination of the following:

(a) Lower atmosphere Earth

(b) Upper atmosphere Earth

(c) Mars

(d) Venus

(e) Jupiter

The programs are selected at the operator's discretion.

When drag is to be included in trajectory computations, a distance test, which varies with the reference system which the vehicle is in, is made. The distance to the center of the reference body is computed and compared with center distances corresponding to the following altitudes:

0 km - used to indicate assumption of no atmospheric drag

80 km - height corresponding to upper level of Mars' atmosphere

180 km - height corresponding to upper level of Venus' atmosphere

210 km - height corresponding to upper level of Earth's lower atmosphere (only used when the Earth's upper atmosphere is ignored)

1160 km - height corresponding to upper level of Earth's upper atmosphere.

If all of the distance tests fail, drag is set equal to zero. If any test passes, drag is computed as follows.

(a) The planetocentric altitude is computed.

(b) The altitude value used by the drag computation subroutine is the distance between the vehicle position and the center of the reference body minus the radius of the reference body. For Mars, Venus and Jupiter, the radius of the reference body is taken to be constant. For the Earth, it varies with the latitude of the vehicle and must be computed from the latitude and the ellipticity of the Earth. Therefore, if the earth is the reference body, the geocentric latitude is computed together with the radius based on an oblate spherical Earth.

(c) Drag is computed using either equation (1) or (3) of paragraph 4.4.2.1, as applicable. (Refer to paragraph 4.4.4.2.)

4.4.4.2 Selection of Drag Equation. Equation (3) of paragraph 4.4.2.1 is used only for the following conditions:

(a) When the computation is to be performed for the Earth's upper atmosphere at altitudes in excess of 100 km, with the Earth as the reference body.

(b) If the computation is to be performed for the Earth's atmosphere in the transition region between continuum flow and free molecular flow, computations are performed using both equations (1) and (3).

Equation (1) is used for all other cases.

Figure 4.4.-1 indicates that altitudes between 120 and 130 km would provide a theoretically desirable transition region. Tables above 120 km are 3-dimensional, i.e., density is tabulated versus solar flux, local solar time, and altitude; tables below 120 km are 1-dimensional, i.e., density is plotted versus altitude only. Thus, to save computer memory space, the range of 100 to 120 km is arbitrarily chosen as the transition region. This choice offers an additional advantage: the discontinuity between the upper and lower atmospheres is bridged by using table values of $\rho \cdot C_{av}$ only with the Harris-Priester model.

For the transition region, both drag equations plus the transition function (paragraph 4.4.2.7) are used.

4.4.4.3 Determination of Drag Equation Parameters

4.4.4.3.1 Air Velocity. The velocity of the vehicle with respect to the air mass (V_a) is computed from the vehicle's inertial velocity (V_i) by subtracting from V_i (1) the velocity of the air mass with respect to the planet, and (2) the velocity of the planet with respect to the coordinate system. The latter comes from the ephemeris tape, the former is

calculated. To calculate velocity of the air mass with respect to the planet, an assumption is made that the air mass is rigidly attached to the planet and rotating with the planet. Wind velocities are neglected.

The magnitude of V_a, the air speed, is used in the calculation of Mach number (for the lower atmosphere). The direction of the drag vector is computed by assuming it to be aligned with $-V_a$.

4.4.4.3.2 Drag Coefficient. The coefficient of drag is computed as a function of Mach number. Mach number is computed from air speed, V_a, and the speed of sound, using stored tabular data (paragraph 4.4.4.4.3) for the speed of sound.

Mach number (M) is used as the independent variable and the coefficient of drag (C_D) computed from it. Two tables are stored, one each for M and C_D (each of 40 values), and linear interpolation is used to find the C_D corresponding to a given M.

4.4.4.3.3 Surface Area. Two values of effective surface area are provided as program inputs: one for use in equation (3) for free molecular flow, and one for use in equation (1) for continuum flow.

4.4.4.3.4 Mass. Mass rates are not considered to be a part of the atmospheric models. Schedules for changes in mass are incorporated into the powered flight analysis of the Program.

4.4.4.4 Tables Required

4.4.4.4.1 General. There are three sets of tables required by the Program; the first two sets are functions of the atmospheric medium but are independent of the vehicle, whereas the third is a function both of the vehicle and the mission but not of the medium.

The first set of tables is used to simulate the density of air at the vehicle position in the upper atmospheric model (Harris-Priester) for the Earth. The second set is used to simulate the density and speed-of-sound for low-level atmospheres, not only for the Earth, but for Mars, Venus and Jupiter, as well. The third set is used, for low-level atmospheric models, to calculate the coefficient of drag of the vehicle (zero lift is assumed) as function of both Mach number and the shape of the vehicle (especially near the nose).

4.4.4.4.2 Earth's Upper Atmosphere Tables. Five tables are needed to simulate the Earth's upper atmosphere. Two of the tables give values of a function of three variables, tabulated at discrete values of each of the three variables. The values of each of the three variables at which the functions (logarithm of Harris-Priester $\rho \cdot C_{av}$ data and logarithm of $\rho \cdot C_{av}$ evaluated at the poles) are tabulated, are in turn, listed in three separate tables of argument values. The three independent variables are altitude, solar flux and local solar time. The altitude table has 16 entries, the solar flux table 4 entries, and the local solar time 13 entries.

The first of the two function tables lists the logarithm (base 10) of the product of density (in units of gm/km^3) and mean particle velocity in the medium (in km/sec). This table is stored at every combination of altitude, solar flux, and local solar time and,

therefore, has 16 x 4 x 13 = 1300 entries. The second function table lists the logarithm (base 10) of the product of air density and mean particle velocity but both are evaluated at twilight, i.e., at the poles. This product is a function of altitude and solar flux, and so the table has 16 x 4 = 64 entries. The data for the upper atmosphere tables are taken directly from the findings of Harris and Priester, except for the mean particle velocity. This quantity is computed using the method described in paragraph 4.4.3.6.2.

4.4.4.2.3 Lower Atmosphere Tables. The independent variable used in the lower atmosphere tables is altitude; density and speed of sound are computed from altitude.

Three tables, 50 values each, are stored for the Earth's lower atmosphere: altitude; logarithm (base 10) of density; speed of sound. For a given value of altitude, a table look-up is performed by linear interpolation in the log density and speed of sound tables. Density is then computed by determining the value given by 10 raised to the power equal to the logarithm of density.

Three similar tables are stored for each of the Mars and Venus atmospheres (15 values per table). Density and speed of sound are found in the same manner as for the Earth.

No data are available for the Jupiter atmosphere.

The three Earth tables are obtained from U.S. Standard Atmosphere, 1962, in which densities and speed of sound at all altitudes below 90 km are listed. Above 90 km, speed of sound was calculated as proportional to the square root of temperature divided by mean molecular weight, both of which are available directly. The tables actually go up to 210 km in altitude so that if it is desired to exclude the upper atmosphere, the lower atmosphere can be extended up to 210 km.

The density data for Mars are obtained from Schilling's "mean" Model II Atmosphere. The speed of sound is obtained from temperature and a constant mean molecular weight (same source). The density for Venus is obtained from reference 13. The speed of sound for Venus was calculated from temperature and a constant molecular weight ontained from the same source.

4.4.4.2.4 Vehicle Dependent Tables. The characteristics of one vehicle consists of a surface area (1 value), a table (40 values) of Mach number (independent variable), and a table containing the drag coefficient (dependent variable) for each Mach Number.

4.5 SOLAR RADIATION PRESSURE

4.5.1 INTRODUCTION. Electromagnetic radiation is known to exert a pressure on an intercepting surface. Orbiting planetary satellites having a large surface-area-to-mass ratio are subject to perturbations due to solar radiation pressure. The value of the vehicle's acceleration due to solar radiation pressure is a function of the degree of solar illumination to which the vehicle is subjected. The satellite at a given time may be in it's planet's shadow (figure 4.5-1); under this condition, the planet obscures from the satellite part of or all of the direct sunlight. Three discrete ranges of illuminations are considered in the following analysis: full sunlight; penumbral illumination; no illumination. (Refer to paragraph 3.1.)

4.5.2 ACCELERATION DUE TO RADIATION PRESSURE. The acceleration, $\bar{P}_5$, due to solar radiation pressure is computed from the following equation:

$$P_5 = PC_P \left[\frac{A}{m}\right] \frac{R_{SV}}{R_{SV}^3} \qquad (1)$$

where

P is an illumination factor which is a function of the amount of direct sunlight to which the vehicle is subjected:

P = 1 in full sunlight

P = 0 in umbral region

P in the penumbral region is a function of the degree of satellite shadowing

C_P is a constant related to the total energy radiated from the Sun

R_{SV} is the position of the Sun with respect to the vehicle

The computation of P for the penumbral region is described in paragraph 4.5.4. It is possible that a satellite may lie within the shadows of two or more bodies, e.g., the Earth and the Moon; in such a case, the illumination factor is properly computed by a consideration of the relative geometry among the vehicle, the Sun, and the bodies involved. However, an adequate approximation is obtained by computing separately the penumbral factors (P's) for each body, and setting the total factor equal to the product of the individual factors, i.e.,

$$P_T = P_1 P_2 \cdot \cdot \cdot \cdot P_n \qquad (2)$$

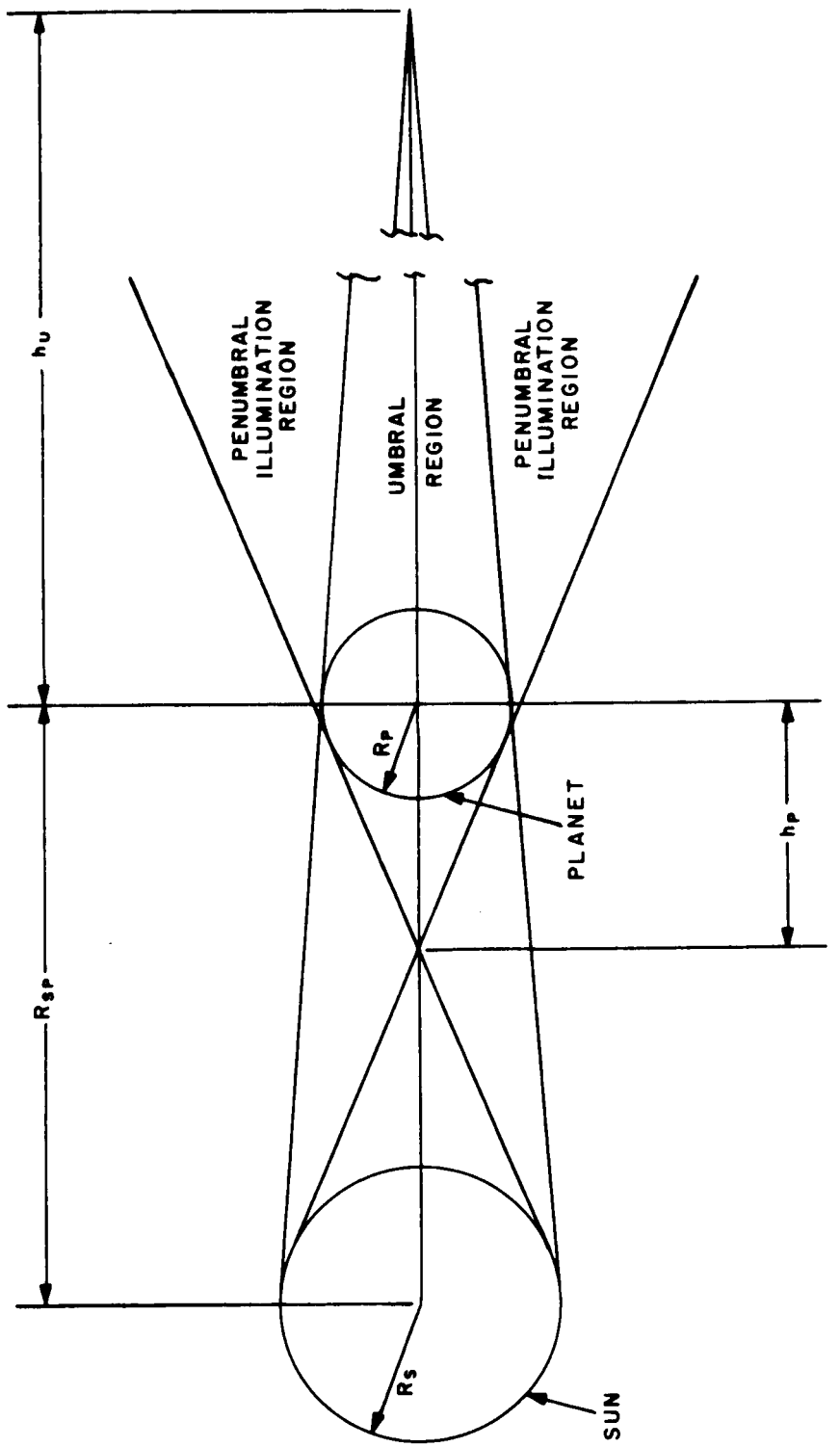

Figure 4.5-1. Satellite Shadowing

4.5.3 SATELLITE SHADOWING. Figure 4.5-1 illustrates the geometry of satellite shadowing, neglecting the effects of atmospheric refraction. By similar triangles, it is seen that the umbral cone has an altitude of

$$h_U = \frac{R_{SP}}{\left[\frac{R_S}{R_P} - 1\right]} \tag{1}$$

Similarly, the altitude of the penumbral cone is given by

$$h_P = \frac{R_{SP}}{\left[\frac{R_S}{R_P} + 1\right]} \tag{2}$$

Atmospheric refraction causes a diffusion of the umbral and penumbral boundaries. Only the Earth's atmosphere is considered dense enough to have a significant effect on these boundaries.

Figure 4.5-2 illustrates the classical approach in defining the semidiameter of the Earth's umbra at the orbit of the Moon, i.e., the semidiameter S_U, of the intersection of the Earth's umbral cone with the plane which (a) passes through the Moon at its mean orbital radius and (b) is normal to the line between centers of the Sun and Earth. From figure 4.5-2,

$$S_U = \pi_M + \pi_S - S_S \tag{3}$$

where

π_M = lunar parallax

π_S = solar parallax

S_S = solar semidiameter

An analogous expression for the semidiameter of the Earth's penumbra, S_P, at the orbit of the Moon may be derived, yielding

$$S_P = \pi_M + \pi_S + S_S \tag{4}$$

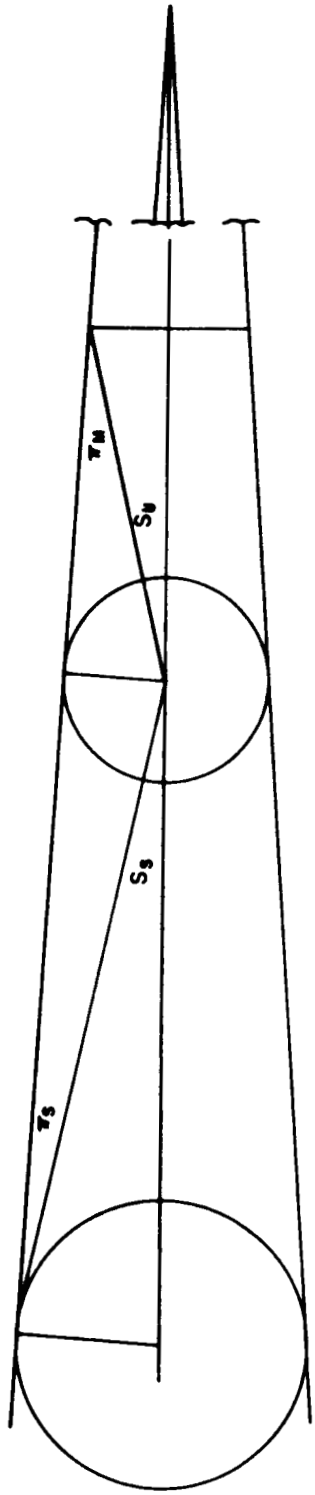

Figure 4.5-2. Semidiameter of Earth's Umbra At Orbit of Moon

Careful observations of lunar eclipses have shown that S_U and S_P are actually about 2% greater than the values given by equations (3) and (4), respectively. Hence,

$$S_U' = 1.02\ (\pi_M + \pi_S - S_S) \tag{5}$$

and

$$S_P' = 1.02\ (\pi_M + \pi_S + S_S) \tag{6}$$

These enlargements arise from refraction due to the Earth's atmosphere (see references 14 and 15). The geometry of both the umbra and penumbra is greatly complicated by the presence of the Earth's atmosphere. The simplest corrections that can be made are to enlarge the central angles of the umbral and penumbral cones.

Criteria will now be developed to determine whether or not a vehicle lies in either of the two shadow zones.

For the umbral region, the planetocentric position P of the cone's apex (figure 4.5-3) is given by

$$P = h_U \frac{R_{SP}}{R_{SP}} \tag{7}$$

Let

$$h_U' = \frac{h_U}{K} \tag{8}$$

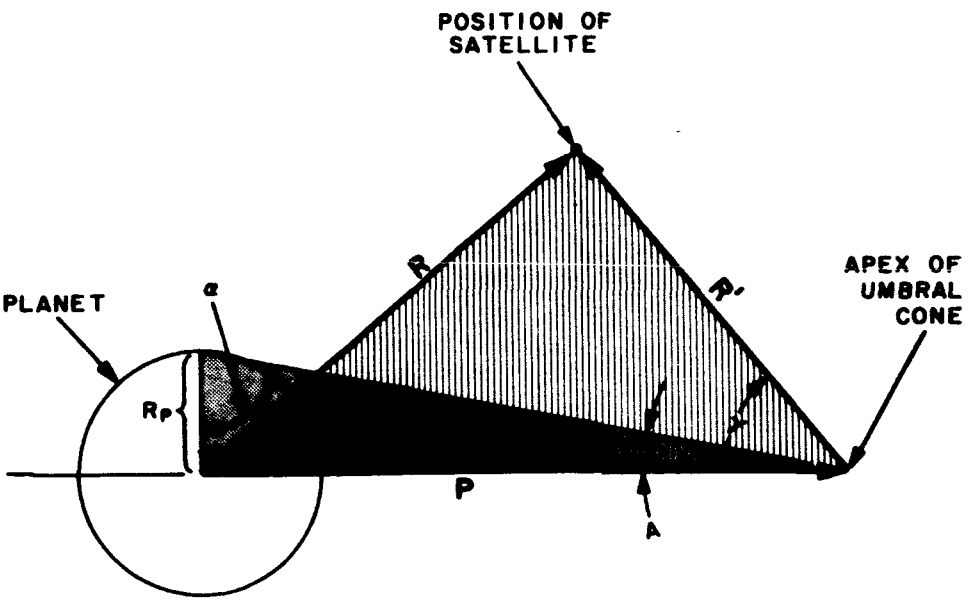

Figure 4.5-3. Umbral Region Geometry

where

$$K = 1.02 \text{ for the Earth}$$

$$K = 1 \text{ for all other planets}$$

From figure 4.5-3, it is seen that the cosine of the cone's central half-angle is equal to sin α:

$$\cos A = \sin \alpha \tag{9}$$

where α includes the effects of refraction.

It can be shown that

$$\cos A = \frac{\frac{h_U'}{R_P}}{\sqrt{1 + \left[\frac{h_U'}{R_P}\right]^2}} \tag{10}$$

If R (figure 4.5-3) represents the satellite's planetocentric position, and if the scalar product $R \cdot P$ is positive, then the satellite is on the side of the planet away from the Sun. Vehicle position with respect to P is given by equation (11)

$$R' = R - P \tag{11}$$

The cosine of the angle, γ, between R' and $-P$ is obtained from the definition of a vector dot product:

$$\cos \gamma = - \frac{(R - P) \cdot R_{SP}}{|R - P| \, R_{SP}} \tag{12}$$

It follows, then, that the satellite lies within the umbral region if cos γ is positive, and if

$$|\cos \gamma| \geq |\cos A|. \tag{13}$$

For the penumbral region, using a similar coordinate system as shown in figure 4.5-4, the position of the cone's apex, Q, is obtained from

$$Q = h_P \frac{R_{SP}}{|R_{SP}|} \tag{14}$$

Let

$$h_P' = \frac{h_P}{K} \tag{15}$$

$$K = 1.02 \text{ for Earth}$$

$$K = 1.0 \text{ for all other planets}$$

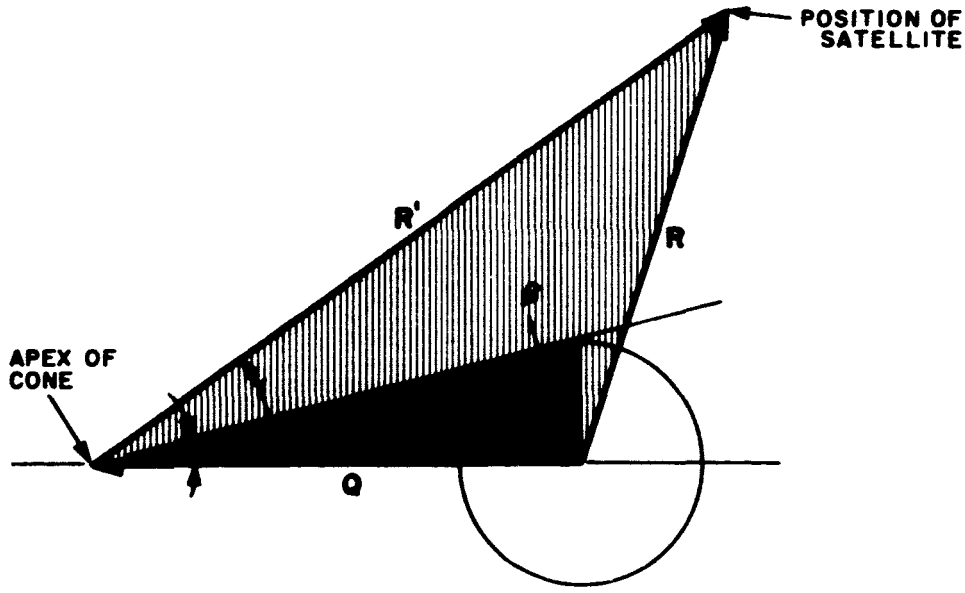

Figure 4.5-4. Penumbral Region Geometry

Then,

$$\cos \beta = \frac{\frac{h_P'}{R_P}}{\sqrt{1 + \left[\frac{h_P'}{R_P}\right]^2}}. \tag{16}$$

Again, if the scalar product, $R \cdot P$, is positive, the satellite is on the shadowed side of the planet. Vehicle position with respect to Q is computed from

$$R' = R - Q. \tag{17}$$

The cosine of the angle between R and -Q is obtained from

$$\cos \gamma = \frac{(R - Q) \cdot R_{SE}}{|R - Q| \, R_{SE}} \tag{18}$$

The satellite lies in the penumbral region if cos γ is positive, and if

$$|\cos \gamma| \geq |\cos B| \tag{19}$$

The foregoing paragraphs have dealt with the problem of satellite shadowing when the Sun is obscured by the body of the object about which the satellite is orbiting. In the Earth-Moon system, another source of shadowing arises, namely, natural eclipses of the Sun by one of the bodies in the system as seen from the other body. Fortunately, the complicated geometry of eclipses need not be computed for the purpose of determining satellite shadowing. The foregoing analysis may be used to account for eclipses. If the satellite is orbiting the Earth, first a test is made to determine whether or not the vehicle lies in

the Earth's shadow; if it does not, a second test is made to see it if lies in the Moon's shadow. Similarly, for a satellite orbiting the Moon, first a test is made to determine if the satellite lies in the Moon's shadow; then a second test is made to determine if it lies in the Earth's shadow.

4.5.4 PENUMBRAL ILLUMINATION FACTOR. To a satellite situated in the penumbra of a planet, the Sun appears as a lune formed by the solar disc and a limb of the planet. (This condition is true, of course, only if the satellite is sufficiently close to the planet; in the limit, as the satellite recedes from the planet, the apparent diameter of the latter becomes so small that the planet appears to be a small speck on the solar disc.) Consequently, the satellite in relatively close proximity to the planet is illuminated by some fraction of the Sun's available radiation, the fraction being a function of the satellite's location within the penumbral region. An expression for this penumbral illumination factor is derived in the following paragraphs.

Consider a satellite at an altitude h above a planet's surface. In this instance, "planet" means any ponderable body in the solar system. To compute the solid angle subtended by the planet from this position, the geometry of figure 4.5-5 is used. From the diagram, it can be shown that

$$c = \sqrt{h\ (h + 2R_P)} \tag{1}$$

$$a = \frac{R_P \sqrt{h\ (h + 2R_P)}}{(R_P + h)} \tag{2}$$

$$b = \frac{hR_P}{(R_P + h)} \tag{3}$$

The angular area of a spherical disc or cap such as the planetary disc shown in figure 4.5-5 is given by the quantity $2\pi H/R$

where

H = depth of disc

R = radius of sphere of which disc is a part

The apparent angular area of the planet's disc is given by

$$\theta_P = \frac{2\pi\ [c - (b + h)]}{c} \tag{4}$$

Substituting equations (32) and (34) into (35) yields

$$\theta_P = 2\pi \left[1 - \frac{\sqrt{h\ (h + 2R_P)}}{(R_P + h)} \right] \tag{5}$$

Similarly, the solid angle subtended by the solar disc from the same position is, approximately,

$$\theta_S = 2\pi \left[1 - \sqrt{1 - \left[\frac{R_S}{R_{SV}} \right]^2} \right] \qquad (6)$$

in which R_{SV} is the distance between the Sun and vehicle and R_S is the solar radius.

Since $R_{SV} >> R_S$,

$$\sqrt{1 - \left[\frac{R_S}{R_{SV}} \right]^2} \approx 1 - \frac{1}{2} \left[\frac{R_S}{R_{SV}} \right]^2 \qquad (7)$$

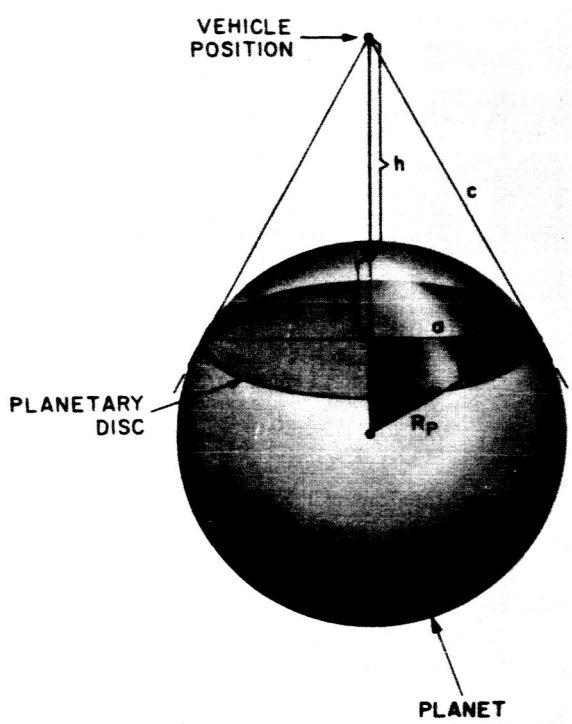

Figure 4.5-5. Planetary Disc

Therefore,

$$\theta_S \simeq \pi \left[\frac{R_S}{R_{SV}} \right]^2 \qquad (8)$$

Similarly, if h becomes large with respect to R_P, equation (5) may be replaced by

$$\theta_P \approx \pi \left[\frac{R_P}{R_P + h} \right]^2 \qquad (9)$$

Equations (5) and (8) establish the relative sizes of the planetary and solar discs. It now remains to compute the percentage obscuration of the former by the latter when the vehicle's position is given. The geometry of this problem is shown in figure 4.5-6. A sphere having a radius greater than $R_{SV} + R_S$ is constructed with the vehicle position as center. Two caps, representing the solar and planetary apparent angular areas, are projected onto the sphere. From the diagram,

$$R_{SV} = R_{SP} + R \tag{10}$$

where

R_{SV} = position of vehicle with respect to the Sun

R_{SP} = position of planet with respect to the Sun

R = position of vehicle with respect to planet

The central angle between the centers of the caps is given by

$$\cos \theta_c = \frac{R \cdot (R_{SP} + R)}{R \, |R_{SP} + R|} \tag{11}$$

$$0 \leq \theta_c \leq \frac{\pi}{2} \tag{12}$$

Figure 4.5-7 illustrates the geometry of the intersection between the two caps. In order to simplify the integration in computing the area of the exposed solar disc, a great circle will be passed through the two points of intersection; this circle will be used to define one of the limits of integration. For the calculations to follow, three coordinate systems are employed:

a. A system (figure 4.5-8) for the cap representing the Sun's disc

b. A system for the cap representing the planet's disc

c. A system for the great circle

All three reference frames are taken to have in common the same y-axis and center of coordinates. Figure 4.5-9 shows the relationships among the three systems. Taking the first system (a) as primary, the second system (b) is related to it by

$$\left.\begin{aligned} x' &= x \cos \theta_c - z \sin \theta_c \\ z' &= z \cos \theta_c + x \sin \theta_c \\ y' &= y \end{aligned}\right\} \tag{13}$$

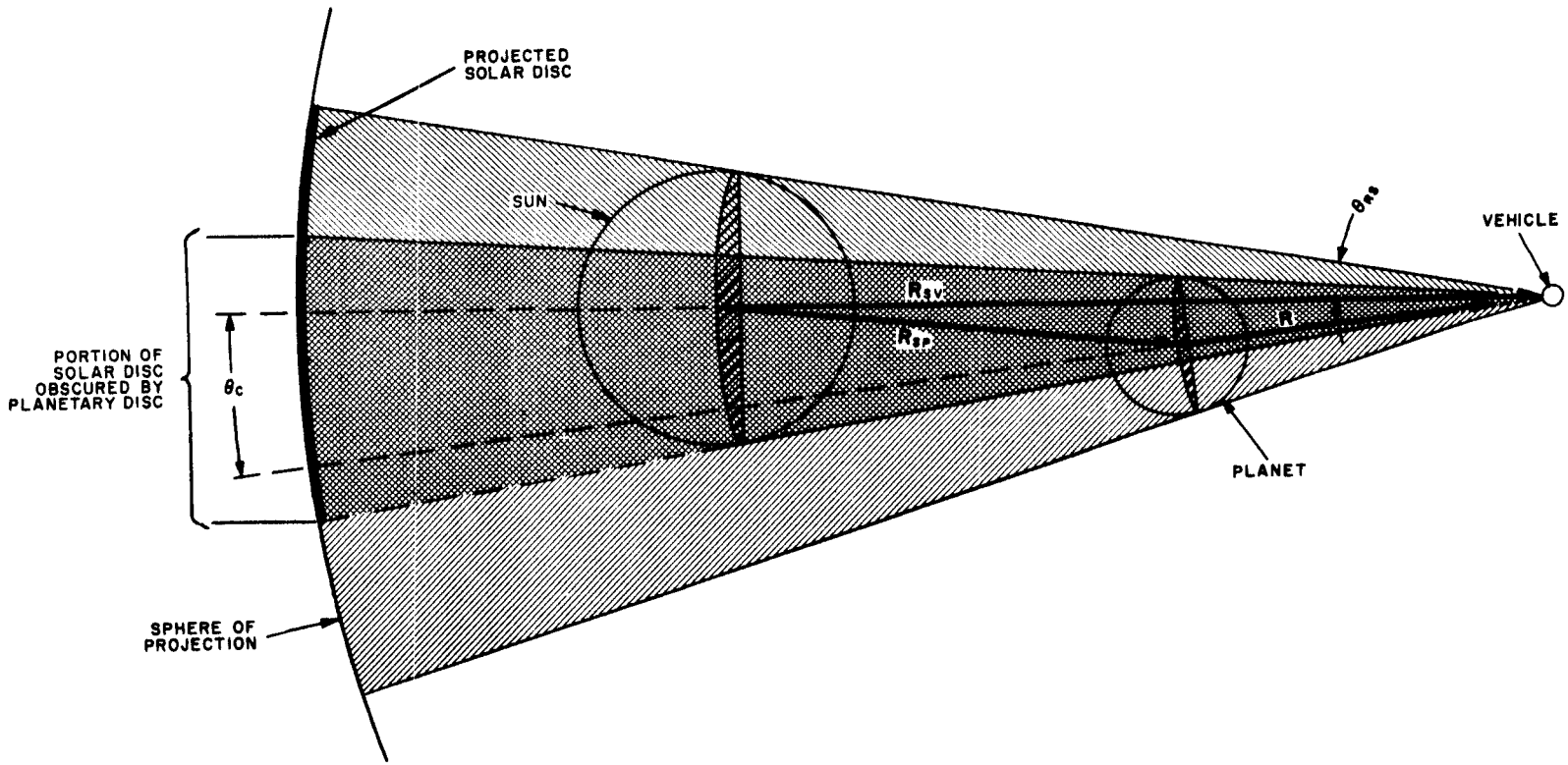

Figure 4.5-6. Solar-Planetary Disc

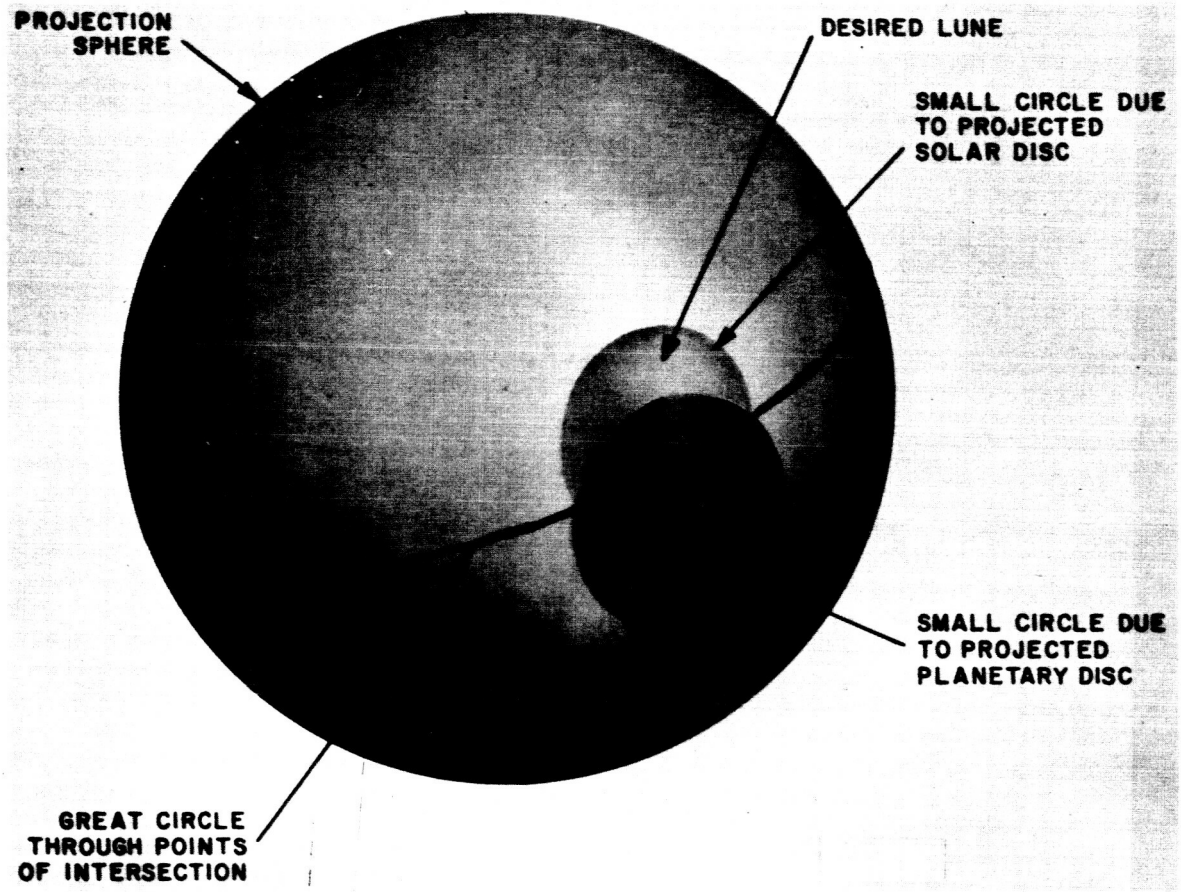

Figure 4.5-7. Solar-Planetary Disc Intersection

where

z' is normal to the planet's disc

and the third system by

$$\left.\begin{aligned} x'' &= x \sin \theta_G + z \cos \theta_G \\ z'' &= z \sin \theta_G - x \cos \theta_G \\ y'' &= y \end{aligned}\right\} \qquad (14)$$

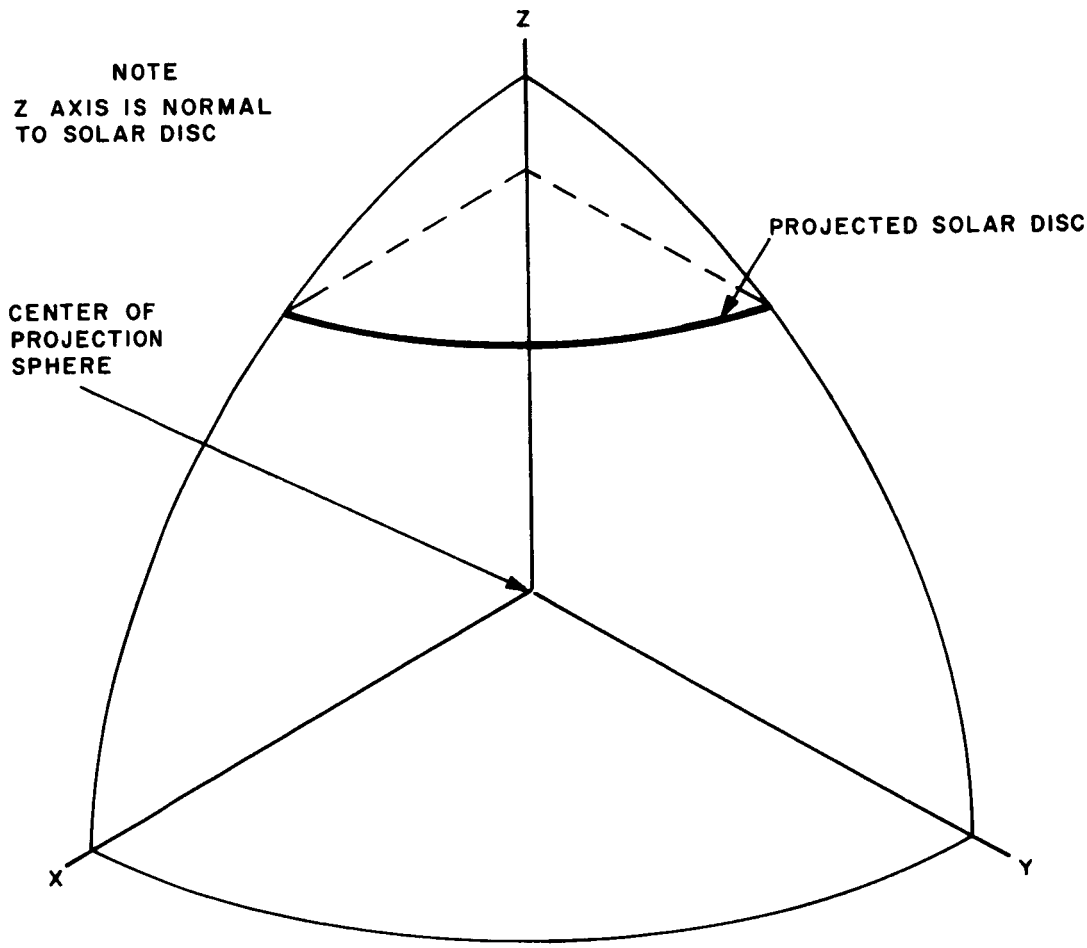

Figure 4.5-8. Orientation of Solar Disc's Coordinate System

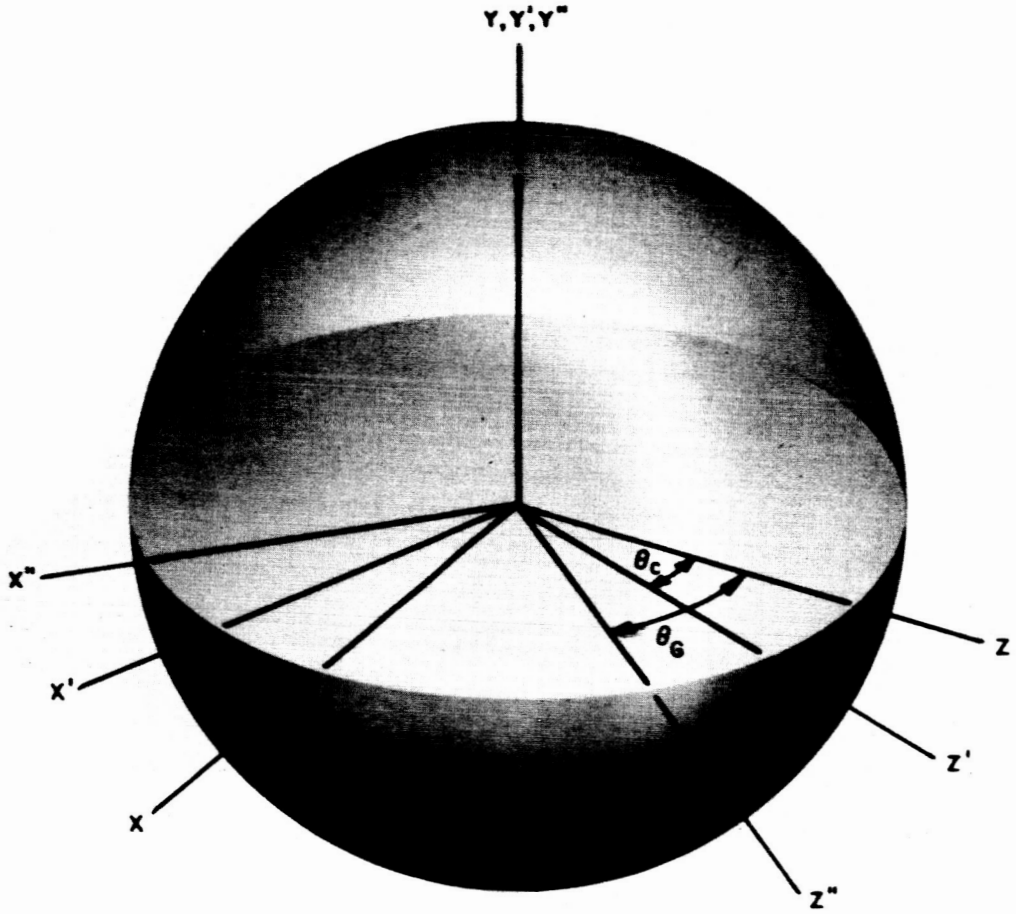

Figure 4.5-9. Coordinate Systems Used in Computations

The set of equations representing the small circle of the Sun's cap is

$$x^2 + y^2 + z^2 = a^2 \tag{15}$$

$$z = (a - H) \tag{16}$$

where

a is the radius of the sphere

H is the height of the cap

Eliminating z from equation (15),

$$x^2 + y^2 = H\ (2a - H) \tag{17}$$

Similarly, the small circle of the planet's cap is given by

$$(x')^2 + y^2 = H'\ (2a - H') \tag{18}$$

Substituting equations (13) into (18) yields

$$(x \cos \theta_c - z \sin \theta_c)^2 + y^2 = H'\ (2a - H') \tag{19}$$

and

$$z' = (a - H') = z \cos \theta_c + x \sin \theta_c \tag{20}$$

Substituting equation (16) into (20) and solving for x:

$$x_P = \frac{a\ (1 - \cos \theta_c) - (H' - H \cos \theta_c)}{\sin \theta_c} \tag{21}$$

where

x_P = x coordinate of point of intersection shown in figure 4.5-8

Solving for y^2 from equation (19)

$$y_P^2 = \frac{H'\ (2a - H') \sin^2 \theta_c - [(a - H') \cos \theta_c - (a - H)]^2}{\sin^2 \theta_c} \tag{22}$$

and

$$z_P = \pm \sqrt{a^2 - x_P^2 - y_P^2} = (a - H) \tag{23}$$

where

y_P and z_P are the y and z coordinates of the point of intersection

For the great circle passing through the intersections of the caps, $z'' = 0$, so that, from equations (14),

$$\tan \theta_G = \frac{x}{z} \tag{24}$$

Evaluating equation (24) at the coordinates of the intersection point:

$$\tan \theta_G = \frac{a\ (1 - \cos \theta_c) - (H' - H \cos \theta_c)}{(a - H) \sin \theta_c} \tag{25}$$

$$-\frac{\pi}{2} \leq \theta_G \leq \frac{\pi}{2} \tag{26}$$

From figure 4.5-6, the angular radius of the solar cap is

$$\theta_{R_S} = \tan^{-1} \frac{R_S}{R_{SV}} \tag{27}$$

Similarly, the angular radius of the planetary cap is given by

$$\theta_{R_P} = \tan^{-1} \frac{a}{h + b} = \tan^{-1} \left[\frac{R_P}{\sqrt{h\ (h + 2R_P)}} \right] \tag{28}$$

The range for θ_c, the angular distance between cap centers can therefore be narrowed to

$$0 \leq \theta_c \leq (\theta_{R_S} + \theta_{R_P})$$

since the sum of $\theta_{R_S} + \theta_{R_P}$ represents the case where the caps are tangent to each other.

Although in the example selected for the previous analysis the solar and planetary discs intersected, it is also possible that (a) they are tangent to each other, or (b) the planetary cap is within the solar cap. (The latter condition arises when the satellite is relatively far from the planet.) To determine whether or not intersections exist, the value of y_P^2 as given in equation (22) may be used as a discriminant:

a. If $y_P^2 > 0$, two intersections exist.

b. If $y_P^2 = 0$, the two caps are tangent, $\theta_c = \theta_{R_S} + \theta_{R_P}$, and there is no obscuration.

c. If $y_P^2 < 0$, the two caps do not intersect and the obscured area is obtained by subtracting the apparent planetary area from the apparent solar area.

Procedures are now developed for computing the percentage obscuration in condition a and c.

The area indicated by the cross-hatched surface (ABC) in figure 4.5-10 corresponds to half of either of the two lunes (figure 4.5-7) formed by the intersection of the great circle and the solar and planetary caps. A general expression will now be developed for the area of this surface. This expression will then be used to compute the areas of the two lunes indicated in figure 4.5-7.

The area of the over-all lune of which the shaded area indicated in figure 4.5-10 is half is given by

$$A_S = 2a^2 \int_0^{\phi_o} d\theta \int_{\theta_a(\phi)}^{\theta_b(\phi)} \sin\theta \, d\theta \qquad (29)$$

where

a is the radius of the sphere

ϕ is the angular displacement, in the x-y plane, from the x axis, positive in the counterclockwise direction

$\theta_a(\phi)$ is the angular displacement of side AC from the z-axis, positive in the counterclockwise direction

$\theta_b(\phi)$ is the angular displacement of side BC from the z-axis, positive in the counterclockwise direction.

Performing the first indicated integration,

$$A_S = 2a^2 \int_0^{\phi_o} \{\cos\theta_a(\phi) - \cos\theta_b(\phi)\} \, d\phi \qquad (30)$$

The maximum area, i.e., when the great circle lies in the x-z plane, which this integral could yield is one-half of the total area of the cap.

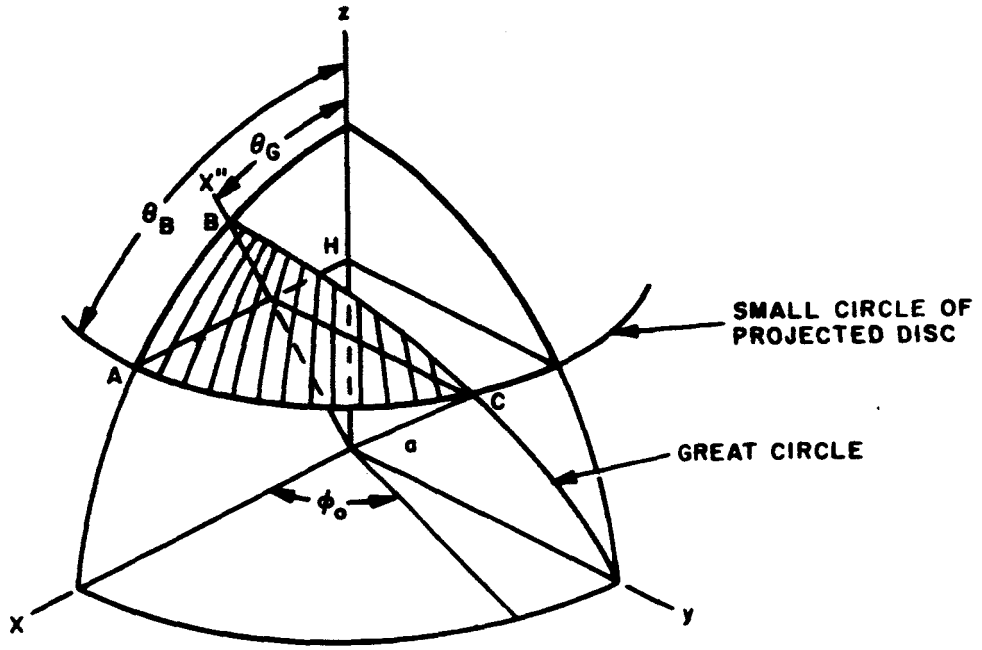

Figure 4.5-10. Area of Spherical Lune

From equation (17), the expression for the small circle of the solar disc is

$$x^2 + y^2 = H\ (2a - H) \tag{31}$$

In polar coordinates,

$$\begin{aligned} x &= a \sin\theta \cos\phi \\ y &= a \sin\theta \sin\phi \\ z &= a \cos\theta \end{aligned} \tag{32}$$

Substituting for x and y in (31):

$$\sin^2\theta \cos^2\phi + \sin^2\theta_b \sin^2\phi = \frac{H(2a - H)}{a^2}$$

For the case of the small circle θ is always equal to θ_b. Therefore,

$$\theta_b(\phi) = \sin^{-1} \frac{\sqrt{H(2a - H)}}{a} \tag{33}$$

The equation of the great circle is

$$(x'')^2 + y^2 = a^2 \tag{34}$$

Substituting from (15),

$$(x \sin\theta_G + z \cos\theta_G)^2 + y^2 = a^2. \tag{35}$$

From (25),

$$\tan\theta_G = \frac{x}{z} \tag{36}$$

Substitution of (36) into (35) yields

$$y^2 \cos^2\theta_G + z^2 = a^2 \cos^2\theta_G \tag{37}$$

Inserting the polar-coordinate relationships from (32):

$$\sin^2\theta \sin^2\phi \cos^2\theta_G + \cos^2\theta = \cos^2\theta_G \tag{38}$$

For the great circle θ is a function of ϕ, i.e., $\theta_a(\phi)$. Therefore,

$$\theta_a(\phi) = \sin^{-1} \frac{\sin\theta_G}{\sqrt{1 - \sin^2\phi \cos^2\theta_G}} \tag{39}$$

Using the limits given by equations (33) and (39) in the integral of equation (30),

$$A_S = 2a^2 \int_0^{\phi_o} \cos\left[\sin^{-1} \frac{\sin \theta_G}{\sqrt{1 - \sin^2\phi \cos^2\theta_G}}\right] d\phi$$

$$- 2a^2\phi_o \cos\left[\sin^{-1} \frac{\sqrt{H\ (2a - H)}}{a^2}\right] \qquad (40)$$

Rewriting equation (40),

$$A_S = 2a^2 \cos \theta_G \int_0^{\phi_o} \frac{\cos \phi\ d\phi}{\sqrt{1 - \sin^2\phi \cos^2\theta_G}} - 2a\ (a - H)\ \phi_o \qquad (41)$$

Rearranging the integral in (38),

$$\cos \theta_G \int \frac{\cos \phi\ d\phi}{\sqrt{1 - \sin^2\phi \cos^2\theta_G}} = \int \frac{\cos \phi\ d\phi}{\sqrt{\sec^2\theta_G - \sin^2\phi}}$$

$$= \int \frac{dx}{\sqrt{c^2 - x^2}} = \sin^{-1} \frac{x}{c} \qquad (42)$$

where

$$x = \sin \phi$$

$$c = \sec \theta_G$$

Therefore,

$$A_S = 2a^2 \sin^{-1}\left[\sin \phi_o \cos \theta_G\right] - a\ (a - H)\ \phi_o \qquad (43)$$

NOTE: In the computation of A_S, the definition of ϕ_o (figure 4.5-10) limits it to the range $0 \leq \phi_o \leq \pi/2$. Therefore, if ϕ_o is actually in the second quadrant, use $(\phi_o - \pi/2)$ for the evaluation of equation (43).

From figure 4.5-10, it is evident that

$$\sin \phi_o = \frac{y_P}{\sqrt{x_P^2 + y_P^2}}$$

$$\cos \phi_o = \frac{x_P}{\sqrt{x_P^2 + y_P^2}}$$

where x_P and y_P are obtained from equations (21) and (22), respectively. The positive sign is taken for the square root when computing y_P. In addition,

$$x_P^2 + y_P^2 = H\ (2a - H) \tag{46}$$

For the planetary cap,

$$A_P = 2a^2 \sin^{-1} \left[\sin \phi_o' \cos \theta_G'\right] - 2a\ (a - H')\ \phi_o' \tag{47}$$

where

$$\tan \theta_G' = \frac{x'}{z'} \tag{48}$$

and ϕ_o' is limited, for the evaluation of equation (47), to values between 0 and $\pi/2$. Taking the values of the intersection point from equations (21) and (23), and transforming them to the planetary cap's coordinate system (x', y', z') by equations (13),

$$\tan \theta_G' = \frac{(H - H' \cos \theta_c) - a\ (1 - \cos \theta_c)}{(a - H')\ \sin \theta_c} \tag{49}$$

$$-\frac{\pi}{2} \leq \theta_G' \leq \frac{\pi}{2} \tag{50}$$

$$\sin \phi_o' = \frac{y_P}{\sqrt{H'\ (2a - H')}} \tag{51}$$

$$\cos \phi_o' = \frac{x_P \cos \theta_c - (a - H) \sin \theta_c}{\sqrt{H'\ (2a - H')}} \tag{52}$$

From the geometry of the intersection of the solar and planetary caps (figures 4.5-7 through 4.5-9), it can be shown that the effective projected area of the solar cap, A_{SC}, varies with the quadrant of ϕ_o and ϕ_o' in the manner shown in table 4.5-1.

Table 4.5-1. Table for Computation of A_{SC}

ϕ_o (quadrant)	ϕ_o' (quadrant)	A_{SC} Equals
First	Second	$2\pi aH - A_S$
Second	Second	A_S
First	First	A_S
Second	First	$2\pi aH - A_S$

The area of the exposed solar-disc is given by

$$A_{EX} = A_{SC} - A_P \tag{53}$$

The forgoing calculations have been made on the basis of a sphere of radius a; these results are now normalized by setting $a = 1$. Normalizing the remaining quantities,

$$\frac{H}{a} = \frac{\theta_S}{2\pi} = 1 - \sqrt{1 - \left[\frac{R_S}{R_{SV}}\right]^2} \tag{54}$$

$$\frac{H'}{a} = \frac{\theta_P}{2\pi} = \frac{1 - \sqrt{h\ (h + 2R_P)}}{(R_P + h)} \tag{55}$$

The penumbral illumination factor is computed from

$$P = \frac{A_{EX}}{\theta_S} \tag{56}$$

For the case where $y_p^2 < 0$, the illumination factor is computed from

$$P = 1 - \frac{\theta_P}{\theta_P}. \tag{57}$$

SECTION 5
STATISTICAL COMPUTATIONS

5.1 INTRODUCTION

The primary function of an orbit determination program is to compute a best estimate of spacecraft position and velocity from observations. In making these computations, the meaning of "best estimate" is defined in some statistical sense, as, for example, minimum variance or least squares. Used as a scientific tool, the program can also update estimates of biases occurring in the dynamic and observational models.

Statistical estimates are obtained for the linearized components of the state vector. The most elementary state vector is composed of the six elements given by $[\delta R\ \delta \dot{R}]^T$, in which δR and $\delta \dot{R}$ represent differential displacements from some nominal trajectory. In practice, the infinitesimal differentials are replaced by finite increments, so that

$$[\Delta R\ \Delta \dot{R}]^T \cong [\delta R\ \delta \dot{R}]^T \tag{1}$$

Using more compact notation to represent the state vector, let

$$\Delta x = [\Delta R\ \Delta \dot{R}]^T \tag{2}$$

Linearization is also applied to the observations. For each data time, an observation is computed from the corresponding point on the nominal trajectory. A vector of observation residuals is formed from

$$\Delta y = O_{ACT} - O_{COMP} \tag{3}$$

where

O_{COMP} is the vector of computed observations;

O_{ACT} is the vector of actual observations.

In terms of these definitions, statistical processing entails inferring Δx given the components of Δy.

For all types of statistical estimation in which linearized variables are employed, three important matrices occur: Φ, the state transition matrix; M, the matrix of observation partial derivatives; and P, the variance-covariance (usually called covariance) matrix of the state vector components. For the state vector of equation (2), the transition matrix relates the state at time t to the state at time t_o:

$$\Delta x(t) = \Phi(t, t_o)\, \Delta x(t_o) \tag{4}$$

The matrix M describes the deterministic relationship between small changes in the state vector and the corresponding changes in the vector of residuals:

$$\Delta y(t) = M(t)\, \Delta x(t) \tag{5}$$

A full treatment of this matrix is given in paragraph 6.3. Turning finally to the covariance matrix, its structure is an array of elements given by:

$$P = \begin{bmatrix} \sigma_x^2 & \rho_{xy}\sigma_x\sigma_y & \rho_{xz}\sigma_x\sigma_y & \cdots & \rho_{x\dot{z}}\sigma_x\sigma_{\dot{z}} \\ \rho_{yx}\sigma_y\sigma_x & \sigma_y^2 & \rho_{yz}\sigma_y\sigma_z & \cdots & \rho_{y\dot{z}}\sigma_y\sigma_{\dot{z}} \\ \vdots & \vdots & \vdots & \vdots & \vdots \\ \rho_{\dot{z}x}\sigma_{\dot{z}}\sigma_x & \rho_{\dot{z}y}\sigma_{\dot{z}}\sigma_y & \rho_{\dot{z}z}\sigma_{\dot{z}}\sigma_z & \cdots & \sigma_{\dot{z}}^2 \end{bmatrix} \tag{6}$$

where

σ_i^2 = the variance of the i^{th} component

$\rho_{ij} = \rho_{ji}$ = the correlation factor between the i^{th} and j^{th} components. Because the correlation between x_i and x_j is the same as the correlation between x_j and x_i, the covariance matrix is symmetrical.

By augmenting the state vector, it is possible to obtain estimates of dynamical and observational biases. Dynamical biases are those parameters which influence a vehicle's orbital motion, and include biases in all gravitational quantities and in the thrust profile of the spacecraft. Observational biases, on the other hand, include those parameters such

as uncertainties in station location or in the speed of light which corrupt the data and contribute to errors in the knowledge of the vehicle state. Both classifications of bias are processed in the same manner in the statistical estimation procedure. The form of the augmented state vector is

$$\delta x_a = [\delta R \quad \delta \dot{R} \quad \delta B_d \quad \delta B_o]^T \tag{7}$$

in which δB_d is a vector of dynamical biases and δB_o a vector of observational biases. These bias parameters have also been linearized, so that δB_d and δB_o represent differential offsets from a set of nominal values.

For δx_a, the state transition matrix becomes

$$\Phi_a(t, t_o) = \left[\begin{array}{c|c|c} \Phi(t, t_o) & \Phi_d(t, t_o) & 0 \\ \hline 0 & I_d & 0 \\ \hline 0 & 0 & I_o \end{array}\right] \tag{8}$$

The partition $\Phi(t, t_o)$ is defined by equation (4). $\Phi_d(t, t_o)$ is a $6 \times k$ matrix relating the differentials of position and velocity to δB_d. The null matrix in the upper right partition has dimension $6 \times \ell$, and relates position and velocity to the observational biases. Dimensions k and ℓ are the number of dynamical parameters and the number of observational parameters, respectively. I_d is a $k \times k$ unit matrix and I_o is an $\ell \times \ell$ unit matrix. The remaining null matrices show that no relation exists between the two classifications of bias, or between the biases and Δx. Overall dimension for $\Phi_a(t, t_o)$ is $(6 + k + \ell) \times (6 + k + \ell)$.

Similarly, the M matrix is expanded to be compatible with the augmented state vector:

$$M_a(t) = [M(t) \quad 0 \quad M_o(t)]. \tag{9}$$

M(t) is defined by equation (5); the null matrix relates the dynamical biases to the observations and has dimension $n \times k$; $M_o(t)$ is a matrix of partial derivatives relating the observational biases to Δy and has dimension $n \times \ell$. The quantity n is the number of observation types.

Augmenting the covariance matrix,

$$P_a = \left[\begin{array}{c|c|c} P & P_{Xd} & P_{Xo} \\ \hline P_{dX} & P_d & P_{do} \\ \hline P_{oX} & P_{od} & P_o \end{array}\right] \tag{10}$$

where P is defined by equation (6), and P_d and P_o are the covariance matrices for the dynamical biases and observational biases, respectively. P has dimensions 6 x 6; P_d is k x k; P_o is ℓ x ℓ. The partitions P_{Xd}, P_{Xo}, and P_{do} contain, respectively, the covariances between ΔX and the dynamical parameters, between ΔX and the observational parameters, and between the two types of parameters themselves. P_a is symmetric and has dimensions $(6+k+\ell) \times (6+k+\ell)$.

5.2 THE GODDARD PARAMETERS

Reference 16 shows that differential correction matrices computed for state vectors like ΔX become singular after a relatively short time. It is further shown in the reference that the optimum set of variables is one in which only one component in the set depends upon the energy of the orbit. Such a set has been developed, and, in this Program, the vehicle state is described by six quantities called the Goddard (or α) parameters. The state transition matrix $\Phi(t, t_o)$ is replaced by the parameter transition matrix $\Psi(t, t_o)$, the matrix of observation partial derivatives M(t) becomes the array of derivatives N(t), and the state variable covariance matrix P(t) is transformed into the parameter covariance matrix Q(t).

The six differential α - parameters are defined as follows (reference 17):

$\Delta\alpha_1$: a small rotation of $\dot{R}$ about R in such a way as to keep $R \cdot \dot{R}$ a constant.

$\Delta\alpha_2$: a small rotation of R about $\dot{R}$ in such a way as to keep $R \cdot \dot{R}$ a constant.

$\Delta\alpha_3$: a small rotation of R and $\dot{R}$ simultaneously about $H = R \times \dot{R}$, the angular momentum vector.

$\Delta\alpha_4$: a small change in 1/a, where a is the major semiaxis of the osculating two-body orbit. This parameter is the only one of the set affected by energy.

$\Delta\alpha_5$: a small change in R, the magnitude of $\mathbf{R}$, such that a and $\mathbf{R} \cdot \dot{\mathbf{R}}$ remain invariant.

$\Delta\alpha_6$: a small change in $\mathbf{R} \cdot \dot{\mathbf{R}}$ caused by a small rotation of $\mathbf{R}$ about $\mathbf{H}$.

The first three differential parameters leave the shape and size of the orbit invariant and change only its orientation in space, whereas the last three affect the orbital configuration.

To use the α - parameters in statistical estimation, it is necessary to establish their relationship with the conventional state vector $\Delta\mathbf{x}$, and then to establish relations between Φ and Ψ, M and N, and between P and Q. The fundamental transformation is

$$\Delta\mathbf{x} = \mathbf{S}\,\Delta\boldsymbol{\alpha}, \tag{11}$$

$\boldsymbol{\alpha}$ being the vector of differential parameters. By definition, the parameter transition matrix relates the new linearized variables at two different times:

$$\Delta\boldsymbol{\alpha}(t) = \Psi(t, t_o)\,\Delta\boldsymbol{\alpha}(t_o) \tag{12}$$

Between Ψ and Φ, the following transformation exists:

$$\Phi(t, t_o) = \mathbf{S}(t)\,\Psi(t, t_o)\,\mathbf{S}^{-1}(t_o). \tag{13}$$

The covariance matrix for the parameters, Q, is related to P by

$$\mathbf{P}(t) = \mathbf{S}(t)\,\mathbf{Q}(t)\,\mathbf{S}^{T}(t), \tag{14}$$

and the matrix of observation partial derivatives, N, is related to M by

$$\mathbf{N}(t) = \mathbf{M}(t)\,\mathbf{S}(t). \tag{15}$$

Augmentation of the transformation matrix S is simply

$$\mathbf{S}_a = \begin{bmatrix} \mathbf{S} & \vdots & \mathbf{0} \\ \cdots & \vdots & \cdots \\ \mathbf{0} & \vdots & \mathbf{I} \end{bmatrix} \tag{16}$$

where S is defined by equation (11). The inverse of S_a is

$$S_a^{-1} = \begin{bmatrix} S^{-1} & 0 \\ 0 & I \end{bmatrix} \tag{17}$$

The matrix S is a point transformation entirely expressable in terms of spacecraft position and velocity at some time.

$$S = \begin{bmatrix} -\frac{H}{V} & 0 & \frac{H \times R}{H} & \frac{H \times R}{H^2} & \frac{\mu D (H \times R)}{2(VH)^2} & \frac{R}{R} - \frac{\mu D (1 - R/a)(H \times R)}{(RVH)^2} \\ 0 & \frac{H}{R} & \frac{H \times \dot{R}}{H} & 0 & -\frac{\mu \dot{R}}{2V^2} & -\frac{\mu \dot{R}}{(RV)^2} \end{bmatrix} \tag{18}$$

$$S^{-1} = \begin{bmatrix} -\frac{VH}{H^2} & 0 \\ 0 & \frac{RH}{H^2} \\ 0 & \frac{H \times \dot{R}}{H V^2} \\ \dot{R} & R \\ -\frac{2R}{R^3} & -\frac{2\dot{R}}{\mu} \\ \frac{R}{R} & 0 \end{bmatrix} \tag{19}$$

In equations (18) and (19),

$$V = |\dot{R}| \tag{20a}$$

$$H = |H| \tag{20b}$$

$$H = R \times \dot{R} \tag{20c}$$

$$D = R \cdot \dot{R} \tag{20d}$$

It is assumed in the Program that a two-body state transition matrix is sufficiently accurate for statistical estimation. With this assumption, Ψ may be expressed in closed form.

$$\Psi(t, t_o) = \left[\begin{array}{ccc|ccc} \frac{V}{V_o} f & -\frac{V}{R_o} g & 0 & 0 & 0 & 0 \\ -\frac{R}{V_o} \dot{f} & \frac{R}{R_o} \dot{g} & & 0 & 0 & 0 \\ 0 & 0 & 1 & a_{3,4} & a_{3,5} & a_{3,6} \\ \hline 0 & 0 & 0 & \dot{g} & a_{4,5} & R_o \dot{f} \\ 0 & 0 & 0 & 0 & 1 & 0 \\ 0 & 0 & 0 & \frac{g}{R} & a_{6,5} & \frac{R_o}{R} f \end{array}\right] \tag{21}$$

where f and g, $\dot{f}$ and $\dot{g}$ are functions describing motion on a Keplerian orbit as defined by equations (1) and (2) of paragraph 3.2.2. The subscript "0" identifies quantities pertaining to the initial time t_o; all other quantities are associated with the time t. This closed-form formulation is computationally more convenient than having to calculate the elements of Φ from the variational equations or by the secant method.

$$a_{3,4} = \frac{H}{V^2}\left\{\left[\frac{\dot{g} - 1}{R^2} - \frac{R_o \dot{f}^2}{\mu} - \frac{\dot{f}}{H^2}\left[\frac{\mu}{R} g - D_o\right]\right]\right. \tag{22}$$

$$a_{3,5} = \frac{\mu \dot{f} H}{2(VV_o)^2}\left\{\left[\dot{g} + \frac{D_o}{H^2}\left[\frac{\mu}{R} g - D_o\right]\right]\right.$$

$$+ \frac{\sqrt{\mu}\, H\beta^2}{2R^3 V^2}\left\{\left[R_o (F_3)^3 + \frac{D_o \beta F_2}{\sqrt{\mu}}\left[(F_3)^2 + F_2\right]\right.\right.$$

$$\left.\left.\left. + \beta^2 (-3 F_6 + F_5 - F_1 F_2 + (F_2)^2 + F_1 (F_3)^2)\right]\right\} \tag{23}$$

$$a_{3,6} = \frac{H \dot{f}}{R_o V^2}\left\{\left[\frac{R_o}{R} F_4 + \left[\frac{R_o}{R}\right]^2 - \frac{\mu \dot{g}}{R_o V_o^2} + \frac{\mu D_o}{H^2 R_o V_o^2}\left[1 - \frac{R_o}{a}\right]\left[\frac{\mu g}{R} - D_o\right]\right]\right\} \tag{24}$$

$$a_{4,5} = \frac{\sqrt{\mu}}{R}\left\{\left[-R_o^2 \beta \Sigma_1 - \frac{D_o R_o}{\sqrt{\mu}} \beta^2 \Sigma_2 - \frac{D_o^2 \beta^3}{\mu} \Sigma_3\right.\right.$$

$$\left.\left. + R_o \beta^3 \Sigma_4 + \frac{D_o \beta^4}{\sqrt{\mu}} \Sigma_5 + \beta^5 \Sigma_6\right]\right\} \tag{25}$$

$$a_{6,5} = \frac{\beta^2}{R}\left\{\left[-\frac{R_o^2}{2} S_1 - \frac{D_o R_o}{\sqrt{\mu}} \beta S_2 + R_o \beta^2 S_3\right.\right.$$

$$\left.\left. + \frac{D_o^2 \beta^2}{\mu} S_4 + \frac{D_o \beta^3}{\sqrt{\mu}} S_5 + \beta^4 S_6\right]\right\} \tag{26}$$

$$F_1 = \frac{1}{6} - \alpha F_6 \tag{27a}$$

$$F_2 = \frac{1}{2} - \alpha F_5 \tag{27b}$$

$$F_3 = 1 - \alpha F_1 \tag{27c}$$

$$F_4 = 1 - \alpha F_2 \tag{27d}$$

$$F_5 = \frac{1}{24} - \alpha F_7 \tag{27e}$$

$$F_6 = \sum_{i=o}^{\infty} \frac{(-\alpha)^i}{(2i + 5)!} \tag{27f}$$

$$F_7 = \sum_{i=o}^{\infty} \frac{(-\alpha)^i}{(2i + 6)!} \tag{27g}$$

$$\alpha = \frac{X^2}{a} \tag{28}$$

where X is Herrick's variable (proportional to differential eccentric anomaly), and a is the major semiaxis of the orbit. The remaining functions are defined as follows:

$$\beta^2 = - a \alpha = - X^2 \tag{29}$$

$$\Sigma_1 = F_3 \cdot F_4 \tag{30a}$$

$$\Sigma_2 = F_2 \cdot (1 + 2 F_4) \tag{30b}$$

$$\Sigma_3 = F_2 \cdot F_3 \tag{30c}$$

$$\Sigma_4 = \frac{3F_2}{2} - \frac{3F_1}{2} - 2 F_2 \cdot F_3 \tag{30d}$$

$$\Sigma_5 = \frac{3F_1}{2} - 3F_5 - 2(F_2)^2 \tag{30e}$$

$$\Sigma_6 = \frac{F_5}{2} - \frac{3F_6}{2} - F_1 \cdot F_2 \tag{30f}$$

$$S_1 = (F_3)^2 \tag{31a}$$

$$S_2 = F_2 \cdot F_3 \tag{31b}$$

$$S_3 = \frac{F_1}{2} - F_5 - F_1 \cdot F_3 \tag{31c}$$

$$S_4 = F_5 - \frac{F_1}{2} - \frac{F_1 \cdot F_3}{2} \tag{31d}$$

$$S_5 = \Sigma_6 \tag{31e}$$

$$S_6 = \frac{F_6}{2} - 2F_7 - \frac{(F_1)^2}{2} \tag{31f}$$

5.3 MINIMUM VARIANCE FILTER

Having available the necessary linearized observations, a state vector, and the associated matrices Φ, M, and P (or Ψ, N, and Q), by what means shall a statistical estimate of the state vector components be obtained? One important estimator is the minimum variance filter, for which the optimum estimate is expressed by

$$\Delta\bar{x} = K\ \Delta y, \tag{32}$$

K being the optimal filter. The error, ϵ, in the estimate is

$$\epsilon = \Delta\bar{x} - K\ \Delta y, \tag{33}$$

and the covariance of this error is the expectation of $\epsilon\epsilon^T$:

$$P = E(\epsilon\epsilon^T) \tag{34}$$

Since the variances of the error components are given by the trace of P, a minimum variance estimate is obtained by solving for those components of Δx which minimize tr(P). Following Battin (reference 18),

$$d\sigma^2 = d\ E(\epsilon^T\ \epsilon) = d[tr(P)] = tr\ [d\ P] \tag{35}$$

where "tr" indicates trace. Substituting (33) and (34) into (35) and setting $d\sigma^2$ equal to zero,

$$d\sigma^2 = tr\ \{ d\ [E(\Delta\bar{x}\ \Delta\bar{x}^T) - E(\Delta\bar{x}\ \Delta y^T)K^T - K\ E(\Delta y\ \Delta\bar{x}^T) + K\ E(\Delta y\ \Delta y^T)\ K^T] \} = 0, \tag{36}$$

or,

$$2\ tr\ [K\ E(\Delta y\ \Delta y^T) - E(\Delta x\ \Delta y^T)]\ d\ K^T = 0. \tag{37}$$

Equation (37) must be valid for arbitrary $d\ K^T$; consequently,

$$K = E(\Delta\bar{x}\ \Delta y^T)\ [E(\Delta y\ \Delta y^T)]^{-1} \tag{38}$$

To evaluate $E(\Delta\bar{x}\ \Delta y^T)$, consider the relation

$$\Delta y = M\ \Delta\bar{x} + e \tag{39}$$

where M is the matrix of partial derivatives relating the observations to the state, and e is the vector of errors in the sensors. Then,

$$E(\Delta\bar{x}\ \Delta y^T) = E(\Delta\bar{x}\ \Delta\bar{x}^T)\ M^T = P\ M^T \tag{40}$$

Using equation (39) again, $E(\Delta x\ \Delta y^T)$ may be computed:

$$E(\Delta y\ \Delta y^T) = MPM^T + \epsilon^2 \tag{41}$$

Hence, the optimum filter is given by

$$K = P\ M^T\ [MP\ M^T + \epsilon^2]^{-1} \tag{42}$$

Employing the Goddard parameters for statistical updating,

$$\Delta\bar{\alpha} = L\,\Delta y \tag{43a}$$

$$L = Q\,N^T\,[NQN^T + \epsilon^2]^{-1} \tag{43b}$$

In the minimum variance procedure, data are processed sequentially, i.e., one data point at a time. There may be several observations at a data point, but they are all simultaneous. The estimate of the state, therefore, depends upon a priori knowledge of the state and its covariance matrix at some initial time, and upon the data gathered between that time and the last data point. Consider a typical minimum variance sequence using, for convenience, conventional state variables rather than the α-parameters. Assume that at t_o, the covariance matrix is $P(t_o)$, and that $\mathbf{R}_o$ and $\dot{\mathbf{R}}_o$ are known. Assume also that the first data point occurs at t_1. Position and velocity are updated by integrating the equations of motion from t_o to t_1 with $\mathbf{R}_o$ and $\dot{\mathbf{R}}_o$ as initial conditions. Between data points, P is updated by means of the state transition matrix:

$$P(t_1^-) = \Phi(t_1,\ t_o)\ P(t_o)\ \Phi^T(t_1,\ t_o) \tag{44}$$

The matrix $P(t_1^-)$ is used in equation (42) to obtain the optimum filter, which, in turn, is used to calculate the optimum estimate of the state from equation (32). A new value for this matrix is computed from

$$P(t_1^+) = (I - KM)\ P(t_1^-) \tag{45}$$

where I is a unit matrix of proper deminsionality, and where the minus and plus superscripts refer to instants just before and just after the processing of data, respectively. Time t_1 now becomes the initial point for the updating process, and the steps just outlined are repeated. Equation (44) may be derived by computing the expectation of $\Delta\bar{\mathbf{x}}(t)$ using the updated linearized state vector

$$\Delta\bar{\mathbf{x}}(t_1) = \Phi(t_1,\ t_o)\ \Delta\bar{\mathbf{x}}(t_o). \tag{46}$$

Equation (45) is obtained by forming the expectation of ϵ, where ϵ is given by equation (33).

Minimum variance estimation is especially useful in error analyses. In this application, a nominal trajectory is specified together with data points along the orbit. An initial estimate of the covariance matrix is needed as well as a measure of the data quality at each point. The matrix P is then propagated from data point to data point, using equation (44) between data times, and equation (45) at a data time. No real data are required and no observations need be computed.

In an earlier version of this Program, an error analysis mode was developed in which P, the covariance matrix of $\Delta\mathbf{x}$, is propagated, but in which the effects of dynamical and observational biases on P are accounted for by additive terms. Between data points, then, equation (44) becomes

$$P(t_1^-) = \Phi(t_1, t_o)\, P(t_o)\, \Phi^T(t_1, t_o) + \Omega(t_1, t_o) \tag{47}$$

in which $\Omega(t_1, t_o)$ is a matrix dependent upon the dynamical biases. At a data point, P is updated by

$$P(t_1^+) = (I - KM)\, P(t_1^-) + \Gamma(t_1), \tag{48}$$

where $\Gamma(t_1)$ is a matrix depending upon both the dynamical and observational biases. Besides its employment in error analyses, this technique has also been used for processing data where it is important to account for the effect of biases but not necessary to compute their values.

5.4 BAYES' ESTIMATION

Consider the normal equations in the classical least-squares formulation:

$$\begin{aligned} M_1\, \Delta x_a &= \Delta y_1 - e_1 \\ M_2\, \Delta x_a &= \Delta y_2 - e_2 \\ &\vdots \\ M_p\, \Delta x_a &= \Delta y_p - e_p \end{aligned} \tag{49}$$

Ordinarily, in orbit determination, each equation in the set obtains at a given time so that the p measurements may be considered data points in time. Each vector Δy_i contains up to n components; the dimensions of Δx_a, on the other hand, are $(6 + k + \ell) \times 1$. Compressing equation (49) into compact notation,

$$B\, \Delta x_a = \Delta y - e \tag{50}$$

where

$$B = [M_1^T \; M_2^T \cdots M_p^T]^T$$

$$\Delta y = [\Delta y_1^T \; \Delta y_2^T \cdots \Delta y_p^T]^T \qquad (51)$$

$$e = [e_1^T \; e_2^T \cdots e_p^T]^T$$

For least squares, the optimization criterion requires the choice of components for Δx_a which minimize the scalar

$$e^2 = e^T e = (B \Delta x_a - \Delta y)^T (B \Delta x_a - \Delta y) \qquad (52)$$

Taking partial derivatives of e^2 with respect to the components of Δx_a and setting the result to zero:

$$\nabla_x e^2 = (B \Delta x_a - \Delta y)^T B + B^T (B \Delta x_a - \Delta y) = 0, \qquad (53)$$

where the operator ∇_x implies taking the gradient in the vector space defined by Δx_a. Since

$$(B \Delta x_a - \Delta y)^T B = [B^T (B \Delta x_a - \Delta y)]^T, \qquad (54a)$$

equation (53) states that the sum of a vector and it transpose are zero. Consequently, the vector itself is identically zero:

$$B^T B \Delta x_a = B^T \Delta y \qquad (54b)$$

The optimum estimate in the least-squares sense is, then,

$$\Delta x_a = (B^T B)^{-1} B^T \Delta y. \qquad (55)$$

The least-square estimate of equation (55) makes no use of a priori information. In orbit determination, such information is usually available in the form of an initial covariance matrix, and the Program can employ this matrix in a least-square calculation called Bayes' estimation. One form of Bayes' theorem relates the conditional probability

distribution of the initial state, given the data, to the conditional probability distribution of the data, given the initial state, and the distributions of the data and the initial state:

$$p(\Delta x_a(0)/\Delta y) = \frac{p(\Delta y/\Delta x_a(0))\ p(\Delta x_a(0))}{p(\Delta y)} \tag{56}$$

In equation (56), $\Delta x_a(0)$ is the initial state vector. The optimization criterion is again the minimization of e^2; expressing this minimization in terms of Bayes' theorem requires finding the components of $\Delta x_a(0)$ which correspond to the mean of the conditional distribution $p(\Delta x_a(0)/\Delta y)$. Since the distributions are assumed to be Gaussian, the distribution of the initial state, within a multiplicative factor, is

$$p(\Delta x_a(0)) = \exp -\frac{1}{2}\{\Delta x_a{}^T(0)\ P^{-1}(0)\ \Delta x_a\}, \tag{57}$$

P 0) being the covariance matrix of $\Delta x_a(0)$. To find $p(\Delta y)$, write equation (50) as

$$\Delta y = B\ \Phi_a\ \Delta x_a(0) + e, \tag{58}$$

where

$$\Phi_a = [\Phi_1{}^T\ \ \Phi_2{}^T \cdots \Phi_p{}^T]^T. \tag{59}$$

Each Φ_i is the state transition matrix from $t = t_o$ to $t = t_i$. The covariance matrix for Δy is the expectation

$$E(\Delta y\ \Delta y^T) = Y = B\ \Phi_a\ P(0)\ \Phi_a{}^T\ B^T + e^2. \tag{60}$$

Hence, within a multiplication factor, the distribution of Δy is

$$p(\Delta y) = \exp -\frac{1}{2}\{\Delta y^T\ Y^{-1}\ \Delta y\}. \tag{61}$$

The conditional distribution of Δy given $\Delta x_a(0)$ is simply proportional to the distribution of the observational errors:

$$p(\Delta y/\Delta x_a(0)) = \exp -\frac{1}{2}\{e^T\ (e^2)^{-1}\ e\} \tag{62}$$

Substituting equations (57), (61), and (62) into equation (56),

$$p(\Delta x_a(0)/\Delta y) = \exp -\frac{1}{2}\{\Delta x_a{}^T(0)\ P^{-1}(0)\ \Delta x_a(0) + e^T(e^2)^{-1}\ e - \Delta y^T\ Y^{-1}\ \Delta y\}. \tag{63}$$

Substituting for Y from equation (60),

$$p(\Delta x_a(0)/\Delta y) = \exp -\frac{1}{2}\{[\Delta x_a{}^T(0) - \Delta y^T\ D^T\ P'(0)][P'(0)]^{-1}[\Delta x_a(0) - P'(0)\ D\ \Delta y]\} \tag{64}$$

where

$$[P'(0)]^{-1} = [P(0)]^{-1} + \Phi^T\ B^T\ [e^2]^{-1}\ B\ \Phi, \tag{65}$$

$$D = \Phi^T\ B^T\ [e^2]^{-1} \tag{66}$$

The optimal estimate for $\Delta x_a(0)$ is that vector which gives the mean value of $p(\Delta x_a(0)/\Delta y)$:

$$\Delta\bar{x}_a(0) = P'(0)\ D\ \Delta y. \tag{67}$$

In the Program, $P'(0)$ and D are computed recursively from the following formulae:

$$[P_i']^{-1} = [P_{i-1}']^{-1} + \Phi_i{}^T\ B_i{}^T\ [e^2]^{-1}\ B_i\ \Phi_i \tag{68}$$

$$D_i = D_{i-1} + \Phi_i{}^T\ B_i{}^T\ \Delta y_i, \tag{69}$$

D being defined by

$$D_i = D_i\ \Delta y \tag{70}$$

At the last point in the data batch, $[P_i']^{-1}$ is inverted and multiplied into D_p to give the optimal estimate of the state:

$$\Delta\bar{x}(0) = P_P'\ D_P \tag{71}$$

Equation (67) gives the updated estimate of the initial state vector and equation (65) gives the updated estimate of the initial covariance matrix. The problem arises, then, of obtaining updated estimates of P and Δx_a at some other time, given the initial estimates. Elements of the state vector pertaining to dynamical and observational biases are constants and so are invariant in time. To obtain updated estimates of position and velocity, one may use the optimal estimates of the initial conditions to integrate forward to any desired time point, or less accurately, the differential elements of the initial state vector may be transferred forward by the state transition matrix. As shown by equation (44), the covariance matrix may also be updated by means of the transition matrix. It is interesting to note that if the elements of $[P(0)]^{-1}$ are set equal to zero, the resulting estimate is exactly that given by a weighted least-squares regression.

Another type of Bayes' estimate employs recursive calculations which give updated estimates of Δx_a and P at each data time. In this procedure, the size of the data batch is limited to one data point. The covariance matrix is computed from

$$P'(t) = P(t) - P(t)\,\Phi^T M^T \left[MP(t)M^T + e^2\right]^{-1} M\Phi P(t),$$

and the optimal estimate of the state vector from

$$\Delta\bar{x}_a(t) = P'(t)\,\Phi^T M^T \left[e^2\right]^{-1} \Delta y$$

This recursive form of Bayes' estimate has been shown to be equivalent to the Kalman filter (reference 19). The equivalency, however, does not imply that the computational methods are the same, as can be seen by comparing equation (73) with equations (32) and (42).

5.5 BIAS ERRORS

Augmentation of the state vector and its associated matrices to accommodate dynamical and observational biases has been discussed in paragraph 5.1. It remains for this paragraph to tabulate the biases included in the program and to describe some of the calculations peculiar to the estimation of these parameters.

The dynamic biases determined by the Program are the uncertainties in the following:

- Products of the universal gravitational constant and the masses of the Earth, Sun, Moon, Mars, Venus, Jupiter and Saturn
- Area-to-mass ratio used in computing radiation pressure
- Magnitude of the solar flux
- Area-to-mass ratio used in computing air drag
- The lunar gravitational coefficients, A, B and C

- Twenty-four of the Earth's gravitational coefficients of the type $C_{n,m}$
- Fifteen of the Earth's gravitational coefficients of the type $S_{n,m}$
- Eighteen coefficients describing thrust acceleration
- The starting and ending times of a thrust period

The observational biases determined by the Program are the uncertainties in the following:

- Geodetic net corrections, Δu, Δv and Δw
- Station orientation angles, Δe_e, Δe_n, Δe_v
- Parameters of the refraction correction model:

  n_o, index of refraction at the Earth's surface;

  h, altitude above Earth;

  h_o, altitude of bottom of F_2 layer;

  h_m, altitude of maximum density of F_2 layer;

  ρ_o, maximum electron density of F_2 layer.

- Measurement timing, Δt
- The velocity of light, Δc.

The partition $\Phi_d(t, t_o)$ (see equation (8)) of the augmented state transition matrix is obtained by means of the secant method. This partition is composed of elements which relate the differentials of position and velocity to the differential dynamic biases. Consequently, numerical derivatives are computed because the variables are not related by a differentiable analytic expression.

Paragraph 6.3 contains the partitions for augmenting the M matrix. Uncertainties in the observations are added to the computed observations of paragraph 6.2.

5.6 POWERED FLIGHT PARAMETERS

5.6.1 GENERAL. As developed in paragraph 3.4, a nominal trajectory is computed during powered flight from the time series solution to equation (3) of that paragraph. To obtain this solution, it is assumed that the thrust acceleration, P_3, is expressible as a polynomial in time. In processing data during a thrust period, uncertainties in the characteristics of the thrust polynomial are included as bias states. These characteristics are the time of the start of burn, the time of the end of burn, and the coefficients of the thrust acceleration polynomial.

It is assumed that the state transition matrix of the nominal trajectory is a sufficiently close approximation to the true transition matrix so that sensitivity coefficients computed from the time series solution may be used for statistical computation during powered flight. Using only the vehicle state and the thrust polynomial coefficients as elements of the state vector, the state transition matrix may be partitioned in this manner:

$$\Phi_a = \left[\begin{array}{c|c|c|c|c|c|c} \Phi & \Phi(0) & \Phi(1) & \cdots & \Phi(5) & \Phi^{(b)} & 0 \\ \hline 0 & \multicolumn{5}{c|}{I} & \end{array}\right] \qquad (74)$$

The partition Φ contains terms of the form $\partial x_i(t)/\partial x_j(t_o)$, the x_i representing components of vehicle position and velocity. Each augmented partition $\Phi^{(0)}$, $\Phi^{(1)}$, $\cdots$, contains partial derivatives relating the x_i to the coefficients of the thrust polynomial. $\Phi^{(0)}$, for example, has terms of the form $\partial x_i(t)/\partial \alpha_o$, $\partial x_i(t)/\partial \beta_o$, $\partial x_i(t)/\partial \gamma_o$. The partition $\Phi^{(b)}$ relates the x_i to the start of burn so that its components are $\partial x_i(t)/\partial t_b$. During powered flight, the last partition, $\Phi^{(f)}$, relating the x_i to the end of burn, is zero. At the completion of powered flight, its elements have the form $\partial x_i(t)/\partial t_f$.

Because of size limitations within the program, the number of biases to be updated has been restricted to twenty. Each of the $\Phi^{(k)}$, $k = 0, 1, 2, \cdots, 5$ are 6×3 arrays, whereas both $\Phi^{(b)}$ and $\Phi^{(f)}$ are 6×1 column vectors. The partition Φ is 6×6. The null matrix in equation (74) is 20×6, and the identity matrix I is 20×20.

5.6.2 THE TRANSITION MATRIX $\Phi(t, t_o)$. Table 5-1 lists the elements of the "conventional" state transition matrix by which the components of the vehicle state are related to their initial values. Since the three elements of each lower half-column are the time derivatives of the three corresponding elements in the upper half-column, only eighteen sets of coefficients need be computed. Typical coefficients are listed in table 5-2.

To compute the coefficients of table 5-2, take derivatives of equations (18), paragraph 3.4.2, with respect to $x_j(0)$, where

$$\begin{aligned} x_1(0) &= x_o \\ x_2(0) &= y_o \\ x_3(0) &= z_o \\ x_4(0) &= \dot{x}_o \\ x_5(0) &= \dot{y}_o \\ x_6(0) &= \dot{z}_o \end{aligned} \qquad (75)$$

Then,

$$\frac{\partial a_{m+2}}{\partial x_j(0)} = \frac{-\mu}{(m+1)(m+2)} \left\{ d_m \frac{\partial x_o}{\partial x_j(0)} + d_{m-1} \frac{\partial \dot{x}_o}{\partial x_j(0)} + \sum_{k=o}^{m-2} d_{m-k-2} \frac{\partial a_{k+2}}{\partial x_j(0)} \right.$$

$$\left. + \sum_{\ell=o}^{m} a_\ell \frac{\partial d_{m-\ell}}{\partial x_j(0)} \right\} \tag{76}$$

$$\frac{\partial b_{m+2}}{\partial x_j(0)} = \frac{-\mu}{(m+1)(m+2)} \left\{ d_m \frac{\partial y_o}{\partial x_j(0)} + d_{m-1} \frac{\partial \dot{y}_o}{\partial x_j(0)} + \sum_{k=o}^{m-2} d_{m-k-2} \frac{\partial b_{k+2}}{\partial x_j(0)} \right.$$

$$\left. + \sum_{\ell=o}^{m} b_\ell \frac{\partial d_{m-\ell}}{\partial x_j(0)} \right\} \tag{77}$$

$$\frac{\partial c_{m+2}}{\partial x_j(0)} \equiv \frac{-\mu}{(m+1)(m+2)} \left\{ d_m \frac{\partial z_o}{\partial x_j(0)} + d_{m-1} \frac{\partial \dot{z}_o}{\partial x_j(0)} + \sum_{k=o}^{m-2} d_{m-k-2} \frac{\partial c_{k+2}}{\partial x_j(0)} \right.$$

$$\left. + \sum_{\ell=o}^{m} c_\ell \frac{\partial d_{m-\ell}}{\partial x_j(0)} \right\} \tag{78}$$

In equations (76) through (78),

$$\frac{\partial x_i(0)}{\partial x_j(0)} = \delta_{ij} \tag{79}$$

Table 5-1. Elements of State Transition Matrix, $\Phi(t, 0)$

	x_o	y_o	z_o	$\dot{x}_o$	$\dot{y}_o$	$\dot{z}_o$
x	$1 + \sum_{m=o}^{\infty} \frac{\partial a_{m+2}\, t^{(m+2)}}{\partial x_o}$	$\sum_{m=o}^{\infty} \frac{\partial a_{m+2}\, t^{(m+2)}}{\partial y_o}$	$\sum_{m=o}^{\infty} \frac{\partial a_{m+2}\, t^{(m+2)}}{\partial z_o}$	$t + \sum_{m=o}^{\infty} \frac{\partial a_{m+2}\, t^{(m+2)}}{\partial \dot{x}_o}$	$\sum_{m=o}^{\infty} \frac{\partial a_{m+2}\, t^{(m+2)}}{\partial \dot{y}_o}$	$\sum_{m=o}^{\infty} \frac{\partial a_{m+2}\, t^{(m+2)}}{\partial \dot{z}_o}$
y	$\sum_{m=o}^{\infty} \frac{\partial b_{m+2}\, t^{(m+2)}}{\partial x_o}$	$1 + \sum_{m=o}^{\infty} \frac{\partial b_{m+2}\, t^{(m+2)}}{\partial y_o}$	$\sum_{m=o}^{\infty} \frac{\partial b_{m+2}\, t^{(m+2)}}{\partial z_o}$	$\sum_{m=o}^{\infty} \frac{\partial b_{m+2}\, t^{(m+2)}}{\partial \dot{x}_o}$	$t + \sum_{m=o}^{\infty} \frac{\partial b_{m+2}\, t^{(m+2)}}{\partial \dot{y}_o}$	$\sum_{m=o}^{\infty} \frac{\partial b_{m+2}\, t^{(m+2)}}{\partial \dot{z}_o}$
z	$\sum_{m=o}^{\infty} \frac{\partial c_{m+2}\, t^{(m+2)}}{\partial x_o}$	$\sum_{m=o}^{\infty} \frac{\partial c_{m+2}\, t^{(m+2)}}{\partial y_o}$	$1 + \sum_{m=o}^{\infty} \frac{\partial c_{m+2}\, t^{(m+2)}}{\partial z_o}$	$\sum_{m=o}^{\infty} \frac{\partial c_{m+2}\, t^{(m+2)}}{\partial \dot{x}_o}$	$\sum_{m=o}^{\infty} \frac{\partial c_{m+2}\, t^{(m+2)}}{\partial \dot{y}_o}$	$t + \sum_{m=o}^{\infty} \frac{\partial c_{m+2}\, t^{(m+2)}}{\partial \dot{z}_o}$
$\dot{x}$	$\sum_{m=o}^{\infty} \frac{(m+2)\, \partial a_{m+2}\, t^{(m+1)}}{\partial x_o}$	$\sum_{m=o}^{\infty} \frac{(m+2)\, \partial a_{m+2}\, t^{(m+1)}}{\partial y_o}$	$\sum_{m=o}^{\infty} \frac{(m+2)\, \partial a_{m+2}\, t^{(m+1)}}{\partial z_o}$	$1 + \sum_{m=o}^{\infty} \frac{(m+2)\, \partial a_{m+2}\, t^{(m+1)}}{\partial \dot{x}_o}$	$\sum_{m=o}^{\infty} \frac{(m+2)\, \partial a_{m+2}\, t^{(m+1)}}{\partial \dot{y}_o}$	$\sum_{m=o}^{\infty} \frac{(m+2)\, \partial a_{m+2}\, t^{(m+1)}}{\partial \dot{z}_o}$
$\dot{y}$	$\sum_{m=o}^{\infty} \frac{(m+2)\, \partial b_{m+2}\, t^{(m+1)}}{\partial x_o}$	$\sum_{m=o}^{\infty} \frac{(m+2)\, \partial b_{m+2}\, t^{(m+1)}}{\partial y_o}$	$\sum_{m=o}^{\infty} \frac{(m+2)\, \partial b_{m+2}\, t^{(m+1)}}{\partial z_o}$	$\sum_{m=o}^{\infty} \frac{(m+2)\, \partial b_{m+2}\, t^{(m+1)}}{\partial \dot{x}_o}$	$1 + \sum_{m=o}^{\infty} \frac{(m+2)\, \partial b_{m+2}\, t^{(m+1)}}{\partial \dot{y}_o}$	$\sum_{m=o}^{\infty} \frac{(m+2)\, \partial b_{m+2}\, t^{(m+1)}}{\partial \dot{z}_o}$
$\dot{z}$	$\sum_{m=o}^{\infty} \frac{(m+2)\, \partial c_{m+2}\, t^{(m+1)}}{\partial x_o}$	$\sum_{m=o}^{\infty} \frac{(m+2)\, \partial c_{m+2}\, t^{(m+1)}}{\partial y_o}$	$\sum_{m=o}^{\infty} \frac{(m+2)\, \partial c_{m+2}\, t^{(m+1)}}{\partial z_o}$	$\sum_{m=o}^{\infty} \frac{(m+2)\, \partial c_{m+2}\, t^{(m+1)}}{\partial \dot{x}_o}$	$\sum_{m=o}^{\infty} \frac{(m+2)\, \partial c_{m+2}\, t^{(m+1)}}{\partial \dot{y}_o}$	$1 + \sum_{m=o}^{\infty} \frac{(m+2)\, \partial c_{m+2}\, t^{(m+1)}}{\partial \dot{z}_o}$

Table 5-2. Typical Coefficients for the State Transition Matrix, $\Phi(t, 0)$

Column 1	Column 2	Column 3	Column 4	Column 5	Column 6
$\frac{\partial a_{n+2}}{\partial x_o}$	$\frac{\partial a_{n+2}}{\partial y_o}$	$\frac{\partial a_{n+2}}{\partial z_o}$	$\frac{\partial a_{n+2}}{\partial \dot{x}_o}$	$\frac{\partial a_{n+2}}{\partial \dot{y}_o}$	$\frac{\partial a_{n+2}}{\partial \dot{z}_o}$
$\frac{\partial b_{n+2}}{\partial x_o}$	$\frac{\partial b_{n+2}}{\partial y_o}$	$\frac{\partial b_{n+2}}{\partial z_o}$	$\frac{\partial b_{n+2}}{\partial \dot{x}_o}$	$\frac{\partial b_{n+2}}{\partial \dot{y}_o}$	$\frac{\partial b_{n+2}}{\partial \dot{z}_o}$
$\frac{\partial c_{n+2}}{\partial x_o}$	$\frac{\partial c_{n+2}}{\partial y_o}$	$\frac{\partial c_{n+2}}{\partial z_o}$	$\frac{\partial c_{n+2}}{\partial \dot{x}_o}$	$\frac{\partial c_{n+2}}{\partial \dot{y}_o}$	$\frac{\partial c_{n+2}}{\partial \dot{z}_o}$

where δ_{ij} is Kronecker's delta. In addition,

$$\frac{\partial d_i}{\partial x_j(0)} = \frac{-1}{i\, D_o} \sum_{\ell=1}^{i} \left[\frac{\ell}{2} + i\right] \left\{ D_\ell \frac{\partial D_{i-\ell}}{\partial x_j(0)} - \frac{D_\ell\, d_{i-\ell}}{D_o} \frac{\partial D_o}{\partial x_j(0)} + d_{i-\ell} \frac{\partial D_\ell}{\partial x_j(0)} \right\}. \quad (80)$$

$$\frac{\partial D_i}{\partial x_j(0)} = \sum_{\ell=o}^{i} \left[\left\{ a_\ell \frac{\partial a_{i-\ell}}{\partial x_j(0)} + a_{i-\ell} \frac{\partial a_\ell}{\partial x_j(0)} \right\} + \left\{ b_\ell \frac{\partial b_{i-\ell}}{\partial x_j(0)} + b_{i-\ell} \frac{\partial b_\ell}{\partial x_j(0)} \right\} \right.$$

$$\left. + \left\{ c_\ell \frac{\partial c_{i-\ell}}{\partial x_j(0)} + c_{i-\ell} \frac{\partial c_\ell}{\partial x_j(0)} \right\} \right] \quad (81)$$

Since

$$D = R_o^2$$

$$d_o = \frac{1}{R_o^3} \quad (82)$$

then

$$\frac{\partial D_o}{\partial x_j(0)} = 2 R_o \frac{\partial R_o}{\partial x_j(0)} \tag{83}$$

$$\frac{\partial d_o}{\partial x_j(0)} = - \frac{3}{R_o^4} \frac{\partial R_o}{\partial x_j(0)} \tag{84}$$

and

$$\frac{\partial R_o}{\partial x_j(0)} = \frac{1}{R_o} \left\{ x_o \frac{\partial x_o}{\partial x_j(0)} + y_o \frac{\partial y_o}{\partial x_j(0)} + z_o \frac{\partial z_o}{\partial x_j(0)} \right\} . \tag{85}$$

or

$$\frac{\partial R_o}{\partial x_j(0)} = \frac{1}{R_o} \{ x_o \delta_{1j} + y_o \delta_{2j} + z_o \delta_{3j} \} . \tag{86}$$

5.6.3 **THE AUGMENTED STATE TRANSITION MATRIX.** The matrices of partial derivatives $\Phi^{(k)}$ have dimensions 6 x 3. A typical matrix of this type may be written as follows:

$$\Phi^{(k)} = \begin{bmatrix} \frac{\partial x}{\partial \alpha_k} & \frac{\partial x}{\partial \beta_k} & \frac{\partial x}{\partial \gamma_k} \\ \frac{\partial y}{\partial \alpha_k} & \frac{\partial y}{\partial \beta_k} & \frac{\partial y}{\partial \gamma_k} \\ \frac{\partial z}{\partial \alpha_k} & \frac{\partial z}{\partial \beta_k} & \frac{\partial z}{\partial \gamma_k} \\ \frac{\partial \dot{x}}{\partial \alpha_k} & \frac{\partial \dot{x}}{\partial \beta_k} & \frac{\partial \dot{x}}{\partial \gamma_k} \\ \frac{\partial \dot{y}}{\partial \alpha_k} & \frac{\partial \dot{y}}{\partial \beta_k} & \frac{\partial \dot{y}}{\partial \gamma_k} \\ \frac{\partial \dot{z}}{\partial \alpha_k} & \frac{\partial \dot{z}}{\partial \beta_k} & \frac{\partial \dot{z}}{\partial \gamma_k} \end{bmatrix} . \tag{87}$$

Since

$$\frac{\partial R_o}{\partial \alpha_k} = 0$$

$$\frac{\partial \dot{R}_o}{\partial \alpha_k} = 0 \tag{88}$$

the first column is given by

$$\frac{\partial x}{\partial \alpha_k} = \sum_{n=o}^{\infty} \frac{\partial a_{n+2}\, t^{(n+2)}}{\partial \alpha_k} \tag{89a}$$

$$\frac{\partial y}{\partial \alpha_k} = \sum_{n=o}^{\infty} \frac{\partial b_{n+2}\, t^{(n+2)}}{\partial \alpha_k} \tag{89b}$$

$$\frac{\partial z}{\partial \alpha_k} = \sum_{n=o}^{\infty} \frac{\partial c_{n+2}\, t^{(n+2)}}{\partial \alpha_k} \tag{89c}$$

$$\frac{\partial \dot{x}}{\partial \alpha_k} = \sum_{n=o}^{\infty} \frac{(n+2)\, \partial a_{n+2}\, t^{(n+1)}}{\partial \alpha_k} \tag{89d}$$

$$\frac{\partial \dot{y}}{\partial \alpha_k} = \sum_{n=o}^{\infty} \frac{(n+2)\, \partial b_{n+2}\, t^{(n+1)}}{\partial \alpha_k} \tag{89e}$$

$$\frac{\partial \dot{z}}{\partial \alpha_k} = \sum_{n=o}^{\infty} \frac{(n+2)\, \partial c_{n+2}\, t^{(n+1)}}{\partial \alpha_k} \tag{89f}$$

Expansions for the second and third columns are similar. As in the "conventional" state transition matrix, the three elements in the lower half-column are the time derivatives of the corresponding elements in the upper half-column. For each value of k, only nine sets of elements need be computed as shown in table 5-3.

Table 5-3. Coefficients for the Augmented Transition Matrix, $\Phi^{(k)}$

Column 1	Column 2	Column 3
$\frac{\partial a_{m+2}}{\partial \alpha_k}$	$\frac{\partial a_{m+2}}{\partial \beta_k}$	$\frac{\partial a_{m+2}}{\partial \gamma_k}$
$\frac{\partial b_{m+2}}{\partial \alpha_k}$	$\frac{\partial b_{m+2}}{\partial \beta_k}$	$\frac{\partial b_{m+2}}{\partial \gamma_k}$
$\frac{\partial c_{m+2}}{\partial \alpha_k}$	$\frac{\partial c_{m+2}}{\partial \beta_k}$	$\frac{\partial c_{m+2}}{\partial \gamma_k}$

Again starting with equations (18), paragraph 3.4.2, and performing the indicated differentiations for the coefficients of the first row:

$$\frac{\partial a_{m+2}}{\partial \alpha_k} = \frac{1}{(m+1)(m+2)}\left\{\delta_{m,k} - \mu \sum_{j=o}^{m}\left[d_{m-j}\frac{\partial a_j}{\partial \alpha_k} + a_j \frac{\partial d_{m-j}}{\partial \alpha_k}\right]\right\} \tag{90a}$$

$$\frac{\partial a_{m+2}}{\partial \beta_k} = \frac{-\mu}{(m+1)(m+2)} \sum_{j=o}^{m}\left[d_{m-j}\frac{\partial a_j}{\partial \beta_k} + a_j \frac{\partial d_{m-j}}{\partial \beta_k}\right] \tag{90b}$$

$$\frac{\partial a_{m+2}}{\partial \gamma_k} = \frac{-\mu}{(m+1)(m+2)} \sum_{j=o}^{m}\left[d_{m-j}\frac{\partial a_j}{\partial \gamma_k} + a_j \frac{\partial d_{m-j}}{\partial \gamma_k}\right] \tag{90c}$$

Let $\xi_k^{\,i}$ be α_k. β_k. γ_k such that

$$\begin{aligned} \xi_k^{\,1} &= \alpha_k \\ \xi_k^{\,2} &= \beta_k \\ \xi_k^{\,3} &= \gamma_k \end{aligned} \tag{91}$$

Then

$$\begin{aligned} \frac{\partial a_o}{\partial \xi_k^{\,i}} &= \frac{\partial a_1}{\partial \xi_k^{\,i}} = 0 \\ \frac{\partial a_2}{\partial \xi_k^{\,1}} &= \frac{\delta_{2,k}}{2} \; ; \frac{\partial a_2}{\partial \xi_k^{\,i}} = 0, \quad i \neq 1. \end{aligned} \tag{92}$$

In addition,

$$\frac{\partial d_{m-j}}{\partial \xi_k^{\,i}} = \frac{-1}{(m-j)\, D_o} \sum_{p=1}^{m-j} \left[\frac{P}{2} + m - j \right] \left[D_p \frac{\partial d_{m-j-p}}{\partial \xi_k^{\,i}} + d_{m-j-p} \frac{\partial D_p}{\partial \xi_k^{\,i}} \right] \tag{93}$$

and

$$\begin{aligned} \frac{\partial D_p}{\partial \xi_k^{\,i}} = \sum_{\ell=o}^{P} \Bigg\{ & a_\ell \frac{\partial a_{p-\ell}}{\partial \xi_k^{\,i}} + a_{p-\ell} \frac{\partial a_\ell}{\partial \xi_k^{\,i}} + b_\ell \frac{\partial b_{p-\ell}}{\partial \xi_k^{\,i}} + b_{p-\ell} \frac{\partial b_\ell}{\partial \xi_k^{\,i}} \\ & + c_\ell \frac{\partial c_{p-\ell}}{\partial \xi_k^{\,i}} + c_{p-\ell} \frac{\partial c_\ell}{\partial \xi_k^{\,i}} \Bigg\} \end{aligned} \tag{94}$$

$$\frac{\partial d_o}{\partial \xi_k^{\,i}} = 0$$

$$\frac{\partial D_o}{\partial \xi_k^{\,i}} = 0 \qquad (95)$$

$$\frac{\partial D_1}{\partial \xi_k^{\,i}} = 0$$

For the coefficients of the second row:

$$\frac{\partial b_{m+2}}{\partial \alpha_k} = \frac{-\mu}{(m+1)(m+2)} \sum_{j=o}^{m} \left[d_{m-j} \frac{\partial b_j}{\partial \alpha_k} + b_j \frac{\partial d_{m-j}}{\partial \alpha_k} \right] \qquad (96a)$$

$$\frac{\partial b_{m+2}}{\partial \beta_k} = \frac{1}{(m+1)(m+2)} \left\{ \delta_{m,k} - \mu \sum_{j=o}^{m} \left[d_{m-j} \frac{\partial b_j}{\partial \beta_k} + b_j \frac{\partial d_{m-j}}{\partial \beta_k} \right] \right\} \qquad (96b)$$

$$\frac{\partial b_{m+2}}{\partial \gamma_k} = \frac{-\mu}{(m+1)(m+2)} \sum_{j=o}^{m} \left[d_{m-j} \frac{\partial b_j}{\partial \gamma_k} + b_j \frac{\partial d_{m-j}}{\partial \gamma_k} \right] \qquad (96c)$$

$$\frac{\partial b_o}{\partial \xi_k^{\,i}} = \frac{\partial b_1}{\partial \xi_k^{\,i}} = 0 \qquad (97)$$

$$\frac{\partial b_2}{\partial \xi_k^{\,2}} = \frac{\delta_{2,k}}{2} \; ; \; \frac{\partial b_2}{\partial \xi_k^{\,i}} = 0, \; i \neq 2$$

Finally, for the third row, the coefficients are:

$$\frac{\partial c_{m+2}}{\partial \alpha_k} = \frac{-\mu}{(m+1)(m+2)} \sum_{j=o}^{m} \left[d_{m-j} \frac{\partial c_j}{\partial \alpha_k} + c_j \frac{\partial d_{m-j}}{\partial \alpha_k} \right] \tag{98a}$$

$$\frac{\partial c_{m+2}}{\partial \beta_k} = \frac{-\mu}{(m+1)(m+2)} \sum_{j=o}^{m} \left[d_{m-j} \frac{\partial c_j}{\partial \beta_k} + c_j \frac{\partial d_{m-j}}{\partial \beta_k} \right] \tag{98b}$$

$$\frac{\partial c_{m+2}}{\partial \gamma_k} = \frac{1}{(m+1)(m+2)} \left\{ \delta_{m,k} - \mu \sum_{j=o}^{m} d_{m-j} \frac{\partial c_j}{\partial \gamma_k} + c_j \frac{\partial d_{m-j}}{\partial \gamma_k} \right\} \tag{98c}$$

$$\frac{\partial c_o}{\partial \xi_k^{\,i}} = \frac{\partial c_1}{\partial \xi_k^{\,i}} = 0$$

$$\frac{\partial c_2}{\partial \xi_k^{\,3}} = \frac{\delta_{2,k}}{2} \; ; \; \frac{\partial c_2}{\partial \xi_k^{\,i}} = 0, \; i \neq 3. \tag{99}$$

The components of $\Phi^{(b)}$ are obtained by translating timing errors at the start of burn into errors in the initial conditions by

$$\delta x_o = \frac{\partial x}{\partial t_b} \cdot \delta t_b = \dot{x}_o \, \delta t_b \; ; \tag{100}$$

$$\delta \dot{x}_o = \frac{\partial \dot{x}}{\partial t_b} \cdot \delta t_b = \ddot{x}_o \, \delta t_b . \tag{101}$$

Consequently

$$\Phi^{(b)} = \Phi \cdot \begin{bmatrix} \dot{x}_o \\ \dot{y}_o \\ \dot{z}_o \\ \ddot{x}_o \\ \ddot{y}_o \\ \ddot{z}_o \end{bmatrix} \tag{102}$$

where Φ is the matrix defined in table 5-1. A similar formulation holds true for $\Phi^{(b)}$, except that the conditions at the end of burn are used for the initial state, and Φ is computed for the period following the thrust interval.

SECTION 6

COMPUTATION OF OBSERVABLES

6.1 INTRODUCTION

6.1.1 OBSERVATION TYPES. Provision has been made in the Program for a total of 25 observation types, of which 23 have been specified. These observations include:

a. Azimuth, A

b. Elevation, E

c. Round-Trip Range, ρ'

d. Range-Rate, $\dot{\rho}$

e. Hour Angle, h

f. Declination , δ

g. ℓ Direction Cosine

h. m Direction Cosine

i. X - Angle

j. Y - Angle

k. Range Equivalent, Δt

l. Range-Rate Equivalent, $\Delta t'$

m. Vehicle Occulation Time, T_{OCV}

n. One-Way Doppler (DSN)

o. Two-Way Coherent Doppler (DSN)

p. Two-Way Non-Coherent Pseudo-Doppler (DSN)

q. Radar Altimeter Ranging, H

r. Stadiometric Ranging

s. Angle Between the Reference Body and Another Planet

t. Angle Between the Reference Body and a Star

u. Angle Between a Landmark and a Star

v. Angle Between Two Landmarks

w. Star Occulation Time, T_{OCS}

6.1.2 DEFINITIONS OF THE MEASUREMENT

6.1.2.1 Azimuth, A, and Elevation, E. Azimuth is measured easterly from station north, from 0 to 2π. Elevation is measured from the station's horizontal plane, positive upward, with a range $\pm \pi/2$. See figure 6-1.

6.1.2.2 Round-Trip Range, ρ'. The round-trip range, ρ', is twice the distance from the station to the vehicle.

6.1.2.3 Range-Rate, $\dot{\rho}$. Range-rate, $\dot{\rho}$, is the time derivative of the magnitude of the vector from the station to the vehicle.

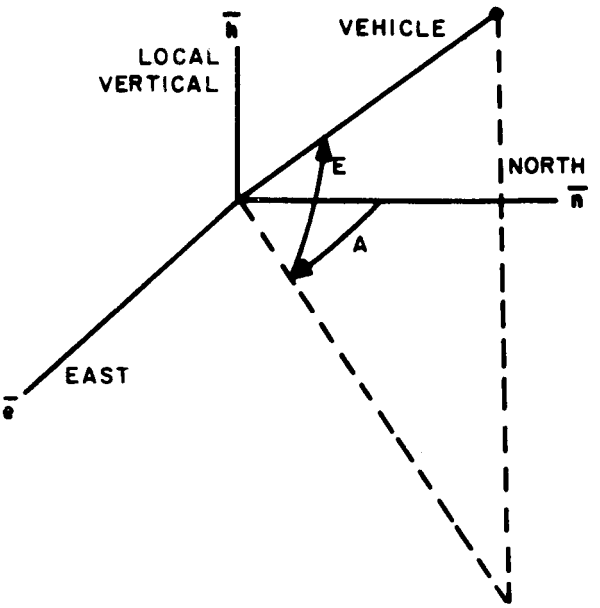

Figure 6-1 Azimuth and Elevation

6.1.2.4 Hour Angle, h, and Declination, δ. Hour angle is the angle between the station meridian and the projection on the true equator of the station-vehicle vector measured in the earth's true equatorial plane, as shown in figure 6-2. It is measured positive westward from 0 to 2π. Declination is the angle made with the true equatorial plane by the station-to-vehicle vector. Declination is measured positive in the northern hemisphere, with limits $\pm \pi/2$.

6.1.2.5 ℓ Direction Cosine, and m Direction Cosine. The ℓ direction cosine, as shown in figure 6-3, is the cosine of the angle between the station-vehicle vector and the station's east vector, the latter vector being taken to lie in the station's horizontal plane, normal to the local meridian, positive eastward in both the northern and southern hemisphere. It has limits of $\pm$ 1.0 in the computation with no dimensions. The m direction cosine is the cosine of the angle between the station-vehicle vector and the station's north vector. The north vector is taken to lie in the station's horizontal plane and is positive in the north direction in both the northern and southern hemispheres. It has limits of $\pm$ 1.0, with no dimensions.

6.1.2.6 X-Angle and Y-Angle. These measurements are shown in figure 6-4. The Y-angle is the angle between the station-vehicle vector and the perpendicular projection of this vector on the station's east-vertical plane. It is positive measured easterly, negative westerly, and has limits of $\pm \pi/2$. The X-angle is measured between the positive vertical vector and the perpendicular projection of the station-vehicle vector in the station's east-vertical plane. It is measured from the positive vertical and lies between $\pm \pi$.

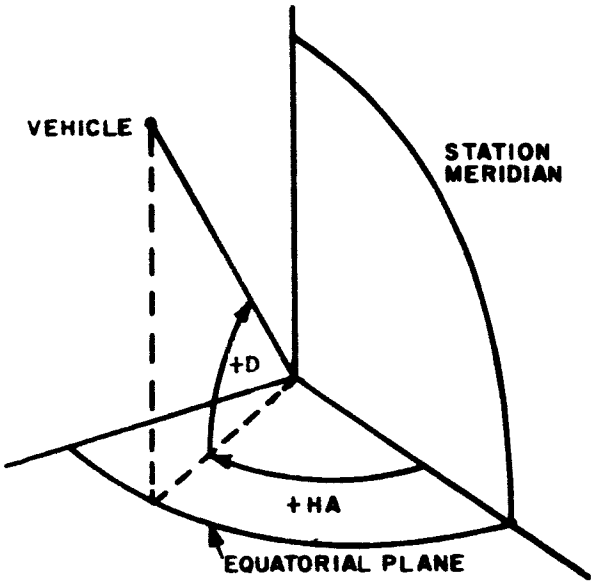

Figure 6-2 Hour Angle and Declination

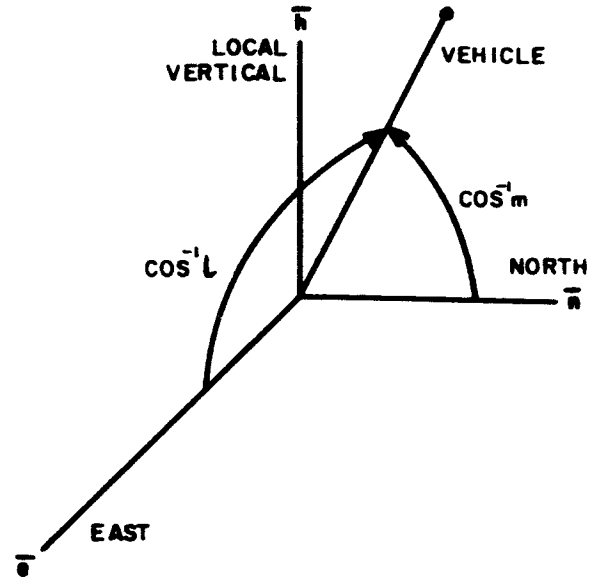

Figure 6-3 Direction Cosines ℓ and m

6.1.2.7 Range and Range-Rate Time Equivalents, Δt, and $\Delta t'$. These measurements are included since the raw data from typical tracking systems are the time between a transmitted and a received signal for range, and the time to count a given number of Doppler cycles for range rate. In most systems, these quantities are first converted to range and range rate units. However, it may be found useful in some cases to use the raw data equivalents.

6.1.2.8 Vehicle Occulation Time T_{OCV}. Time is measured at the instant a spacecraft disappears or reappears behind the limb of the Moon as seen from an Earth-based tracking station.

6.1.2.9 One-Way Doppler. Ground station receives a signal not locked to a ground interrogation.

6.1.2.10 Two-Way Coherent Doppler. Ground station receives a signal from the transponder which is being interrogated by a ground transmitter radiating through the same antenna utilized by the ground receiver.

6.1.2.11 Two-Way Non-Coherent Pseudo-Doppler. Ground station receives a signal from the transponder which is being interrogated by a ground transmitter remotely located with respect to the receiver. The transmitter and receiver reference frequencies are not locked.

6.1.2.12 Radar Altimeter Ranging. The height above the reference body surface is determined by measuring the round trip time of an electromagnetic signal reflected from the surface.

6.1.2.13 **Stadiometric Ranging.** The largest angle between the limbs of the reference body is measured. The range to the body is deduced from knowledge of the body's radius.

6.1.2.14 **Angle Between the Reference Body and Another Planet.** The angle between the two vectors from vehicle to the reference body center and from vehicle to a selected planet's center.

6.1.2.15 **Angle Between the Reference Body and a Star.** The angle between the two vectors from vehicle to the center of a reference body and from vehicle to a selected star.

6.1.2.16 **Angle Between a Landmark and a Star.** The angle between landmarks on the Moon's or Earth's surface and a star.

6.1.2.17 **Angle Between Two Landmarks.** The angle between two landmarks, either both on the Moon, or both on the Earth, or one on each body.

6.1.2.18 **Star Occulation Time, T_{OCS}.** Star occulation time is measured at the instant a selected star disappears or reappears behind the limb of a planet or the Moon as seen from a space vehicle.

6.2 COMPUTATION OF OBSERVATIONS

6.2.1 **INTRODUCTION.** Observations are computed entirely from the relative position and velocity of the spacecraft with respect to the point of observation. In most cases, only relative position is involved so that computing the observables becomes a problem in geometry. In the paragraphs to follow, formulae are given for computing observations from the ground and from a space vehicle in orbit. A separate paragraph is devoted to observations from the Deep Space Net.

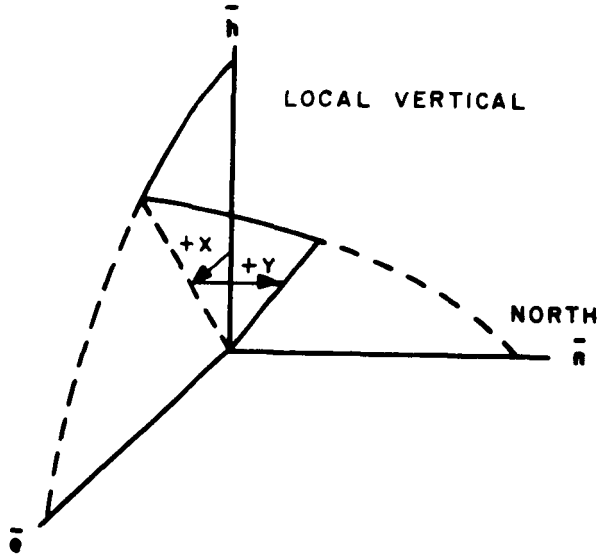

Figure 6-4 X- and Y-Angles

6.2.2 GROUND-BASED OBSERVATIONS

6.2.2.1 **General.** For ground-based sensors, account must be taken of precession and nutation. Refraction corrections should also be added to obtain the most accurate values for the observations.

The station position vector in a coordinate system rigidly attached to the earth is

$$R_{SE} = [\gamma] \left([G]_S \begin{bmatrix} 0 \\ 0 \\ h_G + C \end{bmatrix} - \begin{bmatrix} 0 \\ 0 \\ \epsilon^2 C \sin \phi_G \end{bmatrix} + \begin{bmatrix} \Delta u \\ \Delta v \\ \Delta w \end{bmatrix} \right) \quad (1)$$

where

h_G = geodetic altitude,

ϕ_G = geodetic latitude,

C = correction factor depending on ϕ_G,

ϵ = Earth's eccentricity,

$\Delta u, \Delta v, \Delta w$ = geodetic net correction,

$[G]_S$ = transformation matrix from geodetic to Greenwich system,

$[\gamma]$ = transformation from Greenwich to true system of date.

To transform R_{SE} from the true coordinate system of date to the base date reference frame, nutation and precession matrices must be premultiplied into the vector in that order:

$$R_{SB} = [A] [N] R_{SE} \quad (2)$$

where

$[A]$ = precession matrix

$[N]$ = nutation matrix.

If vehicle position is expressed with respect to some reference body other than the Earth, the station-to-vehicle position is given by

$$\rho_B = R + R_{PB} - R_{SB} \quad (3)$$

where

$\bar{R}$ = vehicle position with respect to reference body

R_{PB} = reference body position with respect to Earth.

If Earth is the reference body, then,

$$\rho_B = R - R_{SB} \tag{4}$$

In the computations to follow, most of the observables will be expressed in a topocentric coordinate system, the unit vectors of this frame being given in the base date system. Using station coordinates, the unit vectors are:

$$\left.\begin{aligned} \bar{x} &= [1 \quad 0 \quad 0]^T \quad \text{east vector} \\ \bar{y} &= [0 \quad 1 \quad 0]^T \quad \text{north vector} \\ \bar{z} &= [0 \quad 0 \quad 1]^T \quad \text{up vector} \end{aligned}\right\} \tag{5}$$

In terms of the base date systems, these vectors are transformed to

$$\left.\begin{aligned} \bar{e}_B &= [T]\,\bar{x} \quad \text{east vector} \\ \bar{n}_B &= [T]\,\bar{y} \quad \text{north vector} \\ \bar{h}_B &= [T]\,\bar{z} \quad \text{up vector} \end{aligned}\right\} \tag{6}$$

$$[T] = [A]\,[N]\,[\gamma]\,[G]_S\,[\alpha], \tag{7}$$

$[\alpha]$ being a rotation matrix to account for misalignment between the station coordinates and the actual east-north-up system.

6.2.2.2 Azimuth, A

$$A = \mathrm{Tan}^{-1}\left[\frac{\rho_B \cdot \bar{e}_B}{\rho_B \cdot \bar{n}_B}\right], \quad 0 \leq A \leq 2\pi. \tag{8}$$

The quadrant of A is obtained from the signs of the numerator and denominator in equation (8).

6.2.2.3 Elevation, E

$$E = \mathrm{Tan}^{-1}\left[\frac{\rho_B \cdot \bar{h}_B}{\sqrt{(\rho_B \cdot \bar{e}_B)^2 + (\rho_B \cdot \bar{n}_B)^2}}\right] \tag{9}$$

The quadrant of E is obtained from the signs of the numerator and denominator in equation (9).

6.2.2.4 Round-Trip Range, ρ'

$$\rho' = 2\,\rho_B$$

6.2.2.5 Range-Rate, $\dot{\rho}$

$$\dot{\rho} = \frac{V_B \cdot \rho_B}{\rho_B}$$

where $V_B = V_B - V_{SB}$, the vehicle velocity relative to the station in the base date system; $V_{SB} = [A]\,[N]\,[W_e]R_{SE}$, the station velocity in the base date system. $[W_e]\,R_{SE} = W_E \times R_{SE}$, where W_E is the Earth's angular velocity vector.

6.2.2.6 Hour Angle, h

$$h = \gamma + (\lambda_G)_S - (RA), \quad 0 \leq h < 2\pi. \tag{12}$$

where

h = the hour angle of ρ_B with respect to the station;

γ = right ascension of Greenwich;

$(\lambda_c)_S$ = station longitude

(RA) = right ascension of ρ_B

In equation (12),

$$(RA) = \text{Tan}^{-1}\left[\frac{\rho_B \cdot \bar{y}}{\rho_B \cdot \bar{x}}\right], \quad 0 \leq (RA) < 2\pi. \tag{13}$$

The quadrant of (RA) is obtained from the signs of the numerator and denominator in equation (13).

6.2.2.7 Declination, δ

$$\delta = \text{Tan}^{-1}\left[\frac{\rho_B \cdot \bar{z}}{\sqrt{(\rho_B \cdot \bar{x})^2 + (\rho_B \cdot \bar{y})^2}}\right], \quad -\frac{\pi}{2} \leq \delta \leq \frac{\pi}{2}. \tag{14}$$

6.2.2.8 ℓ Direction Cosine

$$\ell = \frac{\rho_B \cdot \bar{e}_B}{\rho_B}. \tag{15}$$

6.2.2.9 m Direction Cosine

$$m = \frac{\rho_B \cdot \bar{n}_B}{\rho_B} \tag{16}$$

6.2.2.10 X-Angle

$$X = \text{Tan}^{-1}\left[\frac{\rho_B \cdot \bar{e}_B}{\rho_B \cdot \bar{h}_B}\right], \quad -\pi < X \leq \pi. \tag{17}$$

The quadrant of X is obtained from the signs of the numerator and denominator in equation (17).

6.2.2.11 Y-Angle

$$Y = \mathrm{Tan}^{-1}\left[\frac{\rho_B \cdot \bar{n}_B}{\sqrt{(\rho_B \cdot \bar{e}_B)^2 + (\rho_B \cdot \bar{h}_B)^2}}\right], \quad -\frac{\pi}{2} \leq Y \leq \frac{\pi}{2}. \tag{18}$$

6.2.2.12 Range Equivalent, Δt

$$\Delta t = \frac{2\,\rho_B}{c} = \frac{\rho'}{c} \tag{19}$$

where c is the velocity of light.

6.2.2.13 Range-Rate Equivalent, $\Delta t'$

$$\Delta t' = \frac{\rho_2 - \rho_1}{c}, \tag{20}$$

where ρ_1 and ρ_2 are the ranges evaluated at the beginning and at the end of the measurement, respectively.

6.2.2.14 Vehicle Occultation Time. Unlike the foregoing observations, the calculation of occultation time entails iterations. As shown in figure 6-5, a ground station observes the occultation of a spacecraft by the Moon. The iteration equation is

$$(\phi_2 - \phi_1) + \left[\frac{d(\phi_2 - \phi_1)}{dt}\right]_i (\Delta t)_i = 0 \tag{21}$$

$$T_{OCV} = T_I + \sum_{i=o}^{k} (\Delta t)_i \tag{22}$$

$$\phi_2 = \cos^{-1}\left[\frac{\rho_B \cdot R_{SM}}{\rho_B\, R_{SM}}\right] \tag{23}$$

$$\phi_1 = \sin^{-1}\frac{R_R}{R_{SM}} \tag{24}$$

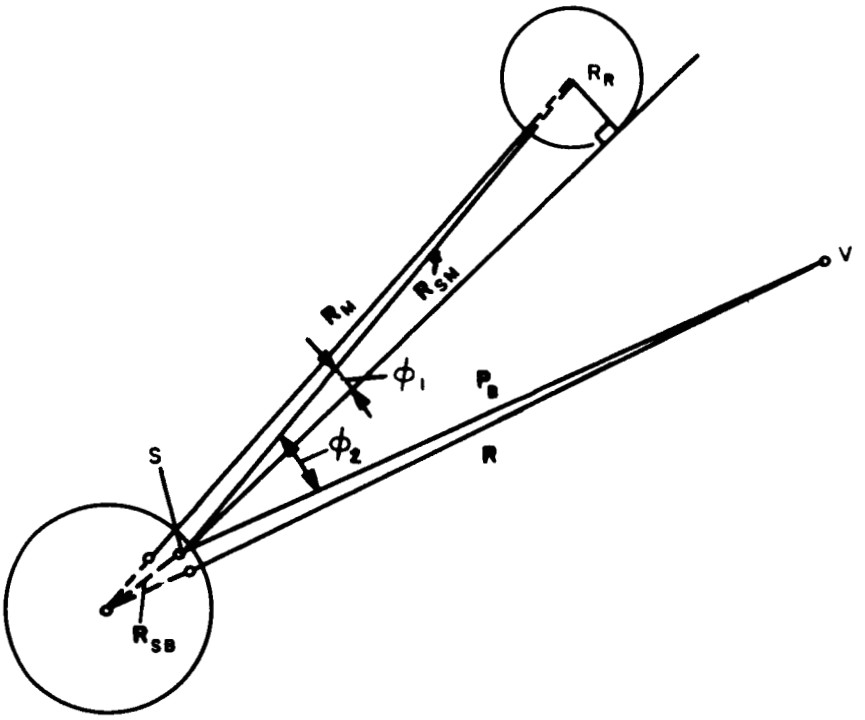

Figure 6-5 Vehicle Occultation By The Moon

In the preceding expressions, ρ_B is the vector from the station to the vehicle, R_{SM} the vector from the station to the Moon's mass center, R_R the mean lunar radius, and T_I the initial time of the iterations. The limit k in equation (22) implies that k + 1 iterations are needed to obtain the desired precision. The derivative is given by

$$\frac{d(\phi_2 - \phi_1)}{dt} = \frac{1}{\rho_B \, R_{SM} \sin \phi_2} \left[(\rho_B \cdot R_{SM}) \left[\frac{\rho_B \cdot \dot{\rho}}{\rho_B^2} + \frac{R_{SM} \cdot \dot{R}_{SM}}{R_{SM}^2} \right] - (\dot{\rho} \cdot R_{SM} + \rho_B \cdot \dot{R}_{SM}) \right]$$

$$+ \frac{R_R \, (R_{SM} \cdot \dot{R}_{SM})}{R_{SM}^3 \cos \phi_1} \qquad (25)$$

$\dot{\rho}$ being the vehicle velocity with respect to the station and $\dot{R}_{SM}$ the velocity of the lunar mass center relative to the station.

6.2.3 OBSERVATIONS FOR THE DEEP SPACE NET

6.2.3.1 Introduction. Three typical DSN observations are given here. However, the method for computing these observables can change depending upon the hardware in use for a particular mission.

6.2.3.2 One-Way Doppler

$$f_1 = 930.150 \times 10^6 - \left[\frac{31}{32}\right](960.10) \times 10^6 \left[1 - \frac{\dot{\rho}}{c}\right] \text{ cycles/second,}$$

where $\dot{\rho}$ is the range rate measured from the station and c is the velocity of light.

6.2.3.3 Two-Way Coherent Doppler

$$f_2 = 0.1 \times 10^6 + 30\left[\frac{96}{89}\right](\text{FRQ})\left[\frac{\dot{\rho}_i + \dot{\rho}_q}{c}\right] \text{ cycles/second,}$$

where (FRQ) is the reference frequency, and where $\dot{\rho}_i$ and $\dot{\rho}_q$ are range-rates from the i^{th} and q^{th} stations, respectively. In general, $\dot{\rho}_i = \dot{\rho}_q$.

6.2.3.4 Two-Way Non-Coherent Pseudo-Doppler

$$f_3 = 930.150 \times 10^6 - 30\left[\frac{96}{89}\right]\left[\frac{31}{32}\right](\text{FRQ})\left[1 - \frac{(\dot{\rho}_i + \dot{\rho}_q)}{c}\right] \text{ cycles/second,} \quad (28)$$

where the i^{th} and q^{th} stations are paired in accordance with the following table:

i	q
1	5
2	3
3	2
4	-
5	1

6.2.4 ON-BOARD OBSERVATIONS

6.2.4.1 Radar Altimeter Ranging

$$H = 2\ H_R \quad \text{earth radii,} \tag{29}$$

where H_R is the height above the reference planet.

6.2.4.2 Stadiometic Ranging

$$(SR) = 2 \sin^{-1} \left[\frac{R_R}{R_D} \right] \quad \text{radians,} \tag{30}$$

R_R being the planet radius and R_D the distance from the planet.

6.2.4.3 Angle Between Reference Body and Planet

$$A_{PP} = \cos^{-1} \left[\frac{Z}{Z} \cdot \frac{R}{R} \right] \quad \text{radians,} \tag{31}$$

where $\mathbf{Z}$ is the vehicle-planet vector, and $\mathbf{R}$ is the vehicle-reference body vector

6.2.4.4 Angle Between a Star and the Reference Body

$$A_{PS} = \cos^{-1} \left(\frac{Z}{Z} \cdot \bar{n} \right) \quad \text{radians,} \tag{32}$$

where $\mathbf{Z}$ is the vehicle-planet vector, and $\bar{n}$ is a unit vector indicating the star direction. This direction is a function of right ascension, (RA), and declination, δ:

$$\bar{n} = [\cos (RA) \cos \delta \quad \sin (RA) \cos \delta \quad \sin \delta] \tag{33}$$

6.2.4.5 Angle Between a Landmark and a Star

$$A_{SLM} = \cos^{-1} \left(\frac{d}{d} \cdot \bar{n} \right) \quad \text{radians,} \tag{34}$$

in which equation $\mathbf{d}$ is the vehicle-landmark vector, and $\bar{n}$ is the unit vector defined above.

6.2.4.6 Angle Between Two Landmarks

$$A_{LL} = \cos^{-1}\left[\frac{\mathbf{d}}{d}\cdot\frac{\mathbf{y}}{y}\right] \text{ radians,} \tag{35}$$

where $\mathbf{d}$ and $\mathbf{y}$ are the vectors from the vehicle to two different landmarks.

6.2.4.7 Star Occultation Time. As in vehicle occultation, star occultation time is computed from a Newton-Raphson iteration:

$$(\phi_2 - \phi_1)_i + \left[\frac{d(\phi_2 - \phi_1)}{dt}\right]_i (\Delta t)_i = 0 \tag{36}$$

$$T_{OCS} = T_I + \sum_{i=o}^{k} (\Delta t)_i \tag{37}$$

where the geometry is defined by figure 6-6. The angles are computed from

$$\phi_2 = \cos^{-1}\left[\frac{\mathbf{R}\cdot\bar{\mathbf{n}}}{R}\right] \tag{38}$$

$$\phi_1 = \sin^{-1}\left[\frac{R_R}{R}\right] \tag{39}$$

In the above expressions, $\mathbf{R}$ is the vector from the occulting body to the vehicle, $\bar{\mathbf{n}}$ defines the direction of the star being occulted, R_R is the radius of the occulting body, T_I is the initial time of the iteration, and the limit k implies that k + 1 iterations are required to obtain the desired precision. The derivative of equation (36) is given by

$$\frac{d(\phi_2 - \phi_1)}{dt} = \frac{1}{R \sin\phi_2}\left\{\mathbf{R}\cdot\bar{\mathbf{n}} - \frac{(\mathbf{R}\cdot\bar{\mathbf{n}})(\mathbf{R}\cdot\dot{\mathbf{R}})}{R^2}\right\} + \frac{R_R(\mathbf{R}\cdot\dot{\mathbf{R}})}{R^3 \sin\phi_1} \tag{40}$$

$\dot{\mathbf{R}}$ being the vehicle velocity with respect to the mass center of the occulting body.

6.3 MATRICES OF PARTIAL DERIVATIVES

6.3.1 INTRODUCTION. In the process of statistical estimation, matrices are employed which have as their elements partial derivatives relating the state vectors to the observations. In differential form,

$$\delta\bar{y} = M\,\delta\bar{x} \qquad (41)$$

in which $\delta\bar{y}$ is the vector of observation residuals and $\delta\bar{x}$ is the state vector. M has dimensions ixj, where i is the number of observables and j is the number of states.

Expressing the observation matrix for a given observation type in general form:

$$M = [M_{OV}\ M_{OS}\ M_{OR}\ M_{OO}\ M_{OC}\ M_{OT}\ M_{OP}] \qquad (42)$$

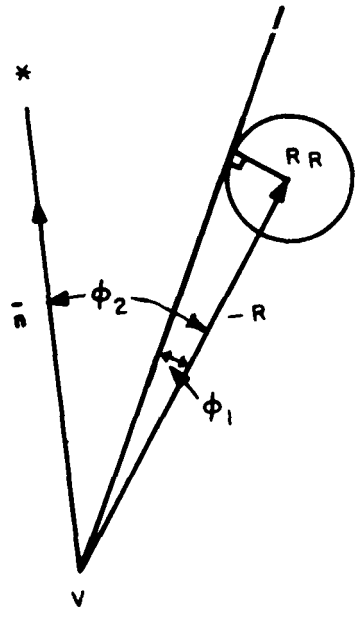

Figure 6-6 Star Occultation

Each submatrix denotes a set of partial derivatives with respect to different components of the state vector.

- M_{OV}: a 1X6 matrix relating the observations to the position and velocity components of the vehicle.
- M_{OS}: a 1X3 matrix relating the observations to errors in the ground station position expressed in the Greenwich coordinate system. In this system, x is taken as positive through the prime meridian, z is positive through the North Pole, and y completes a right-handed system.
- M_{OR}: a 1X3 matrix relating the observations to the ground station orientation angles defined with respect to the local east, north and up vectors.
- M_{OO}: a 1X1 matrix relating the observations to themselves.
- M_{OC}: a 1X1 matrix relating the observations to the speed of light.
- M_{OT}: a 1X1 matrix relating the observations to the observation time.
- M_{OP}: a 1X6 matrix relating the observations to the propagation parameters.

6.3.2 PARTIAL DERIVATIVES FOR GROUND OBSERVATIONS

6.3.2.1 Azimuth, A

$$M_{AV} = \frac{1}{\rho_B \cos E} \left[(\bar{e} \cos A - \bar{n} \sin A) \quad 0 \quad 0 \quad 0 \right] \tag{43a}$$

$$M_{AS} = \begin{bmatrix} \frac{\partial A}{\partial \ell} & \frac{\partial A}{\partial m} \end{bmatrix} \begin{bmatrix} M_{\ell S} \\ M_{mS} \end{bmatrix} \tag{43b}$$

$$\frac{\partial A}{\partial \ell} = \frac{1}{m} \; ; \; \frac{\partial A}{\partial m} = - \frac{1}{\ell} \tag{43c}$$

$$M_{AR} = \begin{bmatrix} \cos\beta \cos\gamma + \tan E \, (\sin A \sin\beta - \cos A \sin\gamma \cos\beta) \\ - (\sin\gamma + \cos A \tan E \cos\gamma) \\ - \sin A \tan E \end{bmatrix}^T \tag{43d}$$

where β and γ are station orientation angles.

$$M_{AA} = 1 \tag{43e}$$

$$M_{AC} = 0 \tag{43f}$$

$$M_{AT} = M_{AV} V_B + M_{AS} [\gamma]^T V_{SB} \tag{43g}$$

$$M_{AP} = 0 \tag{43h}$$

6.3.2.2 Elevation, E

$$M_{EV} = \left[- [\bar{e}_B \sin A \sin E + \bar{n}_B (\cos A \sin E - \cos E)] \quad 0 \quad 0 \quad 0 \right] \tag{44a}$$

$$M_{ES} = \begin{bmatrix} \frac{\partial E}{\partial \ell} & \frac{\partial E}{\partial m} \end{bmatrix} \begin{bmatrix} M_{\ell S} \\ M_{mS} \end{bmatrix} \tag{44b}$$

$$\frac{\partial E}{\partial \ell} = \frac{-1}{\sin A \sin E} \; ; \; \frac{\partial E}{\partial m} = \frac{-1}{\cos A \sin E} \tag{44c}$$

$$M_{ER} = \begin{bmatrix} \cos A \sin \beta + \sin A \sin \gamma \cos \beta \\ \sin A \cos \gamma \\ \cos A \end{bmatrix}^T \tag{44d}$$

$$M_{EE} = 1 \tag{44e}$$

$$M_{EC} = 0 \tag{44f}$$

$$M_{ET} = M_{EV}\, V_B + M_{ES}\, [\gamma]^T\, V_{SB} \tag{44g}$$

$$M_{EP} = \begin{bmatrix} \frac{\partial E}{\partial P_1} & \frac{\partial E}{\partial P_2} & \frac{\partial E}{\partial P_3} & \frac{\partial E}{\partial P_4} & \frac{\partial E}{\partial P_5} & \frac{\partial E}{\partial P_6} \end{bmatrix} \tag{44h}$$

6.3.2.3 Round-Trip Range, ρ'

$$M_{\rho' V} = 2 \begin{bmatrix} \frac{\rho_B}{\rho_B} & 0 & 0 & 0 \end{bmatrix} \tag{45a}$$

$$M_{\rho' S} = -\frac{2}{\rho_B} [(x - x_S)\ (y - y_S)\ (z - z_S)]\ [\gamma] \tag{45b}$$

$$M_{\rho' R} = 0 \tag{45c}$$

$$M_{\rho' \rho'} = 1 \tag{45d}$$

$$M_{\rho' c} = \frac{\rho'}{c} \tag{45e}$$

$$M_{\rho' T} = M_{\rho' V}\, V_B + M_{\rho' S}\, [\gamma]^T\, V_{SB} \tag{45f}$$

$$M_{\rho' P} = \begin{bmatrix} \frac{\partial \rho'}{\partial P_1} & \frac{\partial \rho'}{\partial P_2} & \frac{\partial \rho'}{\partial P_3} & \frac{\partial \rho'}{\partial P_4} & \frac{\partial \rho'}{\partial P_5} & \frac{\partial \rho'}{\partial P_6} \end{bmatrix} \tag{45g}$$

6.3.2 PARTIAL DERIVATIVES FOR GROUND OBSERVATIONS

6.3.2.1 Azimuth, A

$$M_{AV} = \frac{1}{\rho_B \cos E} \left[(\bar{e} \cos A - \bar{n} \sin A) \quad 0 \quad 0 \quad 0 \right] \tag{43a}$$

$$M_{AS} = \left[\frac{\partial A}{\partial \ell} \quad \frac{\partial A}{\partial m} \right] \begin{bmatrix} M_{\ell S} \\ M_{mS} \end{bmatrix} \tag{43b}$$

$$\frac{\partial A}{\partial \ell} = \frac{1}{m} \; ; \; \frac{\partial A}{\partial m} = -\frac{1}{\ell} \tag{43c}$$

$$M_{AR} = \begin{bmatrix} \cos\beta \cos\gamma + \tan E \, (\sin A \sin\beta - \cos A \sin\gamma \cos\beta) \\ -(\sin\gamma + \cos A \tan E \cos\gamma) \\ -\sin A \tan E \end{bmatrix}^T \tag{43d}$$

where β and γ are station orientation angles.

$$M_{AA} = 1 \tag{43e}$$

$$M_{AC} = 0 \tag{43f}$$

$$M_{AT} = M_{AV} V_B + M_{AS} [\gamma]^T V_{SB} \tag{43g}$$

$$M_{AP} = 0 \tag{43h}$$

6.3.2.2 Elevation, E

$$M_{EV} = \left[-[\bar{e}_B \sin A \sin E + \bar{n}_B (\cos A \sin E - \cos E)] \quad 0 \quad 0 \quad 0 \right] \tag{44a}$$

$$M_{ES} = \left[\frac{\partial E}{\partial \ell} \quad \frac{\partial E}{\partial m} \right] \begin{bmatrix} M_{\ell S} \\ M_{mS} \end{bmatrix} \tag{44b}$$

$$\frac{\partial E}{\partial \ell} = \frac{-1}{\sin A \sin E} \; ; \; \frac{\partial E}{\partial m} = \frac{-1}{\cos A \sin E} \tag{44c}$$

$$M_{ER} = \begin{bmatrix} \cos A \sin \beta + \sin A \sin \gamma \cos \beta \\ \sin A \cos \gamma \\ \cos A \end{bmatrix}^T \tag{44d}$$

$$M_{EE} = 1 \tag{44e}$$

$$M_{EC} = 0 \tag{44f}$$

$$M_{ET} = M_{EV}\, V_B + M_{ES}\, [\gamma]^T\, V_{SB} \tag{44g}$$

$$M_{EP} = \begin{bmatrix} \frac{\partial E}{\partial P_1} & \frac{\partial E}{\partial P_2} & \frac{\partial E}{\partial P_3} & \frac{\partial E}{\partial P_4} & \frac{\partial E}{\partial P_5} & \frac{\partial E}{\partial P_6} \end{bmatrix} \tag{44h}$$

6.3.2.3 Round-Trip Range, ρ'

$$M_{\rho' V} = 2 \begin{bmatrix} \frac{\rho_B}{\rho_B} & 0 & 0 & 0 \end{bmatrix} \tag{45a}$$

$$M_{\rho' S} = -\frac{2}{\rho_B} [(x - x_S)\ (y - y_S)\ (z - z_S)]\ [\gamma] \tag{45b}$$

$$M_{\rho' R} = 0 \tag{45c}$$

$$M_{\rho' \rho'} = 1 \tag{45d}$$

$$M_{\rho' c} = \frac{\rho'}{c} \tag{45e}$$

$$M_{\rho' T} = M_{\rho' V}\, V_B + M_{\rho' S}\, [\gamma]^T\, V_{SB} \tag{45f}$$

$$M_{\rho' P} = \begin{bmatrix} \frac{\partial \rho'}{\partial P_1} & \frac{\partial \rho'}{\partial P_2} & \frac{\partial \rho'}{\partial P_3} & \frac{\partial \rho'}{\partial P_4} & \frac{\partial \rho'}{\partial P_5} & \frac{\partial \rho'}{\partial P_6} \end{bmatrix} \tag{45g}$$

6.3.2.4 One-Way Range-Rate, $\dot{\rho}$

$$M_{\dot{\rho}V} = \frac{1}{\rho_B}\left[\left[V_B - \dot{\rho}\frac{\rho_B}{\rho_B}\right]\rho_B\right] \tag{46a}$$

$$M_{\dot{\rho}S} = \begin{bmatrix} \frac{\dot{\rho}}{\rho_B^2}(x - x_S) - \frac{1}{\rho_B}(\dot{x} + \omega_e y) \\ \frac{\dot{\rho}}{\rho_B^2}(y - y_S) - \frac{1}{\rho_B}(\dot{y} - \omega_e x) \\ \frac{\dot{\rho}}{\rho_B^2}(z - z_S) - \frac{\dot{z}}{\rho_B} \end{bmatrix}^T [\gamma] \tag{46b}$$

$$M_{\dot{\rho}R} = 0 \tag{46c}$$

$$M_{\dot{\rho}\dot{\rho}} = 1 \tag{46d}$$

$$M_{\dot{\rho}c} = \frac{\dot{\rho}}{c} \tag{46e}$$

$$M_{\dot{\rho}T} = M_{\dot{\rho}V} V_B + M_{\dot{\rho}S} [\gamma]^T V_{SB} \tag{46f}$$

$$M_{\dot{\rho}P} = \left[\frac{\partial\dot{\rho}}{\partial P_1} \quad \frac{\partial\dot{\rho}}{\partial P_2} \quad \frac{\partial\dot{\rho}}{\partial P_3} \quad \frac{\partial\dot{\rho}}{\partial P_4} \quad \frac{\partial\dot{\rho}}{\partial P_5} \quad \frac{\partial\dot{\rho}}{\partial P_6}\right] \tag{46g}$$

6.3.2.5 Hour Angle, h

$$M_{hV} = \left[\frac{\partial h}{\partial E} \quad \frac{\partial h}{\partial A}\right]\begin{bmatrix} M_{EV} \\ \\ M_{EA} \end{bmatrix} \tag{47a}$$

$$\left.\begin{aligned} \frac{\partial h}{\partial E} &= \frac{\cos \phi_G \sec^2 E \tan^2 h}{\sin^2 A} \\ \frac{\partial h}{\partial A} &= \cot A + \tan^2 h \sin \phi_G \end{aligned}\right\} \quad (47b)$$

$$M_{hS} = \begin{bmatrix} \frac{\partial h}{\partial E} & \frac{\partial h}{\partial A} \end{bmatrix} \begin{bmatrix} M_{ES} \\ M_{AS} \end{bmatrix} \quad (47c)$$

$$M_{hR} = \begin{bmatrix} \frac{\partial h}{\partial E} & \frac{\partial h}{\partial A} \end{bmatrix} \begin{bmatrix} M_{ER} \\ M_{AR} \end{bmatrix} \quad (47d)$$

$$M_{hh} = 1 \quad (47e)$$

$$M_{hc} = 0 \quad (47f)$$

$$M_{hT} = M_{hV} V_B + M_{hS} [\gamma]^T V_{SB} \quad (47g)$$

$$M_{hP} = \frac{\partial h}{\partial E} M_{EP} \quad (47h)$$

6.3.2.6 Declination, δ

$$M_{\delta V} = \begin{bmatrix} \frac{\partial \delta}{\partial E} & \frac{\partial \delta}{\partial A} \end{bmatrix} \begin{bmatrix} M_{EV} \\ M_{AV} \end{bmatrix} \quad (48a)$$

$$\left.\begin{aligned} \frac{\partial \delta}{\partial E} &= \frac{\cos E \sin \phi_G - \sin E \cos A \cos \phi_G}{\cos \delta} \\ \frac{\partial \delta}{\partial A} &= \frac{\sin A \cos A \cos \lambda}{\cos \delta} \end{aligned}\right\} \quad (48b)$$

$$M_{\delta S} = \begin{bmatrix} \frac{\partial \delta}{\partial E} & \frac{\partial \delta}{\partial A} \end{bmatrix} \begin{bmatrix} M_{ES} \\ M_{AS} \end{bmatrix} \tag{48c}$$

$$M_{\delta R} = \begin{bmatrix} \frac{\partial \delta}{\partial E} & \frac{\partial \delta}{\partial A} \end{bmatrix} \begin{bmatrix} M_{ER} \\ M_{AR} \end{bmatrix} \tag{48d}$$

$$M_{\delta \delta} = 1 \tag{48e}$$

$$M_{\delta C} = 0 \tag{48f}$$

$$M_{\delta T} = M_{\delta V}\, V_B + M_{\delta S}\, [\gamma]^T\, V_{SB} \tag{48g}$$

$$M_{\delta P} = \frac{\partial \delta}{\partial E}\, M_{EP} \tag{48h}$$

6.3.2.7 ℓ Direction Cosine

$$M_{\ell V} = \begin{bmatrix} \frac{\partial \ell}{\partial E} & \frac{\partial \ell}{\partial A} \end{bmatrix} \begin{bmatrix} M_{EV} \\ M_{AV} \end{bmatrix} \tag{49a}$$

$$\frac{\partial \ell}{\partial E} = -\sin E \sin A; \quad \frac{\partial \ell}{\partial A} = m \tag{49b}$$

$$M_{\ell S} = \begin{bmatrix} -\frac{1}{\rho_B} & \frac{\ell \tan \phi_G}{R} & \frac{\ell}{R} \end{bmatrix} [G]_S^T + \rho_B{}^T\, [\gamma] \begin{bmatrix} \frac{\ell}{\rho_B{}^2} & \frac{-\sec \phi_G}{\rho_B\, R} & 0 \\ \frac{\sec \phi_G}{\rho_B\, R} & \frac{\ell}{\rho_B{}^2} & 0 \\ 0 & 0 & \frac{\ell}{\rho_B{}^2} \end{bmatrix} \tag{49c}$$

$$M_{\ell R} = \begin{bmatrix} \frac{\partial \ell}{\partial E} & \frac{\partial \ell}{\partial A} \end{bmatrix} \begin{bmatrix} M_{ER} \\ M_{AR} \end{bmatrix} \tag{49d}$$

$$M_{\ell\ell} = 1 \tag{49e}$$

$$M_{\ell C} = 0 \tag{49f}$$

$$M_{\ell T} = M_{\ell V}\, V_B + M_{\ell S}\, [\gamma]^T\, V_{SB} \tag{49g}$$

$$M_{\ell P} = \frac{\partial \ell}{\partial E}\, M_{EP} \tag{49h}$$

6.3.2.8 m Direction Cosine

$$M_{mV} = \begin{bmatrix} \frac{\partial m}{\partial E} & \frac{\partial m}{\partial A} \end{bmatrix} \begin{bmatrix} M_{EV} \\ M_{AV} \end{bmatrix} \tag{50a}$$

$$\frac{\partial m}{\partial E} = -\cos A \sin E; \quad \frac{\partial m}{\partial A} = -\ell \tag{50b}$$

$$M_{mS} = \begin{bmatrix} -\frac{m \tan \phi_G}{R} & -\frac{1}{\rho_B} & -\frac{m}{R} \end{bmatrix} [G]_S^T$$

$$+ \rho_B^T\, [\gamma] \begin{bmatrix} \frac{m}{\rho_B^2} & 0 & \frac{2 \cos \lambda_G}{\rho_B R} \\ 0 & \frac{m}{\rho_B^2} & -\frac{2 \sin \lambda_G}{\rho_B R} \\ -\frac{2 \cos \phi_G}{\rho_B R} & \frac{2 \sin \phi_G}{\rho_B R} & \frac{m}{\rho_B^2} \end{bmatrix} \tag{50c}$$

$$M_{mR} = \begin{bmatrix} \frac{\partial m}{\partial E} & \frac{\partial m}{\partial A} \end{bmatrix} \begin{bmatrix} M_{ER} \\ M_{AR} \end{bmatrix} \quad (50d)$$

$$M_{mm} = 1 \quad (50e)$$

$$M_{mC} = 0 \quad (50f)$$

$$M_{mT} = M_{mV}\, V_B + M_{mS}\, [\gamma]^T\, V_{SB} \quad (50g)$$

$$M_{mP} = \frac{\partial m}{\partial E} M_{EP} \quad (50h)$$

6.3.2.9 X-Angle

$$M_{XV} = \begin{bmatrix} \frac{\partial X}{\partial E} & \frac{\partial X}{\partial A} \end{bmatrix} \begin{bmatrix} M_{EV} \\ M_{AV} \end{bmatrix} \quad (51a)$$

$$\frac{\partial X}{\partial E} = -\frac{\sin 2X}{\sin 2E} \; ; \; \frac{\partial X}{\partial A} = \frac{\sin 2X}{2 \tan A} \quad (51b)$$

$$M_{XS} = \begin{bmatrix} \frac{\partial X}{\partial E} & \frac{\partial X}{\partial A} \end{bmatrix} \begin{bmatrix} M_{ES} \\ M_{AS} \end{bmatrix} \quad (51c)$$

$$M_{XR} = \begin{bmatrix} \frac{\partial X}{\partial E} & \frac{\partial X}{\partial A} \end{bmatrix} \begin{bmatrix} M_{ER} \\ M_{AR} \end{bmatrix} \quad (51d)$$

$$M_{XX} = 1 \quad (51e)$$

$$M_{XC} = 0 \quad (51f)$$

$$M_{XT} = M_{XV}\, V_B + M_{XS}\, [\gamma]^T\, V_{SB} \qquad (51g)$$

$$M_{XP} = \frac{\partial X}{\partial E}\, M_{EP} \qquad (51h)$$

6.3.2.10 Y-Angle

$$M_{YV} = \begin{bmatrix} \frac{\partial Y}{\partial E} & \frac{\partial Y}{\partial A} \end{bmatrix} \begin{bmatrix} M_{EV} \\ M_{AV} \end{bmatrix} \qquad (52a)$$

$$\frac{\partial Y}{\partial E} = -\frac{\cos A \sin E}{\cos Y} \; ; \; \frac{\partial Y}{\partial A} = -\frac{\sin A \cos E}{\cos Y} \qquad (52b)$$

$$M_{YS} = \begin{bmatrix} \frac{\partial Y}{\partial E} & \frac{\partial Y}{\partial A} \end{bmatrix} \begin{bmatrix} M_{ES} \\ M_{AS} \end{bmatrix} \qquad (52c)$$

$$M_{YR} = \begin{bmatrix} \frac{\partial Y}{\partial E} & \frac{\partial Y}{\partial A} \end{bmatrix} \begin{bmatrix} M_{ER} \\ M_{AR} \end{bmatrix} \qquad (52d)$$

$$M_{YY} = 1 \qquad (52e)$$

$$M_{YC} = 0 \qquad (52f)$$

$$M_{YT} = M_{YV}\, V_B + M_{YS}\, [\gamma]^T\, V_{SB} \qquad (52g)$$

$$M_{YP} = \frac{\partial Y}{\partial E}\, M_{EP} \qquad (52h)$$

6.3.2.11 Range Equivalent, Δt

$$M_{\Delta tV} = \frac{1}{c} M_{\rho' V} \tag{53a}$$

$$M_{\Delta tS} = \frac{1}{c} M_{\rho' S} \tag{53b}$$

$$M_{\Delta tR} = 0 \tag{53c}$$

$$M_{\Delta t\Delta t} = 1 \tag{53d}$$

$$M_{\Delta tC} = -\frac{\rho'}{c^2} \tag{53e}$$

$$M_{\Delta tT} = \frac{2\dot{\rho}}{c} \tag{53f}$$

$$M_{\Delta tP} = \frac{1}{c} M_{\rho' P} \tag{53g}$$

6.3.2.12 Range-Rate Equivalent, $\Delta t'$

$$M_{\Delta t' V} = K M_{\dot{\rho} V} \tag{54a}$$

$$K = \frac{2 f_u (\Delta t')^2}{cN} \tag{54b}$$

where

f_u = transmitted frequency;

c = velocity of light;

N = number of cycle counts.

$$M_{\Delta t' S} = K M_{\dot{\rho} S} \tag{54c}$$

$$M_{\Delta t' R} = 0 \tag{54d}$$

$$M_{\Delta t' \Delta t'} = 1 \tag{54e}$$

$$M_{\Delta t' c} = -\frac{K\dot{\rho}}{c} \tag{54f}$$

$$M_{\Delta t' T} = KM_{\dot{\rho} T} \tag{54g}$$

$$M_{\Delta t' P} = KM_{\dot{\rho} P} \tag{54h}$$

6.3.2.13 Vehicle Occultation Time, T_{OCV}

$$M_{T_{OCV}V} = \frac{1}{\bar{l}_P \cdot \dot{\bar{\rho}}} [\bar{l}_P \cdot \bar{i} \;\; \bar{l}_P \cdot \bar{j} \;\; \bar{l}_P \cdot \bar{k} \;\; 0 \;\; 0 \;\; 0], \tag{55a}$$

where $\bar{i}$, $\bar{j}$, and $\bar{k}$ are unit vectors in the base date coordinate system.

$$\bar{l}_P = \bar{l}_N \times \frac{\rho_B}{\rho_B} \tag{55b}$$

$$\bar{l}_N = \frac{\rho_B \times R_{SM}}{|\rho_B \times R_{SM}|} \tag{55c}$$

6.3.3 PARTIAL DERIVATIVES FOR THE DEEP SPACE NET

6.3.3.1 One-Way Doppler

$$M_{f_1 V} = \frac{\partial f_1}{\partial \dot{\rho}} M_{\dot{\rho} V} \tag{56a}$$

$$\frac{\partial f_1}{\partial \dot{\rho}} = \frac{930\ 096\ 875}{c} \tag{56b}$$

$$M_{f_1 S} = \frac{\partial f_1}{\partial \dot{\rho}} M_{\dot{\rho} S} \tag{56c}$$

$$M_{f_1 R} = \frac{\partial f_1}{\partial \dot{\rho}} M_{\dot{\rho} R} \tag{56d}$$

$$M_{f_1 f_1} = 1 \tag{56e}$$

$$M_{f_1 c} = \frac{\partial f_1}{\partial \dot{\rho}} M_{\dot{\rho} c} \tag{56f}$$

$$M_{f_1 T} = \frac{\partial f_1}{\partial \dot{\rho}} M_{\dot{\rho} T} \tag{56g}$$

$$M_{f_1 P} = \frac{\partial f_1}{\partial \dot{\rho}} M_{\dot{\rho} P} \tag{56h}$$

6.3.3.2 Two-Way Coherent Doppler. By the chain rule,

$$M_{f_2 \xi} = \frac{\partial f_2}{\partial \dot{\rho}_1} M_{\dot{\rho}_1 \xi} + \frac{\partial f_2}{\partial \dot{\rho}_q} M_{\dot{\rho}_q \xi} \tag{57a}$$

where ξ stands for any of the elements in the state vector. For closely spaced stations, however,

$$M_{\dot{\rho}_1 \xi} \tilde{=} M_{\dot{\rho}_q \xi}; \frac{\partial f_2}{\partial \dot{\rho}_1} \tilde{=} \frac{\partial f_2}{\partial \dot{\rho}_q} \tag{57b}$$

Hence,

$$M_{f_2 \xi} \tilde{=} \frac{2 \partial f_2}{\partial \dot{\rho}_1} M_{\dot{\rho}_1 \xi} \tag{57c}$$

Let

$$K = \frac{2 \partial f_2}{\partial \rho_1} = \frac{64.719\ 1011}{c} \text{ (FRQ)} \tag{57d}$$

Then,

$$M_{f_2 V} = K M_{\dot{\rho}_1 V} \tag{57e}$$

$$M_{f_2 S} = K M_{\dot{\rho}_1 S} \tag{57f}$$

$$M_{f_2 R} = K M_{\dot{\rho}_1 R} \tag{57g}$$

$$M_{f_2 f_2} = 1 \tag{57h}$$

$$M_{f_2 c} = KM\dot{\rho}_i c \tag{57i}$$

$$M_{f_2 T} = KM\dot{\rho}_i T \tag{57j}$$

$$M_{f_2 P} = KM\dot{\rho}_i P \tag{57k}$$

6.3.3.3 Two-Way Non-Coherent Pseudo-Doppler. Using the same arguments as were given for two-way coherent doppler,

$$M_{f_3 \xi} \simeq \frac{2\partial f_3}{\partial \dot{\rho}_i} M_{\dot{\rho}_i \xi} \tag{58a}$$

Let

$$K' = \frac{2\partial f_3}{\partial \dot{\rho}_i} = \frac{62.696\ 6292}{c} (FRQ) \tag{58b}$$

Then,

$$M_{f_3 V} = K' M_{\dot{\rho}_i V} \tag{58c}$$

$$M_{f_3 S} = K' M_{\dot{\rho}_i S} \tag{58d}$$

$$M_{f_3 R} = K' M_{\dot{\rho}_i R} \tag{58e}$$

$$M_{f_3 f_3} = 1 \tag{58f}$$

$$M_{f_3 C} = K' M_{\dot{\rho}_i C} \tag{58g}$$

$$M_{f_3 T} = K' M_{\dot{\rho}_i T} \tag{58h}$$

$$M_{f_3 P} = K' M_{\dot{\rho}_i P} \tag{58i}$$

6.3.4 PARTIAL DERIVATIVES FOR ON-BOARD OBSERVATIONS

6.3.4.1 Introduction. For on-board observations, only matrices of the type M_{0V} and M_{00} will be used. These matrices relate the observations to vehicle position and velocity, and to the observations themselves, respectively.

6.3.4.2 Radar Altimeter Ranging, H

$$M_{HV} = 2\left[\frac{R}{R}\ 0\ \ 0\ \ 0\right] \tag{59a}$$

$$M_{HH} = 1 \tag{59b}$$

6.3.4.3 Stadiometric Ranging

$$M_{SRV} = \left[\frac{2R_R\ R_D}{R_D{}^3 \cos\frac{(SR)}{2}}\ 0\ \ 0\ \ 0\right] \tag{60a}$$

$$M_{SRSR} = 1 \tag{60b}$$

6.3.4.4 Angle Between Two Planets

$$M_{A_{PP}V} = \frac{\bar{m} - (\bar{n}\cdot\bar{m})\bar{n}}{R\ \sin(APP)} + \frac{\bar{n} - (\bar{n}\cdot\bar{m})\bar{m}}{Z\ \sin(APP)} \tag{61a}$$

$$\bar{m} = \frac{Z}{Z};\ \bar{n} = \frac{R}{R} \tag{61b}$$

$$M_{A_{PP}A_{PP}} = 1 \tag{61c}$$

6.3.4.5 Angle Between a Star and a Planet's Center

$$M_{A_{PS}V} = \frac{\bar{n} - (\bar{n}\cdot\bar{m})\bar{m}}{Z\ \sin(APS)} \tag{62a}$$

$$\bar{m} = \frac{Z}{Z};\ \bar{n} = [\cos(RA)\cos\delta\ \sin(RA)\cos\delta\ \sin\delta] \tag{62b}$$

$$M_{A_{PS}A_{PS}} = 1 \tag{62c}$$

6.3.4.6 Angle Between a Landmark and a Star

$$M_{A_{SLM}V} = \begin{bmatrix} \frac{\rho}{d} & 0 & 0 & 0 \end{bmatrix} \tag{63a}$$

$$\rho = d \times \bar{n} \times d \tag{63b}$$

$$M_{A_{SLM}A_{SLM}} = 1 \tag{63c}$$

6.3.4.7 Angle Between Two Landmarks

$$M_{A_{LL}V} = \begin{bmatrix} \frac{\bar{m} - (\bar{n}\cdot\bar{m})\bar{n}}{d \sin A_{LL}} + \frac{\bar{n} - (\bar{n}\cdot\bar{m})\bar{m}}{y \sin A_{LL}} & 0 & 0 & 0 \end{bmatrix} \tag{64a}$$

$$\bar{m} = \frac{d}{d}; \quad \bar{n} = \frac{y}{y} \tag{64b}$$

$$M_{A_{LL}A_{LL}} = 1 \tag{64c}$$

6.3.4.7 Star Occultation Time, T_{OCS}

$$M_{T_{OCS}V} = \frac{1}{\bar{l}_P \cdot \dot{\bar{R}}} [\, \bar{l}_P \cdot \bar{I} \;\; \bar{l}_P \cdot \bar{J} \;\; \bar{l}_P \cdot \bar{k} \;\; 0 \;\; 0 \;\; 0 \,], \tag{65a}$$

where $\bar{I}$, $\bar{J}$, and $\bar{k}$ are unit vectors in the base date coordinate system.

$$\bar{l}_P = \bar{l}_N \times \bar{n} \tag{65b}$$

$$\bar{l}_N = \frac{R \times \bar{n}}{|R \times \bar{n}|} \tag{65c}$$

$$M_{T_{OCS}T_{OCS}} = 1 \tag{65d}$$

6.4 AMBIGUITY RESOLUTION AND TIME CORRECTION

Prior to the introduction of data into the main Program, the available raw data have been passed through edit and merge routines to time order all data from all sources onto one input tape of standard format. After sorting and merging, there still remain two adjustments to be made before the data are used in the Program:

- The time which is assigned as the instant of an observation must take into account the finite propagation time from transmission to reception at each end of the link
- Some measuring systems produce ambiguous data in the sense that the recorded value differs from the real value by some uncertain multiple of a fixed quantity. The ambiguity is not readily resolvable by the measuring device since a priori information is needed.

The Program handles these two problems in the sequence shown in figure 6-7. The raw data, already time-ordered on the data tape, are read in. Each data time can be associated with up to four data types from any one station. As each time is read in, options are available for:

rejecting data which are marked as being of poor quality

rejecting data of any type from any station

rejecting all data from any station or stations

rejecting any particular data point which is not an integral multiple of an input value. This allows selecting 1n, 2n, 3n, 4n, ... data of any time from any station.

The next raw data time is selected, and two-body theory is used to compute the vehicle's position at that time, from which the station-to-vehicle distance, ρ_B, is computed and those data requiring ambiguity resolution have this correction made. The factor ρ_B/c where c is the velocity of light, is subtracted from the time recorded for each measurement time, translating back to the time the message was sent from the vehicle. The data, corrected for time, are sent to the main Program, where they are used in the statistical estimation process. The next data point is then brought in. Thus, the time correction and ambiguity resolution are continually repeated, the precision increasing as the precision of the orbit improves.

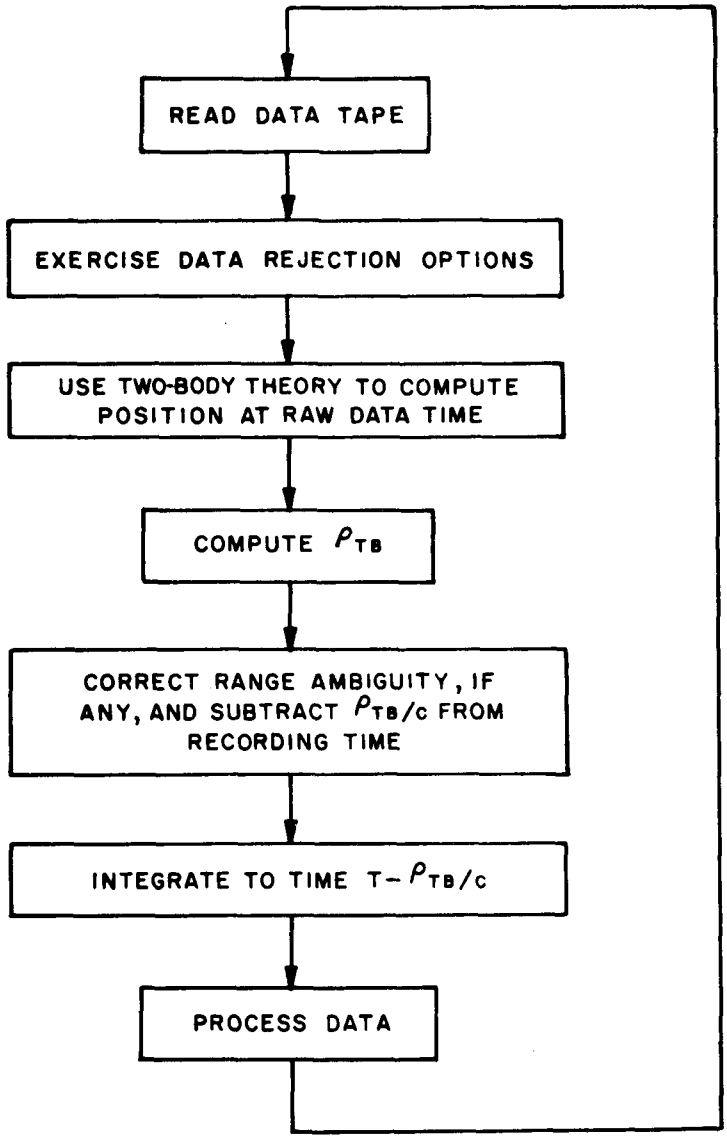

Figure 6-7 Data Selection and Correction

APPENDIX A

COORDINATE SYSTEMS AND TRANSFORMATIONS

A.1 INTRODUCTION

This appendix describes the transformations of vehicle initial conditions and earth and lunar oblateness attractions to the "base date" coordinate system used for trajectory calculations in the Program. The base date system is determined by the direction of the vernal equinox of 0^h0 January 1 of the year subsequent to the launch year. It has been chosen as the basis for calculation because the planetary and solar coordinates are written, on tapes, in that coordinate system. Rather than transform the tape information, the vehicle initial conditions and the oblateness accelerations are transformed into the base date system.

Vehicle initial conditions that are inserted in an earth-referenced system, such as latitude, longitude, and altitude, are transformed first to a system determined by the vernal equinox of date. This system (true earth) differs from the base date system by the Earth's nutation and precession. Transformation by the nutation matrix [N] and the precession matrix [A] then brings the initial conditions into the base date system.

The oblateness attraction of the Earth is calculated from a knowledge of the position of the vehicle from the center of the Earth, expressed in the true earth system. Since vehicle position, as calculated in the trajectory portion of the program is in base date components, these components must be transformed via precession and nutation into the true earth system. After computation, the oblateness attraction is transformed into the base date system.

The oblateness attraction of the moon is calculated from the vehicle position with respect to the moon's center and the lunar oblateness matrix.

The transformations described in this appendix are also employed in calculation of the observations and the matrices of their partial derivatives with respect to the state variables.

A.2 DEFINITION OF COORDINATE SYSTEMS

A.2.1 GENERAL. The transformations described in this appendix all represent rigid rotations of right-handed cartesian-coordinate systems. The following general coordinate systems are employed: direction of vernal equinox at a specified date; moon-referenced axes; geocentric; geodetic; selenocentric.

A.2.2 VERNAL EQUINOX SYSTEMS

A.2.2.1 Mean Vernal Equinox of Base Date. This system employs unit vectors $\bar{x}_B$, $\bar{y}_B$, and $\bar{z}_B$, defined as follows:

$\bar{x}_B$ - Unit vector directed towards the mean vernal equinox of base date, i.e., intersection of ecliptic (mean plane of Earth's motion about the Sun) of base date and mean equatorial plane of base date

$\bar{z}_B$ - Unit vector normal to mean equatorial plane of base date, positive in northern hemisphere

$\bar{y}_B$ - Unit vector completing right-handed orthogonal system with $\bar{x}_B$ and $\bar{z}_B$

A.2.2.2 Mean Vernal Equinox of Date. This system employs unit vectors $\bar{x}_Q$, $\bar{y}_Q$, and $\bar{z}_Q$, defined for the date of interest in the same manner as unit vectors $\bar{x}_B$, $\bar{y}_B$, and $\bar{z}_B$ are defined for the base date (paragraph A.2.2.1).

A.2.2.3 True Vernal Equinox of Date. This system employs unit vectors $\bar{x}_E$, $\bar{y}_E$, and $\bar{z}_E$ defined as follows:

$\bar{x}_E$ - Unit vector directed towards the true vernal equinox of date, i.e., intersection of true equatorial plane and ecliptic plane of date.

$\bar{z}_E$ - Unit vector normal to true equatorial plane, positive in northern hemisphere

$\bar{y}_E$ - Unit vector completing right-handed orthogonal system with $\bar{x}_E$ and $\bar{z}_E$.

A.2.3 MOON-REFERENCED AXES SYSTEM. This system employs unit vectors $\bar{x}_M$, $\bar{y}_M$, and $\bar{z}_M$, defined as follows:

$\bar{x}_M$ - Unit vector along the (A) principal axis of Moon, positive on Earth side

$\bar{z}_M$ - Unit vector along the (C) principal axis of the Moon, positive in the direction of rotation of Moon about its axis

$\bar{y}_M$ - Unit vector along the (B) principal axis of Moon, completing a right-handed system with $\bar{x}_M$ and $\bar{z}_M$.

A.2.4 GEOCENTRIC COORDINATE SYSTEM. This system employs the following parameters (see figure A-1):

$\bar{x}_G$ - Unit vector in true equatorial plane, directed toward intersection of Greenwich meridian with equatorial plane

$\bar{z}_G$ - Unit vector normal to true equatorial plane, positive in northern hemisphere

$\bar{y}_G$ - Unit vector completing a right-handed orthogonal system with $\bar{x}_G$ and $\bar{z}_G$

λ_E - Geocentric right ascension

ϕ_E - Declination of line from center of Earth to vehicle

R_E - Geocentric distance to vehicle

$\bar{\lambda}_E$ - Unit vector normal to vehicle's local meridian, positive eastward

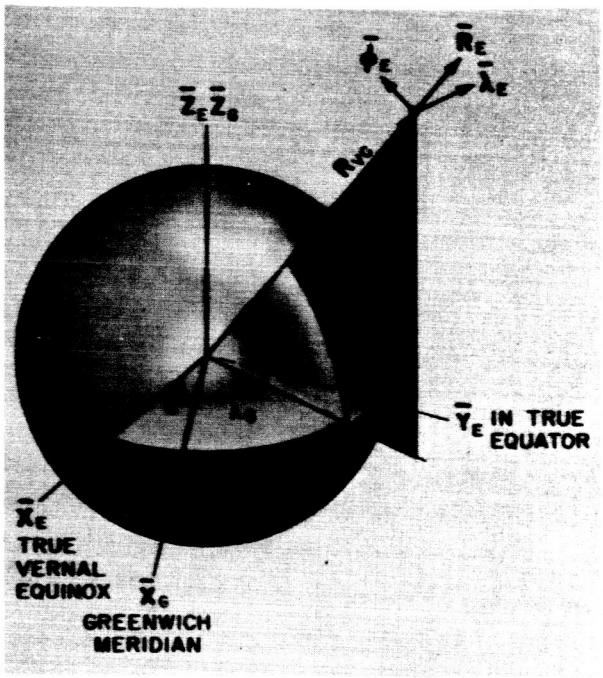

Figure A-1. Geocentric Coordinate System

$\bar{r}_E$ - Unit vector in direction of geocentric radius to vehicle

$\bar{\varphi}_E$ - Unit vector completing right-handed orthogonal system with $\bar{\lambda}_E$ and $\bar{r}_E$

A.2.5 GEODETIC COORDINATE SYSTEM. This system employs the following parameters (see figure A-2):

$\bar{\lambda}_G$ - Unit vector normal to vehicle's local meridian, positive eastward ($\bar{\lambda}_G = \bar{\lambda}_E$)

$\bar{h}_G$ - Unit vector along that normal to the Earth's surface (considered as an ellipsoid) which passes through the vehicle's position

$\bar{\varphi}_G$ - Unit vector completing right-handed orthogonal system with $\bar{\lambda}_G$ and $\bar{h}_G$

λ_G - Geodetic longitude, positive eastward from Greenwich meridian

ϕ_G - Geodetic latitude (angle between equatorial plane and $\bar{h}_G$)

h_G - Altitude above Earth's surface, measured along $\bar{h}_G$.

A.2.6 SELENOCENTRIC COORDINATE SYSTEM. This system employs the following coordinates (see figure A-3):

$\bar{\lambda}_m$ - Unit vector normal to local moon meridian, positive eastward

$\bar{r}_m$ - Unit vector from center of moon to vehicle

$\bar{\varphi}_M$ - Unit vector completing right-handed orthogonal system with $\bar{\lambda}_m$ and $\bar{r}_m$

λ_M - Selenocentric longitude, measured in the $\bar{x}_M$ - $\bar{y}_M$ plane (paragraph A.2.3) in the sense of positive rotation about $\bar{z}_m$

ϕ_M - Selenocentric declination of line from moon center to vehicle

R_M - Selenocentric distance from moon center to vehicle

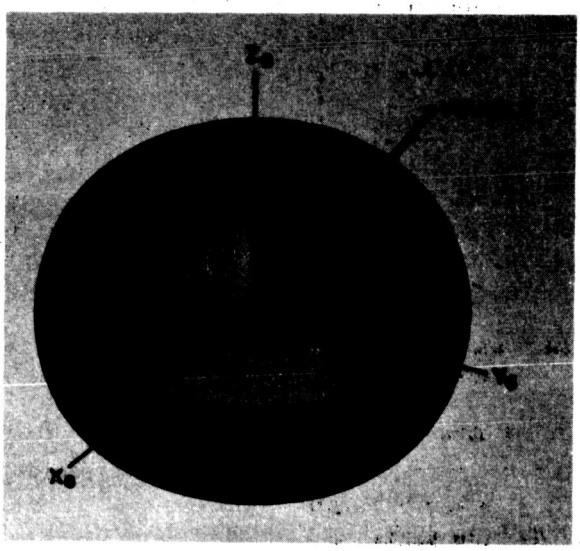

Figure A-2. Geodetic Coordinate System

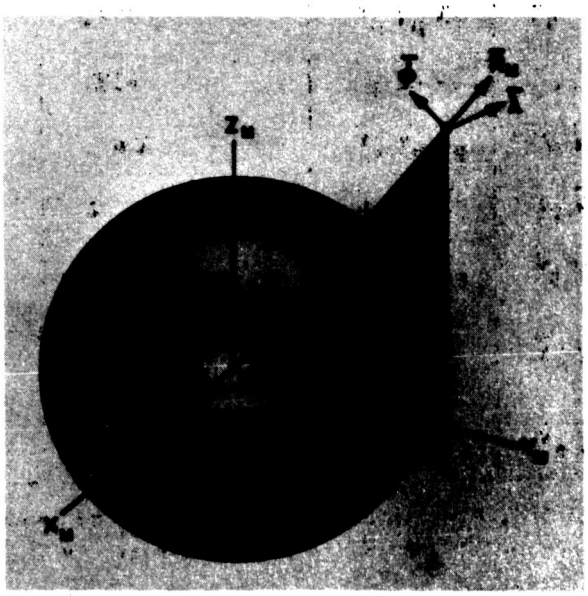

Figure A-3. Selenocentric Coordinate System

A.2.7 AZIMUTH AND FLIGHT PATH ANGLES. The following vehicle flight parameters are employed (see figure A-4):

V - Velocity of vehicle relative to the $\bar{x}_G$, $\bar{y}_G$, $\bar{z}_G$ coordinate system

A_G - Azimuth relative to $\bar{\lambda}_G$, $\bar{\varphi}_G$, $\bar{h}_G$ system

γ_G - Flight path angle relative to $\bar{\lambda}_G$, $\bar{\varphi}_G$, $\bar{h}_G$ system

A_E - Azimuth relative to $\bar{\lambda}_E$, $\bar{\varphi}_E$, $\bar{r}_E$ system

γ_E - Flight path angle relative to $\bar{\lambda}_E$, $\bar{\varphi}_E$, $\bar{r}_E$ system.

A.3 LIST OF TRANSFORMATIONS

Table A-1 lists the coordinate system transformation matrices used in the Program. The coordinate systems under the From and To columns are defined in paragraph A.2. The matrices used are given in paragraph A.4.

Table A-1. Transformation Matrices

Matrix Symbol	Matrix Name	Acronym	From	To
[A]	Precession	PREC	$\bar{x}_Q\ \bar{y}_Q\ \bar{z}_Q$	$\bar{x}_B\ \bar{y}_B\ \bar{z}_B$
[N]	Nutation	NUTA	$\bar{x}_E\ \bar{y}_E\ \bar{z}_E$	$\bar{x}_Q\ \bar{y}_Q\ \bar{z}_Q$
[L]	Libration	LIBRA	$\bar{x}_M\ \bar{y}_M\ \bar{z}_M$	$\bar{x}_E\ \bar{y}_E\ \bar{z}_E$
[γ]	Gamma Matrix	GAMMAT	$\bar{x}_G\ \bar{y}_G\ \bar{z}_G$	$\bar{x}_E\ \bar{y}_E\ \bar{z}_E$
[G]	Geodetic to Greenwich Transformation	GENMAT (λ_G,ϕ_G)	$\bar{\lambda}_G\ \bar{\varphi}_G\ \bar{h}_G$	$\bar{x}_G\ \bar{y}_G\ \bar{z}_G$
[ERA]	Declination, Right Ascension	GENMAT (λ_E,ϕ_E)	$\bar{\lambda}_E\ \bar{\varphi}_E\ \bar{R}_E$	$\bar{x}_E\ \bar{y}_E\ \bar{z}_E$
[S]	Selenographic	GENMAT (λ_M,ϕ_M)	$\bar{\lambda}_M\ \bar{\varphi}_M\ \bar{R}_M$	$\bar{x}_M\ \bar{y}_M\ \bar{z}_M$

NOTE: Since all the transformation matrices listed in table A-1 are orthogonal, the inverse of any is simply its transpose.

A.4 TRANSFORMATIONS

A.4.1 PRECESSION. The spin axis of the Earth is slowly precessing in inertial space due to lunar and solar attractions on the terrestrial bulge. The plane of the Earth's orbit about the Sun (ecliptic) moves slowly because of planetary attractions. As a result

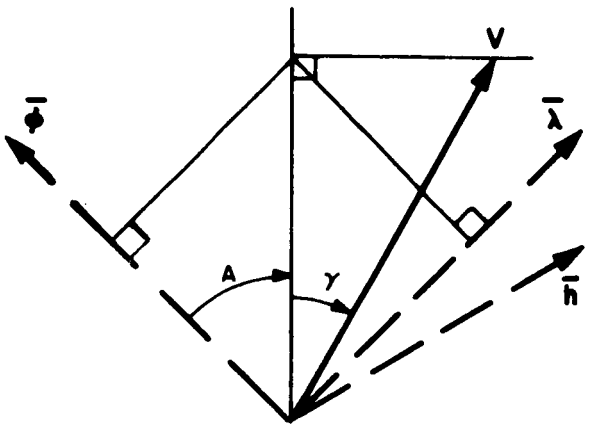

A POSITIVE CW FROM NORTH
γ POSITIVE UP FROM $\bar{\phi}-\bar{\lambda}$ PLANE

Figure A-4. Azimuth and Flight Path Angles

the intersection of the Earth's mean equator and the ecliptic (termed the vernal equinox, γ) undergoes a gradual rotation in space. Therefore, the $\bar{x}_Q$, $\bar{y}_Q$, $\bar{z}_Q$ coordinate system is rotating with respect to the $\bar{x}_B$, $\bar{y}_B$, $\bar{z}_B$ system. Figure A-5 illustrates this rotation of the vernal equinox with respect to its position at base date.

The following form of the precession transformation matrix is derived from the forms in references 6, 20, and 21.

The standard form of the precession matrix is a set of elements $a_{ij}(T)$ that are functions of the time T in Julian centuries of 36525 days from some standard time, usually 0^h0 January 1, 1950, to the present epoch. This transformation $[a(T)]$ takes a vector from the present-time system to the January 1, 1950 system, i.e., through the small angle that the earth has precessed in the time T.*

It is desired to refer vectors to 0^h0 January 1 of year subsequent to launch rather than the 1950 date. Let

T_B = time in Julian centuries from 0^h0 January 1, 1950 to 0^h0 January 1, of year after launch.

ΔT = time in Julian centuries from 0^h0 January 1, of year after launch, to the present (trajectory) time.

$T = T_B + \Delta T$ = time in Julian centuries from 0^h0 January 1, 1950 to trajectory time.

The desired transformation from the present system to the new base date is the product of $[a(T)]$, which transforms from the present date system to the 1950 date system, and $[a(T_B)]^{-1}$ which goes from the 1950 system to the base date system. Thus, the precession matrix, $[A]$, is given by

$$[A] \triangleq [a(T_B)]^{-1} [a(T)]$$

$$= [a(T_B)]^{-1} [a(T_B + \Delta T)]$$

*For an alternative form of the precession matrix used in the Program, see the Programmer's Manual.

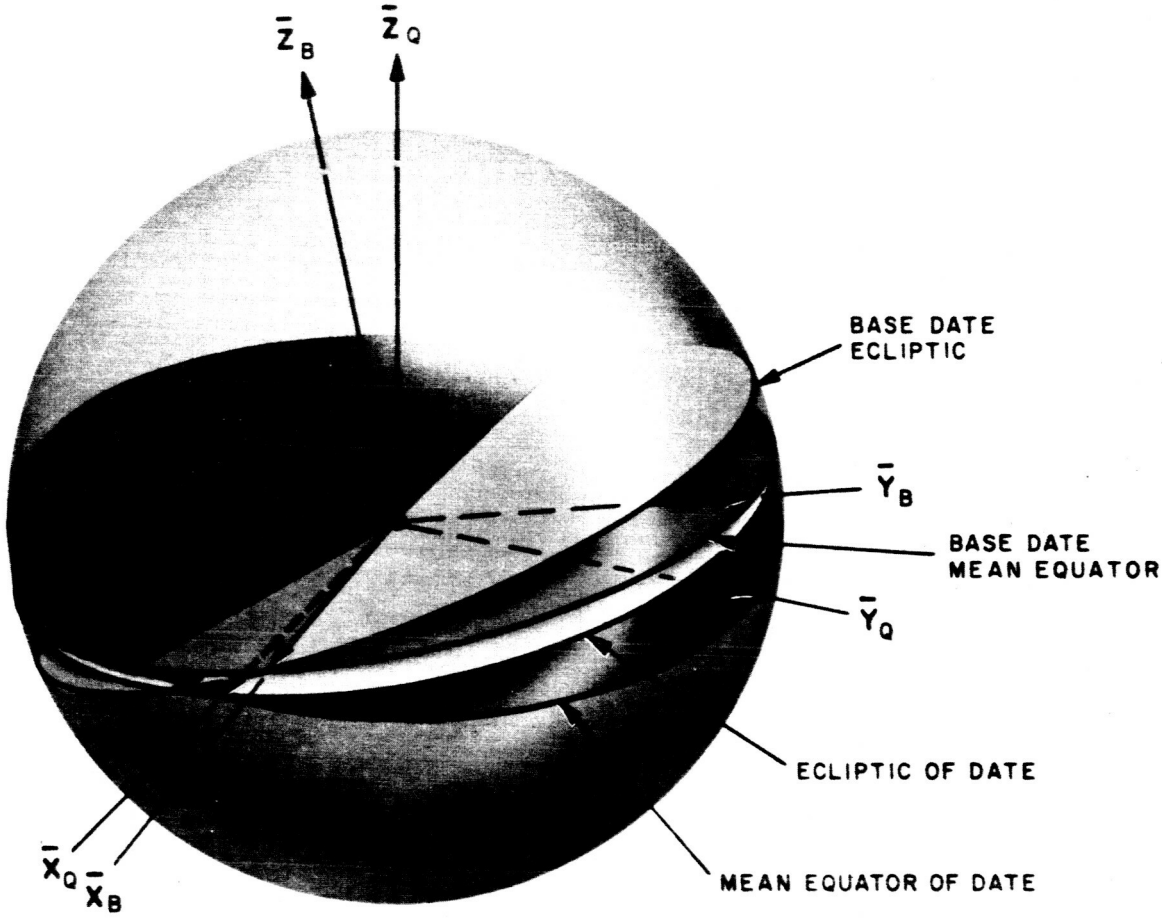

Figure A-5. Precession of Equinoxes

The quantity $a(T_B + \Delta T)$ can be written as a sum:

$$[a(T_B + \Delta T)] = [a(T_B)] + [\Delta a(\Delta T, T_B)]$$

So that

$$[A] = [a(T_B)]^{-1} \{[a(T_B)] + [\Delta a(T_B, \Delta T)]\}$$

$$[A] = [I] + [a(T_B)]^{-1} [\Delta a(T_B, \Delta T)]$$

$$[A] = \begin{bmatrix} 1 & 0 & 0 \\ 0 & 1 & 0 \\ 0 & 0 & 1 \end{bmatrix} + \begin{bmatrix} a_{11} & a_{22} & a_{31} \\ a_{12} & a_{22} & a_{32} \\ a_{13} & a_{23} & a_{33} \end{bmatrix}_{T_B} \begin{bmatrix} \Delta a_{11} & \Delta a_{12} & \Delta a_{13} \\ \Delta a_{21} & \Delta a_{22} & \Delta a_{23} \\ \Delta a_{31} & \Delta a_{32} & \Delta a_{33} \end{bmatrix}_{T_B, \Delta T}$$

where the elements a_{ij} are $a_{ij}(T_B)$, the standard forms of the precession transformation elements evaluated at T_B.

The Δa_{ij} elements are obtained from their definition as follows:

$$a_{ij}(T_B + \Delta T) \stackrel{\Delta}{=} a_{ij}(T_B) + \Delta a_{ij}(\Delta T, T_B)$$

$$\Delta a_{ij}(\Delta T, T_B) = a_{ij}(T_B + \Delta T) - a_{ij}(T_B)$$

Expanding in a power series, using terms up to the third power,

$$\Delta a_{ij}(\Delta T, T_B) = a^0{}_{ij} + a^1{}_{ij}(T_B + \Delta T) + a^2{}_{ij}(T_B + \Delta T)^2 + a^3{}_{ij}(T_B + \Delta T)^3$$

$$- a^0{}_{ij} - a^1{}_{ij}\, T_B - a^2{}_{ij}\, T_B{}^2 - a^3{}_{ij}\, T_B{}^3$$

$$= a^1{}_{ij}\Delta T + a^2{}_{ij}(2T_B\, \Delta T + \Delta T^2) + a^3{}_{ij}(3T_B{}^2\, \Delta T + 3T_B\, \Delta T^2 + \Delta T^3)$$

$$= a^1{}_{ij}\, \tau_1 + a^2{}_{ij}\, \tau_2 + 3a^3{}_{ij}\, \tau_3$$

where

$$\tau_1 \stackrel{\Delta}{=} \Delta T\,,$$

$$\tau_2 \stackrel{\Delta}{=} (2\, T_B\, \Delta T + \Delta T^2),$$

and

$$\tau_3 \stackrel{\Delta}{=} \left(T_B{}^2\, \Delta T + T_B\, \Delta T^2 + \frac{1}{3}\Delta T^3\right)$$

The a_{ij} and Δa_{ij} elements are as follows:

$$a_{11} = 1.0000000 - 0.000296970\ T_B^2 - 0.000000130\ T_B^3$$

$$a_{12} = 0.02234988\ T_B + 0.00076700\ T_B^2 - 0.00000221\ T_B^3$$

$$a_{13} = 0.00971711\ T_B - 0.00000207\ T_B^2 - 0.00000096\ T_B^3$$

$$a_{21} = -a_{12}$$

$$a_{22} = 1.0000000 - 0.00024976\ T_B^2 - 0.00000015\ T_B^3$$

$$a_{23} = -0.00010859\ T_B^2 - 0.000000030\ T_B^3$$

$$a_{31} = -a_{13}$$

$$a_{32} = a_{23}$$

$$a_{33} = 1.0000000 - 0.00004721\ T_B^2 + 0.000000020\ T_B^3$$

and

$$\Delta a_{11} = - 0.00029697\ \tau_2 - 0.000000390\ \tau_3$$

$$\Delta a_{12} = 0.02234988\ \tau_1 + 0.00000676\ \tau_2 - 0.00000663\ \tau_3$$

$$\Delta a_{13} = 0.00971711\ \tau_1 - 0.00000207\ \tau_2 - 0.00000288\ \tau_3$$

$$\Delta a_{21} = -\Delta a_{12}$$

$$\Delta a_{22} = -0.00024976\ \tau_2 - 0.000000450\ \tau_3$$

$$\Delta a_{23} = -0.00010859\ \tau_2 - 0.000000090\ \tau_3$$

$$\Delta a_{31} = -\Delta a_{13}$$

$$\Delta a_{32} = +\Delta a_{23}$$

$$\Delta a_{33} = -0.00004721\ \tau_2 + 0.000000060\ \tau_3$$

The elements of the precession matrix are computed whenever needed with the exception that if the matrix has been computed within the previous 1322 seconds, the previous value is used.

A.4.2 NUTATION. Nutation is the periodic angular motion experienced by the Earth's spin axis. The Earth's mean equatorial plane is the mean plane of the oscillatory motion. The oscillatory motion of the $\bar{x}_E$, $\bar{y}_E$, $\bar{z}_E$ system about its mean position, the $\bar{x}_Q$, $\bar{y}_Q$, and $\bar{z}_Q$ system, is described by the transformation between the two systems. The nutation matrix [N] is as follows:

$$[N] = \begin{bmatrix} 1 & -\delta\psi \cos \epsilon_Q & -\delta\psi \sin \epsilon_Q \\ \delta\psi \cos \epsilon_Q & 1 & -\delta\epsilon \\ \delta\psi \sin \epsilon_Q & \delta\epsilon & 1 \end{bmatrix}$$

The geometric significance of $\delta\psi$, $\delta\epsilon$, and ϵ_Q is shown in figure A-6; refer to paragraph A.4.6 for a discussion of these parameters.

The preceding expression for [N] matrix is an approximation, valid to about 0.5×10^{-8}. The exact transformation is given in reference 6, pp. 67-68. More complete discussions of nutation may be found in references 22 and 23.

The nutation terms are recomputed if needed and if the prior values are more than 0.1 day old.

A.4.3 LIBRATION. It is possible for an orbiting satellite in a circular orbit to have an angular rotation in a direction such that the satellite tends to keep a constant face to its attracting body. This condition can only exist in a truly circular orbit. In an eccentric orbit, $\dot{\theta}$ (figure A-7) is not constant; hence, to an observer on the attracting body, the satellite appears to oscillate or librate.

In the Program, the libration matrix, [L], is used to correct, when necessary, for the Moon's libration; this matrix gives the transformation from the Moon-referenced axes system, $\bar{x}_M$ $\bar{y}_M$ $\bar{z}_M$, to the $\bar{x}_E$ $\bar{y}_E$ $\bar{z}_E$ system axes as shown in figure A-8.

$$[L] = \begin{bmatrix} \ell_{11} & \ell_{12} & \ell_{13} \\ \ell_{21} & \ell_{22} & \ell_{23} \\ \ell_{31} & \ell_{32} & \ell_{33} \end{bmatrix}$$

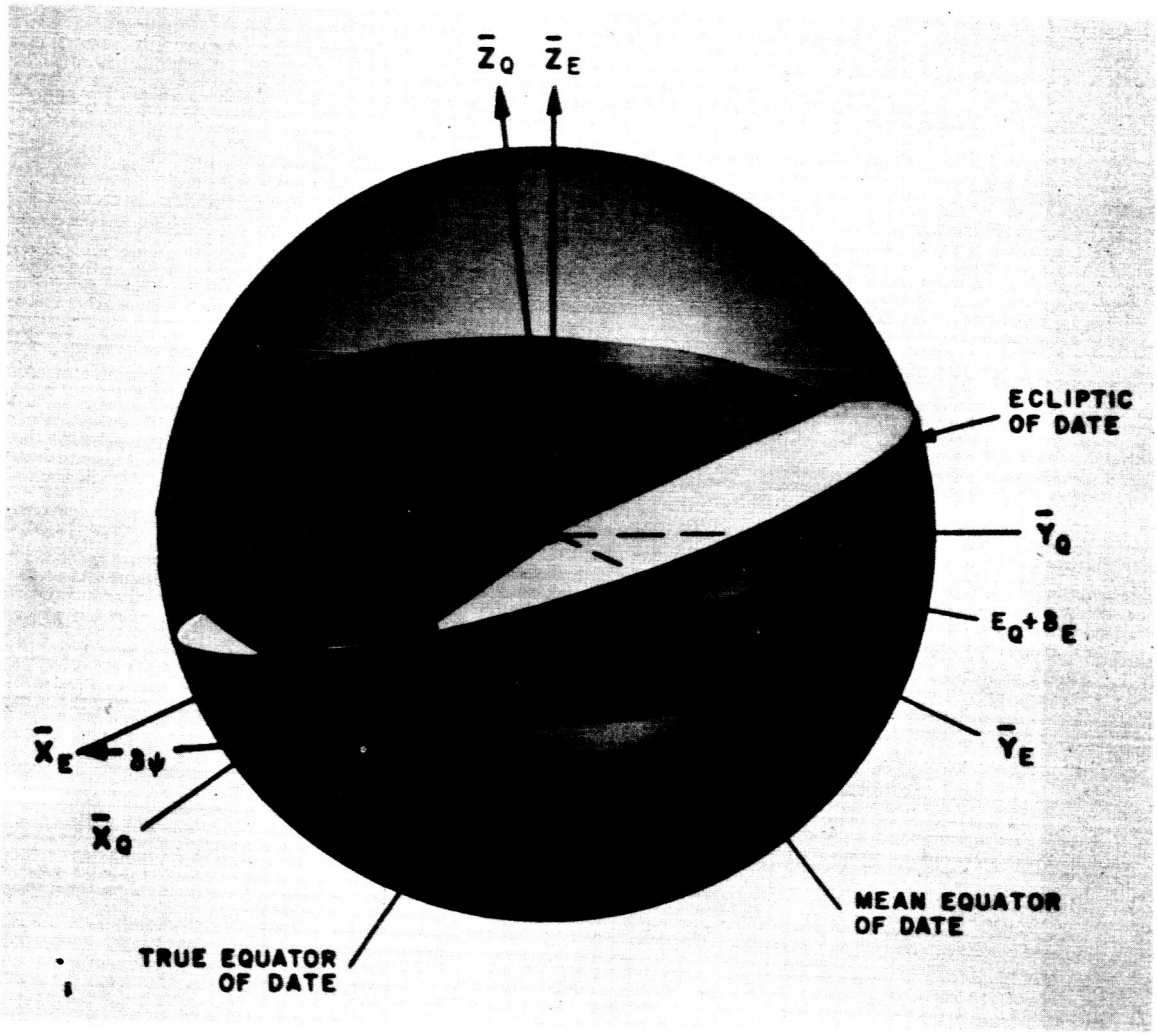

Figure A-6. Nutation Angles

where the ℓ_{ij} are given in terms of the three angles Ω', Λ, i:

$$\ell_{11} = \cos \Omega' \cos \Lambda - \sin \Omega' \sin \Lambda \cos i$$

$$\ell_{12} = - \cos \Omega' \sin \Lambda - \sin \Omega' \cos \Lambda \cos i$$

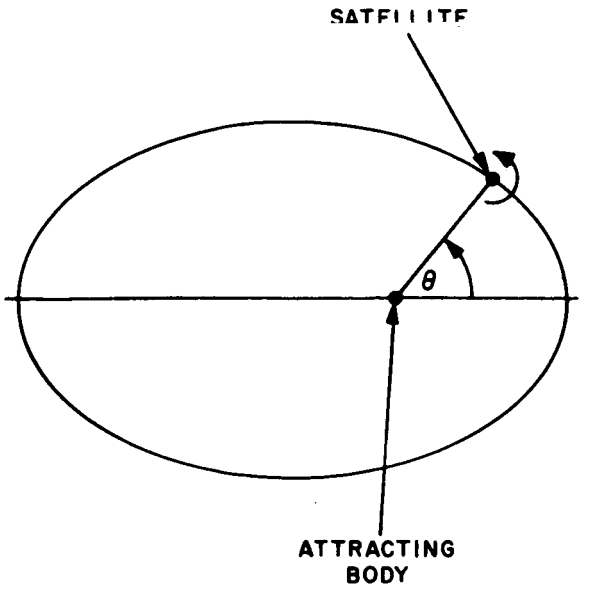

Figure A-7. Libration Geometry

$$\hat{\imath}_{13} = \sin\Omega' \sin i$$

$$\ell_{21} = \sin\Omega' \cos\Lambda + \cos\Omega' \sin\Lambda \cos i$$

$$\ell_{22} = -\sin\Omega' \sin\Lambda + \cos\Omega' \cos\Lambda \cos i$$

$$\ell_{23} = -\cos\Omega' \sin i$$

$$\ell_{31} = \sin\Lambda \sin i$$

$$\ell_{32} = \cos\Lambda \sin i$$

$$\ell_{33} = \cos i$$

The angles Ω', Λ, i are obtained as follows:

$$\sin\Omega' = -\sin(\Omega + \sigma + \delta\psi) \sin(I + \rho) \csc i, \qquad -90° < \Omega' < +90°$$

$$\Lambda = \Delta + \text{(illegible)} - \Omega + \tau - \sigma, \qquad 0° \leq \Lambda \leq 360°$$

$$\cos i = \cos(I + \rho) \cos\epsilon_E + \sin\epsilon_E \sin(I + \rho) \cos(\Omega + \sigma + \delta\psi), \qquad 0° < i < 90°$$

where

$$I = 1° 32.1'$$

$$\sin\Delta = -\sin(\Omega + \sigma + \delta\psi) \csc i \sin\epsilon_E \qquad 0° \leq \Delta < 360°$$

$$\cos\Delta = -\cos(\Omega + \sigma + \delta\psi) \cos\Omega' - \sin(\Omega + \sigma + \delta\psi) \sin\Omega' \cos\epsilon_E$$

$$\sigma = \frac{1}{\sin I} [-0.°0302777 \sin g + 0.°0102777 \sin(g + 2\omega) - 0.°00305555 \sin(2g + 2\omega)]$$

$$\tau = -0.°003333 \sin g + 0.°0163888 \sin g' + 0.°005 \sin 2\omega$$

$$\rho = -0.°0297222 \cos g + 0.°0102777 \cos(g + 2\omega) - 0.°00305555 \cos(2g + 2\omega)$$

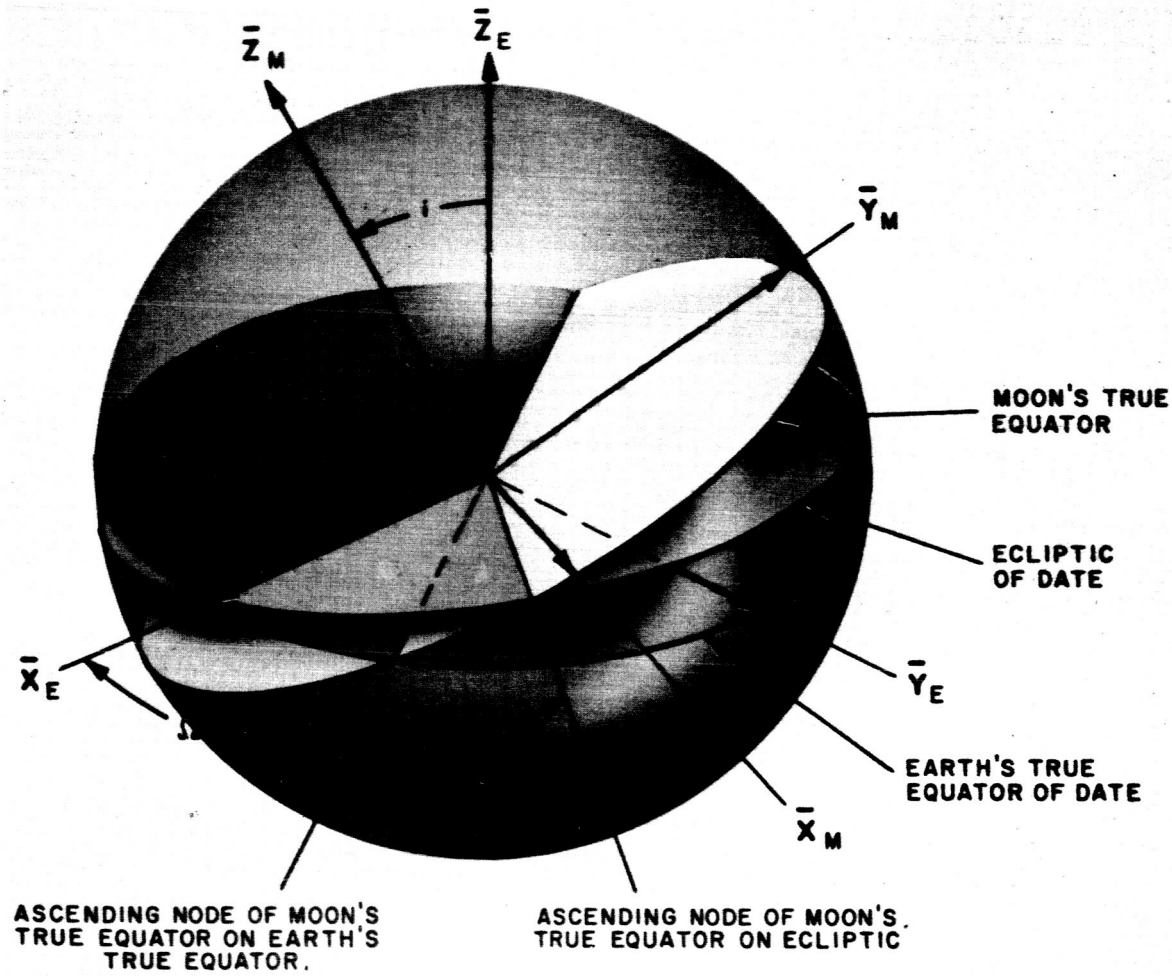

Figure A-8. Libration Angles

and

$$g = 215.^{\circ}54013 + 13.^{\circ}064992\ (d - d_{50})$$

$$g' = 358.^{\circ}009067 + 0.^{\circ}9856005\ (d - d_{50})$$

$$\omega = 196.^{\circ}745632 + 0.^{\circ}1643586\ (d - d_{50})$$

$$\epsilon_E = \epsilon_Q + \delta\epsilon$$

The libration formulas are taken from reference 6, and may be found also in references 6 and 20. A description of ϵ_Q, $\delta\epsilon$, Ω, $\mathfrak{Q}$, and $\delta\psi$ is given in paragraph A.4.6.

The libration matrix is recomputed when needed, except that the prior values are used if they were calculated less than 0.01 day previously.

A.4.4 GAMMA MATRIX. The gamma matrix, $[\gamma]$, transforms a vector from the x_G, y_G, z_G system to the x_E, y_E, z_E system. From references 6 and 20, the expression for $[\gamma]$ is

$$[\gamma] = \begin{bmatrix} \cos\gamma & -\sin\gamma & 0 \\ \sin\gamma & \cos\gamma & 0 \\ 0 & 0 & 1 \end{bmatrix}$$

where $\gamma = \gamma_M + \delta\alpha$ degrees

$$\gamma_M = \begin{bmatrix} 100^\circ.07554260 + 0^\circ.9856473460\ di \\ +2^\circ.9015 \times 10^{-13}\ (di)^2 + \omega_e t' \end{bmatrix} \text{ modulo } 360^\circ$$

where

$$di = IP\ [d - d_{50}] \qquad \text{(dimensionless)}$$

$$t' = [3600\ (t - t_\ell + hrs) + 60H\ min + sec]$$

$$- \left[IP \left[\frac{3600\ (t - t_\ell + hrs) + 60H\ min + sec}{86400} \right] \right] 86400$$

$$\omega_e = \frac{0.72921158558 \times 10^{-4}}{(1 + 5.21 \times 10^{-13}\ d_i)} \quad \frac{\text{radians}}{\text{sec}}$$

$IP\ [X]$ = integral part of $[X]$

$\delta\alpha = \delta\psi \cos\epsilon_Q$

A.4.5 GENERAL PURPOSE ORTHOGONAL TRANSFORMATION MATRICES. The [G], [DRA] and [S] transformation matrices listed in table A-1 all have the same form:

$$[G] = \begin{bmatrix} -\sin\lambda_G & -\sin\phi_G \cos\lambda_G & \cos\phi_G \cos\lambda_G \\ \cos\lambda_G & -\sin\phi_G \sin\lambda_G & \cos\phi_G \sin\lambda_G \\ 0 & \cos\phi_G & \sin\phi_G \end{bmatrix}$$

where λ_G and ϕ_G are the geodetic longitude and latitude of the sub-vehicle point or of the observation station.

For the [DRA] matrix, the right ascension λ_E of the vehicle or station replaces λ_G, and the declination ϕ_E replaces ϕ_G.

For the [S] matrix, the lunar longitude λ_M of the vehicle replaces λ_G and lunar latitude ϕ_M replaces ϕ_G.

The above transformations may be obtained by inspection of figures A-1 through A-3.

A.4.6 NUTATION AND LIBRATION PARAMETERS. The nutation and libration matrices use, among others, the following parameters: mean obliquity, ϵ_Q (figure A-6); nutation in obliquity, $\delta\epsilon$; mean longitude of descending node of the Moon's mean equator on the ecliptic, Ω; mean longitude of the Moon, ℓ ; nutation in longitude, $\delta\psi$. The expression for these parameters, given in references 6 and 20, are as follows:

$$\epsilon_Q = 23.^\circ 4457874 - 0.^\circ 01301376T - 0.^\circ 8855 \times 10^{-6}T^2 + 0.^\circ 503 \times 10^{-6}T^3 \quad (1)$$

$$\delta\epsilon = \Delta\epsilon + d\epsilon \text{ degrees} \quad (2)$$

$$\begin{aligned}\Delta\epsilon = {} & + 0.^\circ 255833 \times 10^{-2} \cos\Omega - 0.^\circ 25 \times 10^{-4} \cos 2\Omega \\ & + 0.^\circ 1530555 \times 10^{-3} \cos 2L + 0.^\circ 61111 \times 10^{-5} \cos(3L - \Gamma) \\ & - 0.^\circ 25 \times 10^{-5} \cos(L + \Gamma) - 0.^\circ 194444 \times 10^{-5} \cos(2L - \Omega) \\ & - 0.^\circ 8333 \times 10^{-6} \cos(2\Gamma' - \Omega)\end{aligned} \quad (3)$$

$$\begin{aligned}d\epsilon = {} & + 0.^\circ 24444 \times 10^{-4} \cos 2\ell + 0.^\circ 5 \times 10^{-5} \cos(2\ell - \Omega) \\ & + 0.^\circ 30555 \times 10^{-5} \cos(3\ell - \Gamma') - 0.^\circ 13888 \times 10^{-5} \cos(\ell + \Gamma') \\ & - 0.^\circ 8333 \times 10^{-6} \cos(\ell - \Gamma' + \Omega) + 0.^\circ 8333 \times 10^{-6} \cos(\ell - \Gamma' - \Omega) \\ & + 0.^\circ 5555 \times 10^{-6} \cos(3\ell - 2L + \Gamma') + 0.^\circ 5555 \times 10^{-6} \cos(3\ell - \Gamma' - \Omega)\end{aligned} \quad (4)$$

$$\begin{aligned}\Omega = {} & 12.^\circ 1127902 - 0.^\circ 0529539222\ (d - d_{50}) + 0.^\circ 20795 \times 10^{-2}T \\ & + 0.^\circ 2081 \times 10^{-2}T^2 + 0.^\circ 2 \times 10^{-5}T^3\end{aligned} \quad (5)$$

$$\ell = 64.^{\circ}37545167 + 13.^{\circ}1763965268\ (d - d_{50}) - 0.^{\circ}1131575 \times 10^{-2}T$$

$$- 0.^{\circ}113015 \times 10^{-2}T^2 + 0.^{\circ}19 \times 10^{-5}T^3 \qquad (6)$$

$$\delta\psi = \Delta\psi + d\psi \text{ (degrees)} \qquad (7)$$

$$\Delta\psi = -[0.^{\circ}47895611 \times 10^{-2} + 0.^{\circ}47222 \times 10^{-5}T] \sin\Omega$$

$$+ 0.^{\circ}580550 \times 10^{-4} \sin 2\Omega - 0.^{\circ}35333 \times 10^{-3} \sin 2L$$

$$+ 0.^{\circ}350 \times 10^{-4} \sin (L - \Gamma) - 0.^{\circ}13888 \times 10^{-4} \sin (3L - \Gamma)$$

$$+ 0.^{\circ}58333 \times 10^{-5} \sin (L + \Gamma) + 0.^{\circ}3333 \times 10^{-5} \sin (2L - \Omega)$$

$$+ 0.^{\circ}13888 \times 10^{-5} \sin (2\Gamma' - \Omega) + 0.^{\circ}11111 \times 10^{-5} \sin (2L - 2\Gamma')$$

$$d\psi = -0.^{\circ}56666 \times 10^{-4} \sin (2\ell) + 0.^{\circ}18888 \times 10^{-4} \sin (\ell - \Gamma')$$

$$+ 0.^{\circ}83333 \times 10^{-6} \sin 2(\ell - \Gamma') - 0.^{\circ}94444 \times 10^{-5} \sin (2\ell - \Omega)$$

$$- 0.^{\circ}7222 \times 10^{-5} \sin (3\ell - \Gamma') + 0.^{\circ}41666 \times 10^{-5} \sin (\ell - 2L + \Gamma')$$

$$+ 0.^{\circ}30555 \times 10^{-5} \sin (\ell + \Gamma') + 0.^{\circ}16666 \times 10^{-5} \sin 2 (\ell - L)$$

$$+ 0.^{\circ}16666 \times 10^{-5} \sin (\ell - \Gamma' + \Omega) + 0.^{\circ}16666 \times 10^{-5} \sin (\ell - \Gamma' - \Omega)$$

$$- 0.^{\circ}13888 \times 10^{-5} \sin (3\ell - 2L + \Gamma') - 0.^{\circ}1111 \times 10^{-5} \sin (3\ell - \Gamma' - \Omega) \qquad (9)$$

where Γ, Γ', L are obtained from

$$\Gamma = 282.^{\circ}08053028 + 0.^{\circ}470684 \times 10^{-4}\ (d - d_{50}) + 0.^{\circ}45525 \times 10^{-3}T$$

$$+ 0.^{\circ}4575 \times 10^{-3}T^2 + 0.3 \times 10^{-5}T^3 \qquad (10)$$

$$\Gamma' = 208.^{\circ}8439877 + 0.^{\circ}1114040803(d - d_{50}) - 0.^{\circ}010334T - 0.^{\circ}010343T^2 - 0.^{\circ}12 \times 10^{-4}T^3 \qquad (11)$$

$$L = 280.^{\circ}08121009 + 0.^{\circ}9856473354\ (d - d_{50}) + 0.^{\circ}302 \times 10^{-3}T + 0.^{\circ}302 \times 10^{-3}T^2 \qquad (12)$$

APPENDIX B

TRANSFORMATION FROM A POWER SERIES TO A CHEBYSHEV POLYNOMIAL SERIES

B.1 INTRODUCTION

Lanczos (reference 24) has pointed out that for a specified tolerable error in a given function, the Chebyshev polynomial expansion of the function converges more rapidly than any other polynomial representation. Stated another way, for a given number of terms, the Chebyshev expansion is the most accurate. In addition, a simple algorithm may be used to compute the $(k + 1)^{th}$ Chebyshev polynomial given the k^{th} and $(k - 1)^{th}$ terms. Consequently, it is sometimes desirable to convert a function from a power series representation to a Chebyshev expansion. A general procedure is described here for obtaining coefficients of the Chebyshev expansion given the power series coefficients.

B.2 CHEBYSHEV POLYNOMIALS

Consider an arbitrary integrable function of bounded variation,

$$y = f(x) \tag{1}$$

which is defined over some interval $-x_M \leq x \leq x_M$. Let the power series expansion of equation (1) be

$$f(x) = P_o' + P_1'x + P_2' x^2 + \ldots . \tag{2}$$

With appropriate normalization of the independent variable, equation (1) may equally well be developed in a series of Chebyshev polynomials,

$$f(t) = \frac{K_o}{2} + K_1 T_1(t) + K_2(t) + \ldots . , \tag{3}$$

where the $T_n(t)$ are functions of the normalized variable, t, or in a series of shifted Chebyshev polynomials

$$f(t') = \frac{K_o'}{2} + K_1' T_1^*(t') + K_2 T_2^*(t') + \ldots . \tag{4}$$

where the $T_n^*(t')$ are functions of the normalized variable, t'. The series of equation (3) is obtained from equation (1) by normalizing x such that

$$\frac{x}{x_M} = \cos\theta = t \tag{5}$$

For this normalized variable, the K_r coefficients are given by

$$K_r = \frac{2}{\pi}\int_{-1}^{1} f(t)T_r(t)\,\frac{dt}{\sqrt{1 - t^2}}. \tag{6}$$

Also, given that

$$\begin{aligned} T_0(t) &= 1 \\ T_1(t) &= t \end{aligned} \tag{7}$$

the recursive formula for $T_{r+1}(t)$ is

$$T_{r+1}(t) = 2tT_r(t) - T_{r-1}(t) \tag{8}$$

Similarly, the series of equation (4) is obtained by defining a normalized variable, t', having a range only from 0 to 1:

$$\frac{x}{x_M} = \frac{1 + \cos\theta}{2} = t' \tag{9}$$

Given that

$$\begin{aligned} T_0^*(t') &= 1 \\ T_1^*(t') &= 2t' - 1 \end{aligned} \tag{10}$$

the recursive formula for $T_{r+1}^*(t')$ is

$$T_{r+1}^*(t') = 2(2t' - 1)T_r^*(t') - T_{r-1}^*(t') \tag{11}$$

It follows from the normalizing equations, (5) and (9), that the relation between the shifted and unshifted polynomials is

$$T_r(t) = T_r(2t' - 1) = T_r^*(t') \tag{12}$$

Consequently, the coefficients of the series of equations (3) and (4) are equal so that

$$K_r' = K_r \tag{13}$$

Evaluation of equation (6) therefore provides the coefficients for both series. It remains now to determine the K_r coefficients given the P_j' coefficients of equation (2).

B.3 DETERMINATION OF THE CHEBYSHEV COEFFICIENTS

The series of equation (2) when rewritten in terms of the normalized variable t becomes

$$f(t) = P_0' + P_1' x_M \left(\frac{x}{x_M}\right) + P_2' x_M^2 \left(\frac{x}{x_M}\right)^2 + \ldots . \tag{14}$$

Redefining the coefficients of the expansion such that

$$P_r = P_r' (x_M)^r \tag{15}$$

equation (14) becomes

$$f(t) = P_0 + P_1 t + P_2 t^2 + \ldots . \tag{16}$$

If the integrand of equation (6), $f(t)\, T_r(t)$, is expanded in a power series in t, the functional form of the typical integral for a given term in the series will be

$$I_n' = \int_{-1}^{1} \frac{t^n dt}{\sqrt{1 - t^2}} \tag{17}$$

Evaluating I'_n

$$I_n' = \begin{cases} 0, \text{ if } n \text{ is odd} \\ \pi, \text{ if } n = 0 \\ \dfrac{(n-1)(n-3)(n-5)\ldots 3 \cdot 1}{n(n-2)(n-4)\ldots 4 \cdot 2} \cdot \pi, \text{ if } n \text{ is even} \end{cases} \tag{18}$$

Multiplying I_n' by the $2/\pi$ factor of equation (6),

$$\frac{2}{\pi} I_n' = I_n = \begin{cases} 0, & \text{if } n \text{ is odd} \\ 2, & \text{if } n = 0 \\ \dfrac{(n-1)(n-3)(n-5)\ldots 3 \cdot 1.2}{n(n-2)(n-4)\ldots 4 \cdot 2}, & \text{if } n \text{ is even} \end{cases} \tag{19}$$

If equation (16) is rewritten as

$$f(t) = \sum_{j=0}^{\infty} P_j t^j, \tag{20}$$

equation (6) becomes

$$K_r = \frac{2}{\pi} \sum_{j=0}^{\infty} \left[P_j \int_{-1}^{1} t^j T_r(t) \frac{dt}{\sqrt{1 - t^2}} \right] \tag{21}$$

From equations (19) and (21), the first coefficient is

$$K_o = 2P_o + 2 \sum_{q=1}^{\infty} C_o(2q) P_{2q} \tag{22}$$

where

$$C_o(2q) = \frac{(2q-1)(2q-3)(2q-5)\ldots 3 \cdot 1}{(2q)(2q-2)(2q-4)\ldots 4 \cdot 2} \tag{23}$$

2q is substituted for n in equation (19) since only even values of n yield non-zero values of I_n.

The remaining coefficients may be inferred by induction:

$$K_r = 2 \sum_{q=1}^{\infty} C_r C_o(2q) P_{2q}, \quad \text{if } r \text{ is even} \tag{24}$$

$$K_r = 2 \sum_{q=1}^{\infty} C_r' C_o(2q) P_{2q-1}, \quad \text{if } r \text{ is odd} \tag{25}$$

where

$$C_r = \frac{(2q)(2q-2)(2q-4)\ldots(2q-r+2)}{(2q+2)(2q+4)(2q+6)\ldots(2q+r)}, \quad r \text{ even} \tag{26}$$

$$C_r' = \frac{(2q-2)(2q-4)(2q-6)\ldots(2q-r+1)}{(2q+2)(2q+4)(2q+6)\ldots(2q+r-1)}, \quad r \text{ odd} \tag{27}$$

The summations of equations (22), (24), and (25) are carried out to a finite limit commensurate with the desired accuracy.

APPENDIX C

PROPAGATION CORRECTIONS

C.1 INTRODUCTION

The bending of radio waves passing through the troposphere and ionosphere limits the inherent precision of modern electronic tracking systems. Therefore, some form of correction for refractive effects is necessary to achieve the maximum accuracy of the satellite tracking system.

Tropospheric error can be corrected either analytically or numerically. The analytical method assumes the index of refraction decays exponentially as altitude increases. The tropospheric errors for range and elevation, resulting from refraction, are therefore solvable in closed form as a function of the elevation angle.

The numerical method does not assume a specific variation of index of refraction with altitude; any model describing the variations can be used. The tropospheric errors are determined by numerically integrating over the total propagation path, the index of refraction at each integration point being determined by the assumed model.

Because of the complex nature of the ionosphere, it is very difficult to find a simple model to use as a basis for an analytical solution to the ionospheric errors; therefore, a numerical approach is indicated. As a refinement, the refraction correction is made dependent upon the predicted evaluation angle rather than the measured elevation angle. Since the predicted angle is subject to error, a test is made on the variance of the predicted angle. If the variance is above a predetermined limit, an iteration is made to include the data point and thereby provide a better estimate of the elevation angle before making the final correction. The refraction correction is then based upon the new elevation angle, and the results of the iteration are used by the statistical filter. The Program uses a numerical approach for the correction of tropospheric errors to be compatible with the numerical solution of the ionospheric model. As a result, integration over the tropospheric and ionosphere may be performed by the same routine.

In addition to refractive bending, the problem of signal retardation which results in range error, and the effect of refractive bending on range rate measurements are included in the following analysis.

C.2 METHOD USED

C.2.1 GENERAL. The method used to determine refraction corrections in both the troposphere and the ionosphere is a simple one which was derived by S. Weisbrod (reference 25). In Weisbrod's method, there are no limitations on the shape of the index of refraction profile or angle of elevation. The following assumptions are made:

a. The gradient of the index of refraction varies only with altitude, i.e., radially.

b. The index of refraction profile can be approximated by a number of linear segments, the length of each segment being very small compared to the Earth's radius.

C.2.2 INDEX OF REFRACTION MODELS

C.2.2.1 General. It is an almost impossible task to analyze completely the atmospheric propagational effects from all possible conditions. Therefore, atmospheric models representative of average conditions are employed to simplify the computational problem. In the models used, the following assumptions are made:

a. The troposphere extends to approximately 40 kilometers with refractivity decreasing with height.

b. The region between the end of the troposphere and the beginning of the ionosphere is assumed to have zero refractivity.

c. The ionosphere lies between a height h_o (refer to paragraph C.2.2.3.1) and 2000 kilometers.

d. The refractivity is zero in the region beyond 2000 kilometers.

In general, the equations used to compute range and elevation errors are the same for both the troposphere and the ionosphere. Refractivity, however, is computed differently for each.

Computed solutions can only be as accurate as the models assumed. However, since profiles of the index of refraction in the atmosphere (especially for the ionosphere) are not precisely known under all conditions, a more exact solution is not warranted at this time.

C.2.2.2 Tropospheric Model. In the tropospheric model, refractivity is assumed to decay exponentially, with the ground index of refraction and the scale height as parameters. The equation for the tropospheric model is as follows:

$$N = N_o \, e^{-h/H} = (n - 1) \, 10^6 \qquad (1)$$

where

N_o = 313 (refractivity at sea level)

h = height above the Earth

H = 7 kilometers (scale height)

n = index of refraction.

For the tropospheric model, the refractive errors are considered to be independent of signal frequency since the index of refraction is virtually independent of frequency up to 30,000 megacycles.

C.2.2.3 Ionospheric Model

C.2.2.3.1 Ionospheric Parameters. In the ionospheric model, the index of refraction is dependent upon more parameters than those considered for the tropospheric model. The ionosphere consists of several belts of charged particles. The F layer is very much larger than any other layer, and therefore contains a greater number of charged particles than the other layers. The F layer is the one closest to the Earth's surface. It is subdivided into the F1 and F2 layers. In the ionospheric model, the index of refraction is primarily dependent upon the height, h_o, of the base of the ionosphere's F2 layer, the maximum electron density of the F2 layer, and the height of the maximum electron density of the F2 layer.

Both index of refraction and the height h_o are dependent upon diurnal, solar activity, seasonal, and geographical variations as well as other miscellaneous sporatic variations. Unlike the tropospheric model, the refractive errors in the ionospheric model are frequency dependent.

In constructing the model, the range of the signal frequency has been limited to frequencies above 100 megacycles since this range of the spectrum both represents the situation of greatest interest and enables equation simplification.

C.2.2.3.2 Electron Density Profile. The relationship between the index of refraction (n) the angular frequency of the incident signal (ω), and the electron density in the ionosphere (reference 25) is given by

$$n = \left[1 - \frac{\rho_e \, e^2}{\epsilon_o \, m \, \omega^2} \right]^{1/2} \qquad (2)$$

where

ρ_e = electron density per cubic meter

e = electron charge (1.6×10^{-19})

m = electron mass (9.08×10^{-31})

ϵ_o = permittivity of free space (8.854×10^{-12})

Using the first two terms of the binomial expansion as an approximation, the equation for the index of refraction reduces to

$$n = 1 - 40.3 \frac{\rho_e}{f^2} \tag{3}$$

where $f = \omega/2\pi$. This equation is true for frequencies above the critical frequency, f_c, which is defined as

$$f_c = 8.97\ \rho_o^{1/2} \times 10^{-6} \quad \text{megacycles per second} \tag{4}$$

where ρ_o is the maximum electron density per cubic meter.

From the definition of N of equation (1), equation (3) can be written as

$$N = -4.03 \frac{\rho_e}{f^2} \times 10^{-5}. \tag{5}$$

The model selected for electron density versus height consists of a parabolic variation below the height of maximum electron density matched to a hyperbolic secant profile above the maximum. The relationships are as follows:

$$\rho_e = \rho_o \left[1 - (1 - \sigma)^2\right] \qquad 0 \leq \sigma \leq 1$$

$$\rho_e = \rho_o \operatorname{sech}\left[\frac{\pi}{4}(\sigma - 1)\right] \qquad \sigma \geq 1 \tag{6}$$

where

$$\sigma = \frac{h - h_o}{h_m - h_o}$$

h = height above the Earth

h_o = height of the base of the F2 layer

h_m = height of the maximum electron density in the F2 layer

The model has the following characteristics:

a. The model has three degrees of freedom (h_o, h_m, and ρ_o) which uniquely specify the entire distribution. These parameters can be obtained from ionogram data.

b. The electron distribution is parabolic below the maximum electron density height, nearly parabolic immediately above the maximum, and exponential at great heights.

c. The electron content of the distribution above the maximum electron density height is three times that below it.

d. The entire electron density profile and its derivatives are continuous everywhere.

Figure C-1 is a plot of the ionosphere model normalized with respect to σ and 1/2 (ρ_e/ρ_o). The h_o, h_m, and ρ_o parameters refer to the ionosphere's F layer. Using this

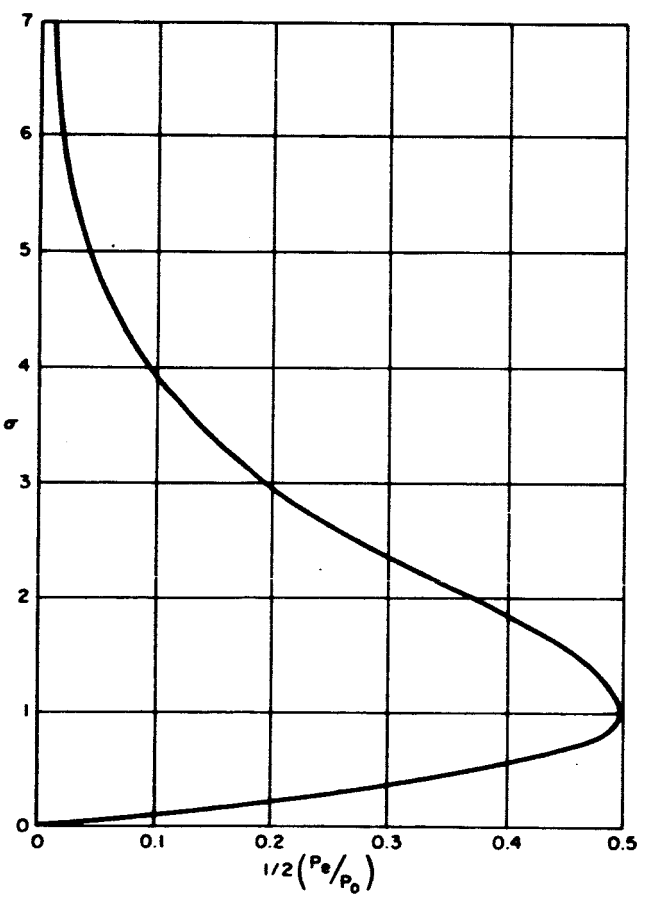

Figure C-1 Normalized 3-Parameter Model of Atmosphere

model, the refractive effects of the D and E layers are not singled out, because they are quite small in comparison with those due to the F layer and are approximately accounted for by allowing the electron density at the bottom edge of the F layer to be zero.

C.2.3 Detailed Analysis

C.2.3.1 Computation of Ray Bending. Consider a ray (figure C-2) entering, at an angle of β, an infinitesimal layer of thickness dP. Since the curvature of the ray is equal to the component of the refractive gradient normal to the ray divided by the index of refraction,

$$\frac{1}{K} = \frac{1}{n} \frac{dn}{dP} \cos \tag{7}$$

where K is the radius of curvature.

The length of the ray path in the layer is

$$K \, d\gamma = \csc \beta \, d\beta \tag{8}$$

which, when combined with equation (7), gives

$$d\gamma = \frac{1}{n} \frac{dn}{dP} \cot \beta \, dP. \tag{9}$$

The $d\gamma$'s of all elementary layers are directly additive; therefore, considering $d\gamma$'s due to bending between points Q and R, it follows that the contribution to the total bending γ, from a layer bounded by the heights P_j and P_k is

$$\gamma_{jk} = \int_{P_j}^{P_k} \frac{1}{n} \frac{dn}{dP} \cot \beta \, dP. \tag{10}$$

If the ray departs from the Earth's surface with an elevation angle of θ_o, then from Snell's law for spherical stratifiction

$$n_o \, a \cos \theta_o = nP \cos \beta = \text{constant} \tag{11}$$

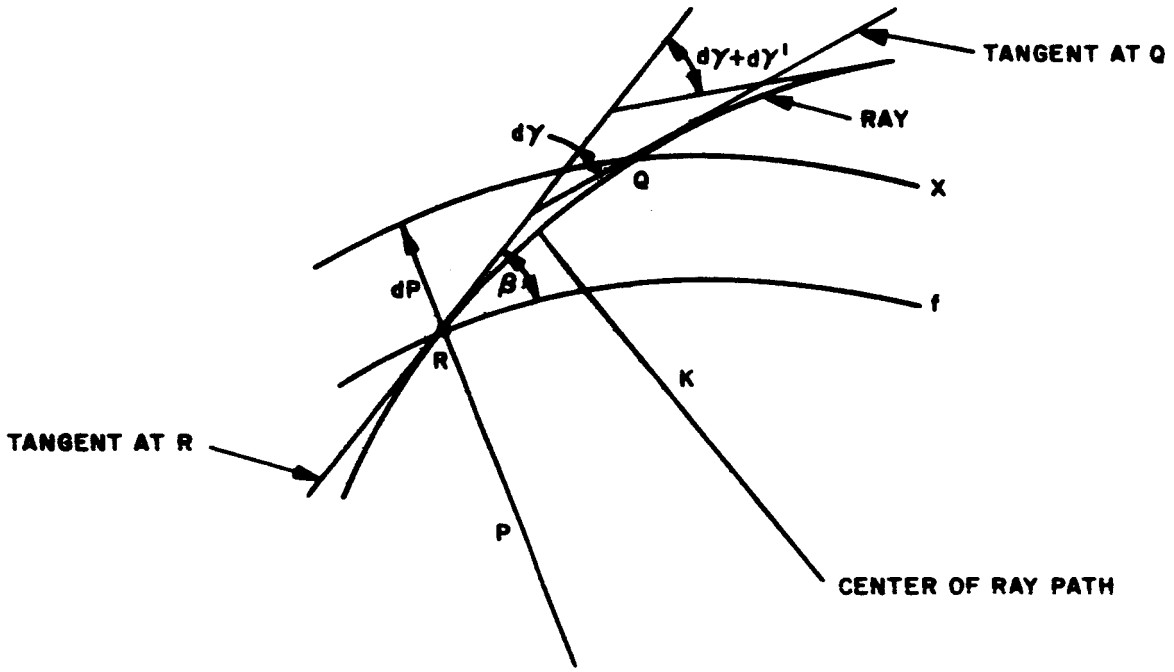

Figure C-2 Geometry of Bending Through an Infinitesimal Layer

where

n_o = index of refraction at the Earth's surface

a = Earth's radius

P = a + h

h = height above Earth

n = index of refraction at h

From equation (11),

$$\cos \beta = \left[\frac{n_o\ a}{nP}\right] \cos \theta_o = \left[\frac{n_i\ P_i}{nP}\right] \cos \beta_i \qquad (12)$$

$$\sin \beta = \left[\frac{n_o\ a}{nP}\right]\left[\left[\frac{nP}{n_o\ a}\right]^2 - \cos^2 \theta_o\right]^{1/2}$$

$$= \left[\frac{n_i\ P_i}{nP}\right]\left[\left[\frac{nP}{n_i\ P_i}\right]^2 - \cos^2 \beta_i\right]^{1/2} \qquad (13)$$

$$\cot \beta = \left[\left[\frac{nP}{n_o\ a}\right]^2 - \cos^2 \theta_o\right]^{1/2} \cos \theta_o$$

$$= \left[\left[\frac{nP}{n_i\ P_i}\right]^2 - \cos^2 \beta_i\right]^{1/2} \cos \beta_i \qquad (14)$$

where n, P, and β are the values of these parameters at h.

Equation (14) can be substituted into equation (10) to give the general equation for refractive bending:

$$\gamma_{jk} = \int_{P_j}^{P_k} \frac{1}{n}\ \frac{dn}{dp}\ \frac{\cos \theta_o}{\left[\left[\frac{nP}{n_o\ a}\right]^2 - \cos^2 \theta_o\right]^{1/2}}\ dP$$

$$= \int_{P_j}^{P_k} \frac{1}{n}\ \frac{dn}{dP}\ \frac{\cos \beta_i}{\left[\left[\frac{nP}{n_j\ P_j}\right]^2 - \cos^2 \beta_j\right]^{1/2}}\ dP \qquad (15)$$

Assume that

a. $\frac{dn}{dP} = -k$, where k is a constant.

b. $P_k - P_j \ll P_j$

c. The index of refration n is very nearly equal to unity.

On the basis of the assumptions and from figure C-2,

$$k = \frac{(N_j - N_k)}{(P_k - P_j)} \times 10^{-6} = \frac{(N_j - N)}{(P - P_j)} \times 10^{-6} \tag{16}$$

and

$$\left[\frac{nP}{n_j P_j}\right]^2 = \left\{\left[1 - (N_j - N)\ 10^{-6}\right]\left[1 + \frac{(P - P_j)}{P_j}\right]\right\}^2 \tag{17}$$

Expanding equation (17) and using only the first two terms,

$$\left[\frac{nP}{n_j P_j}\right]^2 \cong 1 + \frac{2(P - P_j)\ (1 - k P_j)}{P_j} \tag{18}$$

and, substituting in equation (15)

$$\gamma_{jk} = k \cos \beta_j \int_{P_j}^{P_k} \left[\sin^2 \beta_j + 2(P - P_j)\ (1 - k P_j)/P_j\right]^{-1/2} dP$$

$$= \frac{k P_j \cos \beta_j}{1 - k P_j} \left\{\left[\sin^2 \beta_j + 2(P_k - P_j)\ (1 - k P_j)/P_j\right]^{1/2} - \sin \beta_j\right\} \tag{19}$$

From equations (12) and (18) and Snell's Law,

$$\sin \beta_k = \left[\frac{n_j P_j}{n_k P_k}\right]\left[\left[\frac{n_k P_k}{n_j P_j}\right]^2 - \cos^2 \beta_j\right]^{1/2}$$

$$= \frac{\cos \beta_k}{\cos \beta_j}\left[\sin^2 \beta_j + \frac{2 (P_k - P_j) (1 - k P_j)}{P_j}\right]^{1/2} \qquad (20)$$

and combining with equation (19)

$$\gamma_{jk} = \frac{k P_j \cos^2 \beta_j}{1 - k P_j} (\tan \beta_k - \tan \beta_j). \qquad (21)$$

From equations (14), (16), and (18)

$$\frac{k P_j}{1 - k P_j} = \frac{2(N_j - N_k) \sec^2 \beta_j}{\sec^2 \beta_k - \sec^2 \beta_j} \cdot 10^{-6}$$

$$= \frac{2(N_j - N_k) \sec^2 \beta_j}{\tan^2 \beta_k - \tan^2 \beta_j} \cdot 10^{-6}, \qquad (22)$$

which, when substituted in equation (21), gives

$$\gamma_{jk} = \frac{1}{2} \frac{(N_j - N_k)}{(\tan \beta_j + \tan \beta_k)} \cdot 10^{-6}$$

$$= \frac{(N_j - N_k)}{500 (\tan \beta_j + \tan \beta_k)} \text{ milliradians.} \qquad (23)$$

Total bending through the atmosphere is simply the sum of the individual contributions; therefore,

$$\gamma = \sum_{i=1}^{n} \frac{(N_{i-1} - N_i)}{500\ (\tan \beta_{i-1} + \tan \beta_i)} \text{ milliradians.} \qquad (24)$$

It is frequently convenient to measure the refractive error in terms of the angle subtended from the Earth's center. This quantity, ϵ, is readily obtained from figure C-3.

$$\epsilon = \gamma - (\theta - \beta) \qquad (25)$$

The quantity $(\theta - \beta)$ is found from Snell's Law and equations (12) and (17):

$$n_o \cos \theta = n \cos \beta$$

$$\cos \beta = \cos [\theta - (\theta - \beta)]$$

$$= [1 + (N_o - N)\ 10^{-6}] \cos \theta$$

$$\cos \theta = \cos [\beta + (\theta - \beta)]$$

$$= [1 - (N_o - N)\ 10^{-6}] \cos \beta \qquad (26)$$

Expansion of equation (26) and the application of small angle approximations results in

$$(\theta - \beta) = \left\{1 - [1 - 2(N_o - N)\ 10^{-6} \cot^2 \theta]^{1/2}\right\} \tan \theta$$

$$= \left\{[1 + 2(N_o - N)\ 10^{-6} \cot^2 \beta]^{1/2} - 1\right\} \tan \beta \qquad (27)$$

For rays departing tangentially at heights above the troposphere, or for angles of elevation greater than 100 milliradians at any height, the angles θ and β are very nearly equal and equation (27) reduces to

$$(\theta - \beta) \cong (N_o - N)\ 10^{-6} \cot \theta$$

$$\cong (N_o - N)\ 10^{-6} \cot \beta. \qquad (28)$$

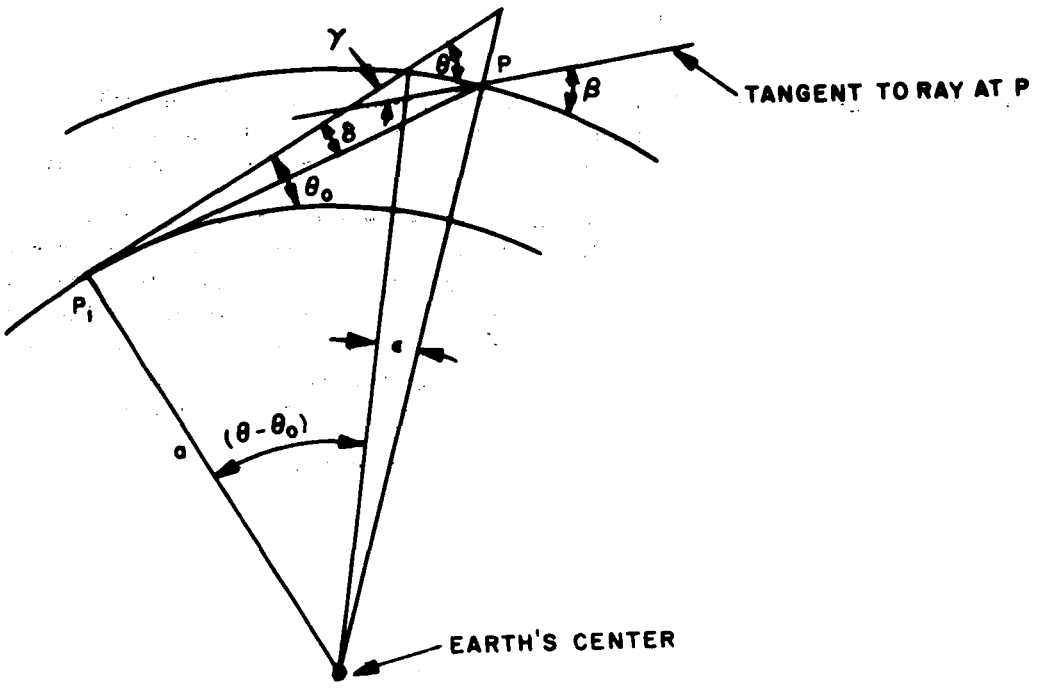

Figure C-3 Geometry of Bending Through a Refractive Layer

C.2.3.2 Computation of Errors in Principal Measurements

C.2.3.2.1 Elevation Angle Error. In most practical applications, the quantity of greatest interest is the elevation angle error, δ. This quantity is obtained from figure C-3 by the use of the law of sines:

$$a \cos \theta_0 = P \cos \theta$$

$$a \cos (\theta_0 - \delta) = P \cos [(\theta + \epsilon) - \delta] \qquad (29)$$

From equation (29),

$$\tan \delta = \frac{\sin \epsilon \tan \theta + (1 - \cos \epsilon)}{\sin \epsilon + \cos \epsilon \tan \theta - \tan \theta_0} .$$

and when ϵ is a small angle,

$$\delta = \frac{\epsilon \tan \theta + \epsilon^2/2}{\epsilon + \tan \theta - \tan \theta_o} . \tag{30}$$

Omitting $\epsilon^2/2$ in the numerator of equation (30) results in an error of about five percent in the troposphere for a tangentially departing ray. At higher angles of elevation or greater heights, this error becomes negligible.

It should be noted that whereas angles γ and ϵ, due to the passage of the ray through various layers, are directly additive, the elevation angle errors are not. Thus, to evaluate δ at ionospheric heights or above, it is first necessary to combine the tropospheric and the ionospheric ϵ's or δ's and then use equation (30). However, in nearly all practical cases above the troposphere, $\epsilon^2/2$ is very much less than ϵ and ϵ is very much less than $(\tan \theta - \tan \theta_o)$. Consequently, the omission of $\epsilon^2/2$ in the numerator and ϵ in the denominator usually results in less than five percent error at heights in the F region.

Equation (30) can thus be approximated by

$$\delta \cong \frac{\epsilon \tan \theta}{\tan \theta - \tan \theta_o} . \tag{31}$$

It is, therefore, justifiable to add directly the tropospheric and ionospheric δ's to obtain the total elevation angle error.

At astronomical distances all three quantities (γ, ϵ, and δ) become numerically equal.

C.2.3.2.2 Signal Retardation in a Constant Refractive Gradient Region. The signal retardation, $d\tau$, caused by a layer of thickness dP (figure C-2) is given by

$$d\tau = \left[\frac{1}{v} - \frac{1}{c}\right] \csc \beta \, dP$$

$$= \left[\frac{c}{v} - 1\right] \csc \beta \frac{dP}{c} = \frac{N \csc \beta \, dP}{c} \cdot 10^{-6} \tag{32}$$

where

c = signal velocity in free space

v = signal velocity in the medium.

The range propagation error, Δr, is given by

$$\Delta r_{ik} = \int_{P_i}^{P_k} c \, d\tau = \int_{P_i}^{P_k} \frac{N \times 10^{-6}}{\sin \beta} \, dP \tag{33}$$

Substituting equation (14) into equation (16) and solving equation (23),

$$\gamma_{ik} = \int_{P_i}^{P_k} \frac{(dn/dP)}{\tan \beta} \, dP = \int_{P_i}^{P_k} \frac{dn}{\tan \beta} = \frac{2(N_i - N_k)}{(\tan \beta_i + \tan \beta_k)} \cdot 10^{-6} \tag{34}$$

The value of the integral for the case of a constant radial gradient is found to be very nearly equal to the value of the integral obtained when taking the average value of the denominator of the integral and treating it as a constant. The integral in equation (33) can justifiably be treated in a similar manner for two reasons. One reason is that the sine and tangent of small angles are very nearly the same, and the other reason is that the rate of change of the sine is very slow at large angles.

To evaluate equation (33), set

$$\Delta r_{ik} = \int_{P_i}^{P_k} \frac{N \times 10^{-6}}{\tan \beta} \, dP = \frac{2 \times 10^{-6}}{\sin \beta_i + \sin \beta_k} \int_{P_i}^{P_k} N \, dP \tag{35}$$

From equation (16),

$$\int_{P_i}^{P_k} N \, dP = \int_{P_i}^{P_k} [N_i - k(P - P_i)] \, dP$$

$$= N_i (P_k - P_i) - \frac{1}{2} (N_i - N_k) (P_k - P_i)$$

$$= \frac{1}{2} (N_i + N_k) (P_k - P_i) \tag{36}$$

Substituting this value,

$$\Delta r_{ik} = \frac{(N_k - N_i)\ (P_k - P_i)}{\sin \beta_k + \sin \beta_i} \cdot 10^{-6}$$

To compute signal retardation for a double passage through the layer, the value of equation (37) must be doubled. Therefore,

$$\Delta r = 2 \times 10^{-3} \sum_{i=1}^{n} \frac{|N_{i-1} + N_i|\ (h_i - h_{i-1})}{\sin \beta_{i-1} + \sin \beta_i} \text{ meters.} \qquad (38)$$

In the ionosphere, the equation for range propagation error is

$$\Delta r = \left[1 + \left[\frac{f_2}{f_1}\right]^2\right] \times 10^{-6} \sum_{i=1}^{n} \frac{|N_{i-1} + N_i|\ (h_i - h_{i-1})}{\sin \theta_{i-1} + \sin \theta_i} \text{ meters} \qquad (39)$$

where

f_1 = up frequency

f_2 = down frequency

C.2.3.2.3 Doppler Error. Due to refractive bending, there is an error in the measurement of the radial component of the target velocity. The equation describing this error can be readily derived with the aid of figure C-4. Let

$\mathbf{R}$ = station location vector in inertial coordinates

Γ = position of satellite with respect to the Earth's center in inertial coordinates

ρ' = position of satellite with respect to the station in inertial coordinates

ρ = position of satellite with respect to the station in topocentric local moving coordinates

Ω = Earth's rotation velocity vector in inertial coordinates

$[A]$ = coordinate conversion transformation matrix

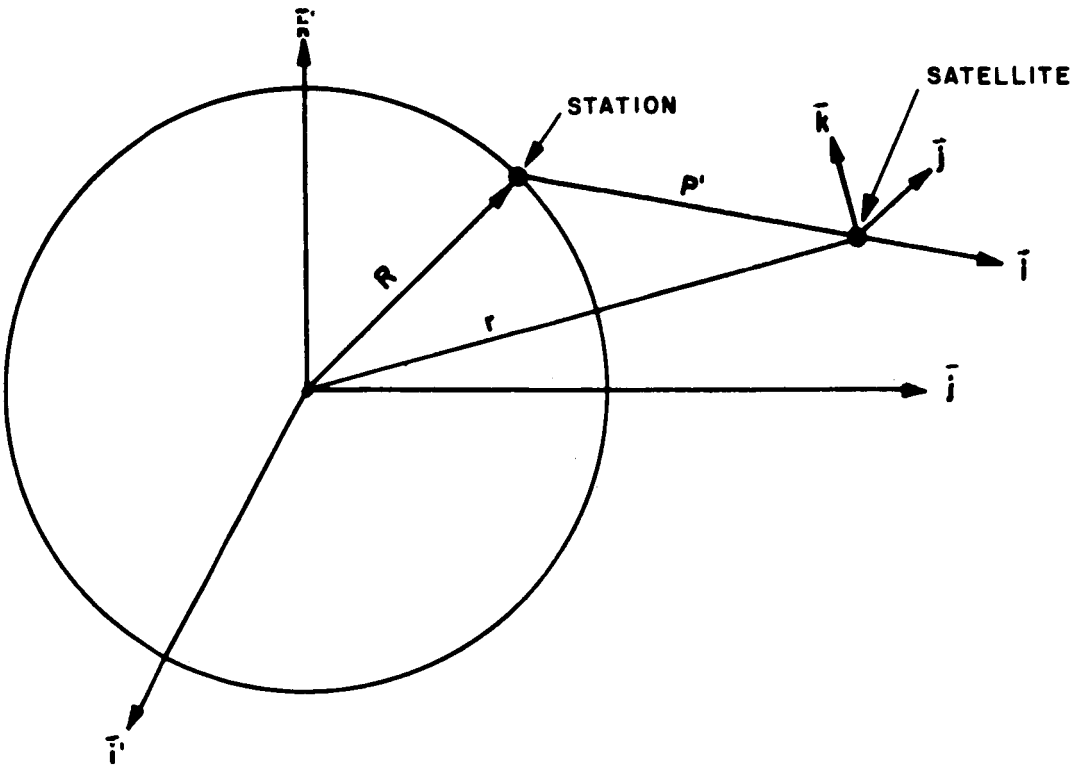

Figure C-4 Doppler Error Geometry

$\bar{I}', \bar{J}', \bar{K}'$ = unit vectors in the inertial coordinate system

$\bar{I}, \bar{J}, \bar{K}$, = unit vectors in the topocentric moving coordinate system

Therefore,

$$\left.\begin{aligned} \Gamma &= X\,\bar{I}' + Y\,\bar{J}' + Z\,\bar{K}' \\ \dot{\Gamma} &= \dot{X}\,\bar{I}' + \dot{Y}\,\bar{J}' + \dot{Z}\,\bar{K}' \\ \dot{R} &= \Omega \times R \\ \rho' &= \Gamma - R \\ \dot{\rho}' &= \dot{\Gamma} - \dot{R} = \dot{\Gamma} - \Omega \times R \\ \rho &= [A]\,\rho' = [A]\,(\Gamma - R) \\ \dot{\rho} &= [A]\,\dot{\rho}' + [\dot{A}]\,\rho' \end{aligned}\right\} \qquad (38)$$

where X, Y and Z are the magnitudes of the x-, y-, and z- components of Γ. Let

$$\bar{I} = \frac{\rho'}{|\rho'|} = A_{11}\,\bar{I}' + A_{12}\,\bar{J}' + A_{13}\,\bar{k}' \tag{39}$$

$$\bar{k} = \frac{\rho' \times R}{|\rho' \times R|} = A_{31}\,\bar{I}' + A_{32}\,\bar{J}' + A_{33}\,\bar{k}' \tag{40}$$

$$\bar{J} = \bar{k} \times \bar{I} = A_{21}\,\bar{I}' + A_{22}\,\bar{J}' + A_{23}\,\bar{k}' \tag{41}$$

where

$$[A] = \begin{bmatrix} A_{11} & A_{12} & A_{13} \\ A_{21} & A_{22} & A_{23} \\ A_{31} & A_{32} & A_{33} \end{bmatrix} \tag{42}$$

In the moving coordinate system, the relative velocity between station and vehicle is described by

$$\dot{\rho} = \dot{\rho}_x\,\bar{I} + \dot{\rho}_y\,\bar{J} + \dot{\rho}_z\,\bar{k}\ , \tag{43}$$

where

$\dot{\rho}_x$ = velocity component along the local range vector

$\dot{\rho}_y$ = velocity component normal to the local range vector in a plane determined by the transmitter beam and the Earth's center

$\dot{\rho}_z$ = velocity component normal to a plane determined by the transmitter beam and the Earth's center

From figure C-3, the measured value of range rate is along the apparent path or along the tangent to the path at the satellite. Here,

$$V \text{ measured} = \dot{\rho}_x \cos(\gamma - \delta) - \dot{\rho}_y \sin(\gamma - \delta)$$

$$V \text{ radial} = \dot{\rho}_x$$

Therefore, the range rate error, Δv_r, is

$$\Delta V_r = V \text{ radial} - V \text{ measured}$$

$$= \dot{\rho}_x - \dot{\rho}_x \cos(\gamma - \delta) + \dot{\rho}_y \sin(\gamma - \delta) \quad (44)$$

and since $(\gamma - \delta)$ is a very small angle, then

$$\Delta V_\Gamma = \dot{\rho} \quad (\gamma - \delta) \quad (45)$$

and is doubled for the round trip error.

In the ionosphere, the correction for range rate is modified as follows

$$\Delta V_r = \left[1 + \left[\frac{f_2}{f_1}\right]^2\right] \dot{\rho}_y \quad (\gamma - \delta) \quad (46)$$

C.3 COMPUTATION OF ERRORS IN SECONDARY ANGULAR MEASUREMENTS

NOTE: The elevation angle error δ must be transformed into the coordinate system of the secondary angular measurements in order to determine the equivalent error in these systems.

C.3.1 COORDINATE CONVERSIONS. To convert from the azimuth angle ϕ and elevation angle θ system to other systems, see figures C-5 and C-6. From figure C-5, the following relations hold for the x-y angles:

$$\begin{aligned} \sin y &= \cos\theta \cos\phi \\ \cos y \sin x &= \cos\theta \sin\phi \\ \cos y \cos x &= \sin\theta \end{aligned} \quad (47)$$

hence,

$$\tan x = \cot\theta \sin\phi \quad (48)$$

where

x is the X- antenna angle

y is the Y- antenna angle

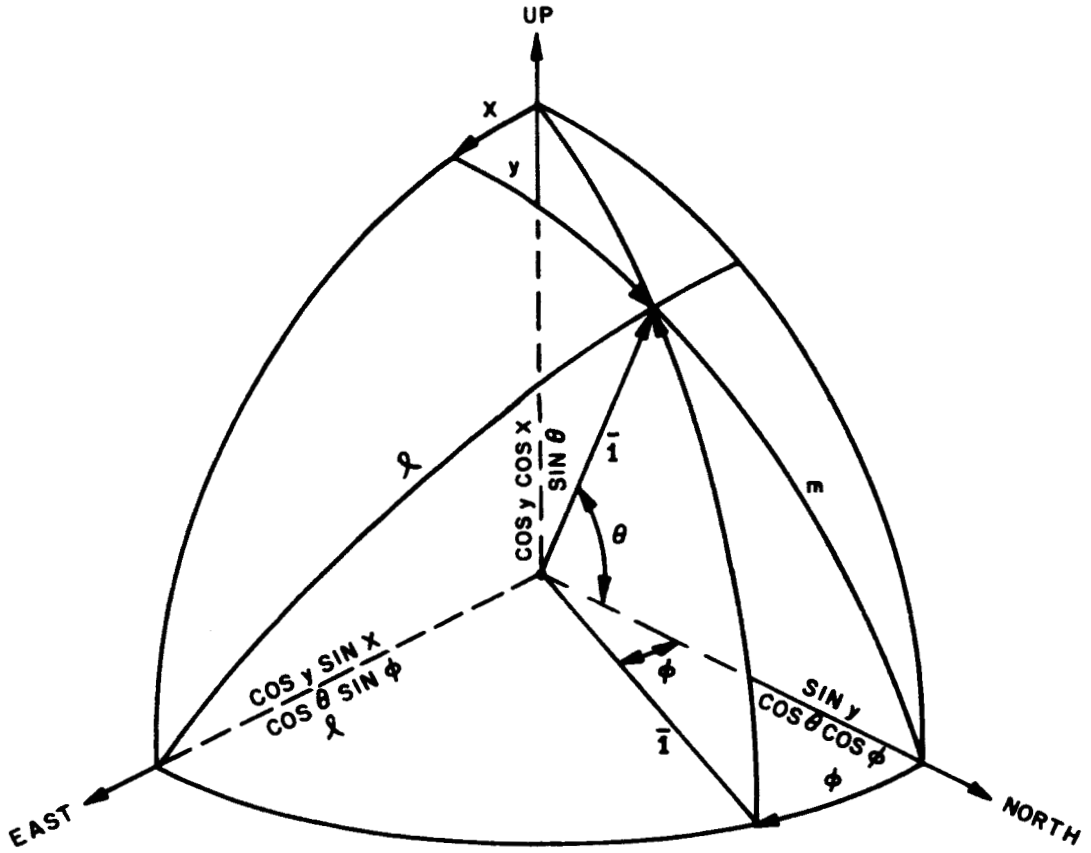

Figure C-5 Geometry for Converting to x-y and ℓ-m System

From figure C-5, the following relations hold for the ℓ-m direction cosine system:

$$\ell = \cos\theta \sin\phi$$

$$m = \cos\theta \cos\phi \qquad (49)$$

where

ℓ is the measured ℓ direction cosine

m is the measured m direction cosine

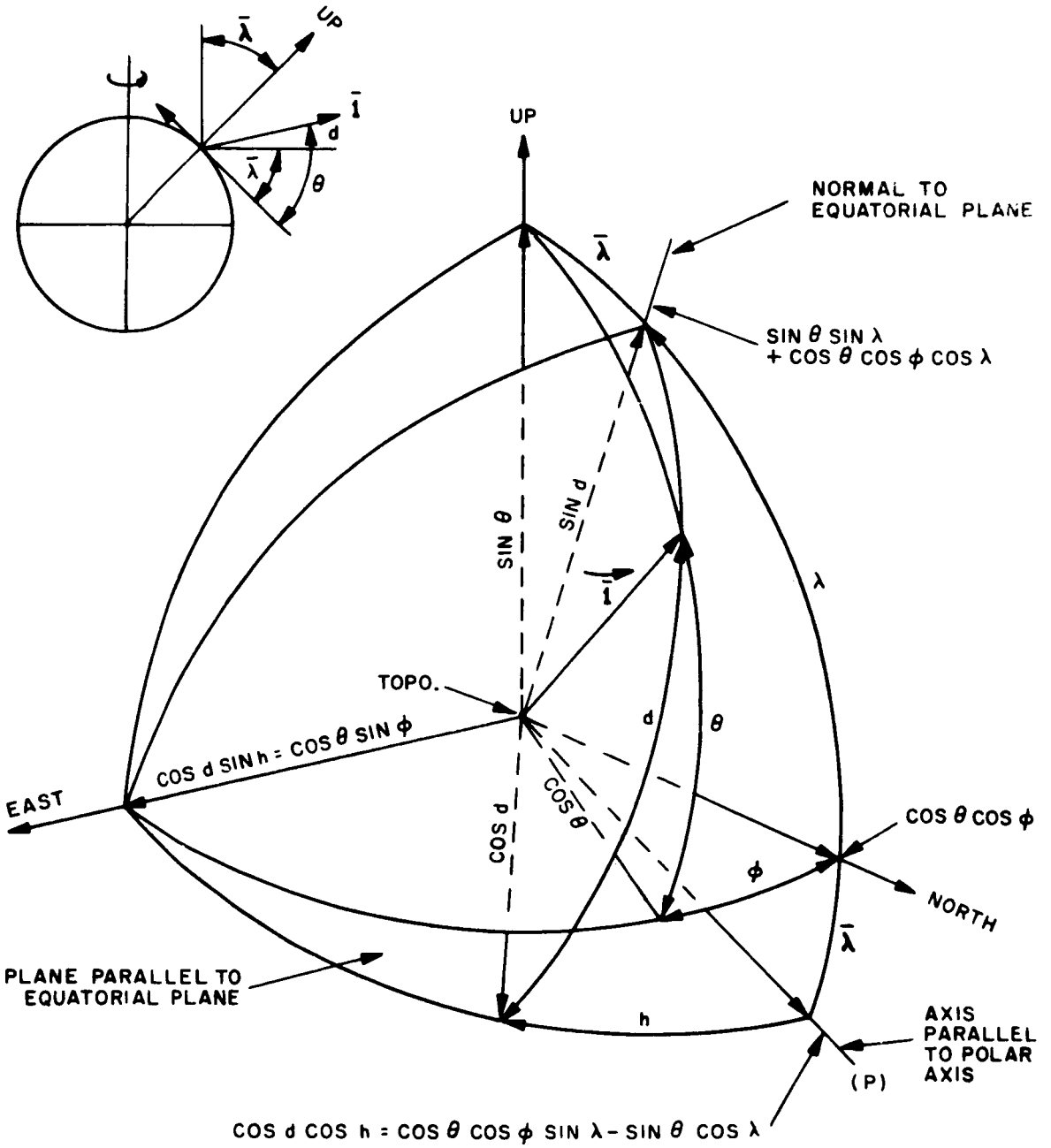

Figure C-6 Geometry for Converting to Hour Angle - Declination System

From figure C-6, the following relations hold for the hour angle-declination system:

$$\begin{aligned} \sin d &= \sin\theta \sin\lambda + \cos\theta \cos\phi \cos\lambda \\ \cos d \sin h &= \cos\theta \sin\phi \\ \cos d \cos h &= \cos\theta \cos\phi \sin\lambda - \sin\theta \cos\lambda \end{aligned} \tag{50}$$

hence,

$$\tan h = \frac{\sin\phi}{\cos\phi \sin\lambda - \tan\theta \cos\lambda} \tag{51}$$

where

d is the measured declination

h is the measured hour angle

λ is the station location latitude

C.4.3.2 ERROR COMPONENTS. A small deviation in the elevation angle θ will cause a small deviation in the secondary angles. The magnitudes of the errors are determined by differentiating the coordinate conversion expressions found in paragraph C.4.3.1 with respect to the elevation angle.

For the x - y system

$$\begin{aligned} \frac{\partial x}{\partial\theta} &= -\frac{\sin\phi \csc^2\theta}{\sec^2 x} = -\frac{\sin\phi \cos^2 x}{\sec^2\theta} \\ \frac{\partial y}{\partial\theta} &= -\frac{\cos\phi \sin\theta}{\cos y} \end{aligned} \tag{52}$$

hence,

$$\begin{aligned} \Delta x &= \frac{\partial x}{\partial\theta}\,\delta \\ \Delta y &= \frac{\partial y}{\partial\theta}\,\delta \end{aligned} \tag{53}$$

where δ is the elevation angle error found in paragraph C.4.2.1.

For the ℓ -m system

$$\frac{\partial \ell}{\partial \theta} = - \sin \theta \sin \phi$$

$$\frac{\partial m}{\partial \theta} = - \sin \theta \cos \phi \qquad (54)$$

hence,

$$\Delta \ell = \frac{\partial \ell}{\partial \theta} \delta$$

$$\Delta m = \frac{\partial m}{\partial \theta} \delta \qquad (55)$$

For the hour angle - declination system

$$\frac{\partial d}{\partial \theta} = \frac{\cos \theta \sin \lambda - \sin \theta \cos \phi \cos \lambda}{\cos d}$$

$$\frac{\partial h}{\partial \theta} = \frac{1}{\sec^2 h} \left[\frac{\sin \phi \cos \lambda \sec^2 \theta}{(\cos \phi \sin \lambda - \tan \theta \cos \lambda)^2} \right] \qquad (56)$$

$$= \frac{\sin \phi \cos \lambda \cos^2 h}{(\cos \theta \cos \phi \sin \lambda - \sin \theta \cos \lambda)^2} \qquad (57)$$

REFERENCES

1. Nordsieck, Arnold, "On Numerical Integration of Ordinary Differential Equations", Mathematics of Computation, Vol. 16, No. 77, January, 1962, pp. 22-49.

2. Gill, S., "A Process for the Step-by-Step Integration of Differential Equations in an Automatic Digital Computing Machine ", Proceedings of Cambridge Philosophical Society, Vol. 47, Part 1, pp. 96-108 .

3. Ehricke, Krafft A., "Interplanetary Operations", Chapter 8 of Space Technology, edited by Howard Seiffert, John Wiley and Sons, Inc., New York, 1959.

4. Lunar Flight Handbook, NASA SP-34 Part 1, prepared by the Space Systems Division of the Martin Co.

5. Battin, Astronautical Guidance, Mc-Graw Hill Book Co., New York, 1964, pp. 11 and 190.

6. Holdridge, D.B., Space Trajectories Program for the IBM 7090 Computer, Technical Report No. 32-223, Jet Propulsion Laboratory, Pasadena, Calif., September 1, 1962.

7. U.S. Standard Atmosphere 1962.

8. Ketchum, Harold B., Advances in Astronautical Sciences, Plenum Press, 1957 Vol. I, pp. 31-41.

9. Schilling, G.F., Limiting Model Atmospheres of Mars, Re-order No. 62-239, RAND Corporation, Santa Monica, Calif., 1962.

10. Harris, I. and Priester, W., Theoretical Models for the Solar Cycle Variation of the Upper Atmosphere, NASA TND-1444, Goddard Space Flight Center, 1962.

11. Harris, I. and Priester, W., Relation Between Theoretical and Observational Models of the Upper Atmosphere, NASA X-640-63-145, Goddard Space Flight Center, 1963.

12. Roemer, M., Fourier Analysis of Atmospheric Densities Given by the Harris-Priester Models, Report to COSPAR Working Group IV.

13. Kaplan, L.D., A Preliminary Model of the Venus Atmosphere, 1962.

14. Chauvenet, W., A Manual of Spherical and Practical Astronomy, Volume One, Dover Publications, Inc. New York, 1960.

15. Kopal, Zdeněk. Physics and Astronomy of the Moon, Academic Press, New York and London 1962.

16. Pines S., Wolf, H., and Payne, M., Asymptotically Singular Differential Correction Matrices, NASA NAS 5-293, Republic Aviation Corporation.

17. Bailey, Ann, Goddard Variational Parameters, Analytical Mechanics Association, February 6, 1964.

18. Battin, Richard H., "A Statistical Optimizing Navigations Procedure for Space Flight", ARS Journal, November, 1962, pp. 1681-1696.

19. Smith, Gerald L., Schmidt, Stanley F., and McGee, Leonard A., Application of Statistical Filter Theory to the Optimal Estimation of Position and Velocity On Board a Circumlunar Vehicle, NASA TR R-135, 1962.

20. American Ephemeris and Nautical Almanac 1960. U.S. Government Printing Office, Washington, D.C.

21. Explanatory Supplement to Astronomical Ephemeris and the American Ephemeris and Nautical Almanac, Issued by H.M. Nautical Almanac Office, London, 1961.

22. Astronomical Papers American Ephemeris, Vol. XV, Part I, p. 153, 1953.

23. Sterne, T.E., An Introduction to Celestial Mechanics, Interscience Publishers, Inc., New York, 1960.

24. Lanczos, Cornelius, Applied Analysis Prentic-Hall Inc., Englewood Cliffs, N.J., 1961.

25. Weisbrod, S. and Anderson, L.J., "A Simple Method for Computing Tropospheric and Ionospheric Effects on Radio Waves", Proceedings of the IRE, October, 1959, pp. 1770-1777.

DISTRIBUTION LIST

Copy No.		Mail Station
1-50 + reproducible	R.K. Squires of Goddard Space Flight Center (via C.I. Smith, 3R112)	
51	J.J. Carroll	3R112
52	D.W. Proctor	3R112
53-68 + reproducible	C.I. Smith	3R112
69	K. Dodge	3R112
70	E. Burgess	SY7
71	A.B. Wolfman	1P30
72	Inventions Research	3S118
73	Engineering Library	1A38
74	R.T. Hamlett	1P30
75-76	Publications Security	G31